Phonon Superradiance in Dilute Gas Bose-Einstein Condensates

Sarah L. W. Midgley

Supervisor: Craig Savage

A thesis submitted for a Graduate Diploma in Science (Physics) at The Australian National University

November, 2006

Declaration

This thesis is an account of research undertaken between March 2006 and November 2006 at the Australian National University, Canberra, Australia.

Except where acknowledged in the customary manner, the material presented in this thesis is, to the best of my knowledge, original and has not been submitted in whole or part for a degree in any university.

Sarah L. W. Midgley
November, 2006

Acknowledgements

This year has been a valuable and enjoyable experience thanks to a bunch of great people. It has been a privilege to work with my supervisor, Craig Savage, on what I found a challenging but exciting research topic. I would like to thank Craig for his ability to explain concepts that seemed intractable to me at first. Also, for his comments on research principles and for teaching me about the "Tortoise and the Hare" in regards to computational physics (a lesson I will no doubt learn a few more times). Finally, I would also like to say thanks for the time he spent working on this project with me and his willingness to distill my often muddled thoughts. Thanks also to Joe and Sebastian for their extremely useful help with XMDS. This work would not have been possible without the use of the APAC National Facility and University of Queensland Taniwha Cluster. In particular, thanks to the APAC helpdesk for answering all of my queries no matter how minor.

I have had the pleasure of meeting some interesting characters this year. To Angela, it has been brilliant to get to know you and share lunch together. I appreciate you allowing me to talk through my project progress each day and your acceptance of my unique tennis skills and my record pace when crawling up Black Mountain. Thanks to Antony for sharing your office with me and providing humorous respite from my work. Also, thanks everyone in the GR group, particularly Andrew for the vegan pizza, and Simon who seemed to venture downstairs.

Finally, to Phyl and Bec for the fun we had at Holt and for understanding that bark is natures toast. Thanks for putting up with my insanity, for teaching me so many great recipes, reciting the little book of calm and associated quotes from Black Books and demonstrating how to tie my shoe laces etc. On a serious note, thanks for ensuring I had computer access at home when my laptop self-destructed again. Mom, thanks for the peanut butter cookies and choc beetroot muffins. To dad, jess and al - hope to see you sometime.

Abstract

The analogy between the propagation of a massless scalar field in curved spacetime and the propagation of sound waves in a Bose-Einstein Condensate (BEC) gives rise to the possibility of observing the analogues of black hole radiance effects, such as Hawking Radiation and superradiance, in the laboratory. In order to provide a solid foundation for realising such analogue gravity models in an experimental setting, we have conducted a numerical investigation of phonon scattering from a BEC vortex by solving the time-dependent Gross-Pitaevskii (GP) equation, describing the dynamics of dilute gas BECs. The consideration of phonon superradiance in BECs in advance of Hawking Radiation is motivated by the fact superradiance may be easier to detect.

We first present the results of one-dimensional simulations of sound waves propagating in a BEC and reflecting from a vortex-like density profile. Using these results as a guide, two-dimensional simulations of sound propagation in a BEC, and reflection from a BEC vortex, are performed. The technique of propagating the wavefunction in imaginary time was employed to find the vortex ground state. The accuracy of the simulations and the convergence of the solution to the vortex ground state was verified using a range of numerical diagnostics. Finally, preliminary simulations were performed within the superradiant frequency regime for the purposes of determining whether the amplification of incoming waves occurs given an appropriate choice of parameters. Overall, the two-dimensional modelling of reflection of cylindrical waves from a BEC vortex provides a basis for a systematic study of phonon superradiance in BECs.

Contents

List of Figures

List of Tables

Chapter 1

Introduction

Black Holes, regions of immense gravitational attraction from which not even light can escape, are associated with several astrophysical phenomena as predicted by Einstein's General Theory of Relativity. Although some of the predictions of Einstein's theory have been experimentally verified, some effects related to Black Holes are inaccessible to experiment and do not lend themselves to observation by means of astronomy.

One such effect is Hawking Radiation or "Black Hole Evaporation", predicted by Hawking in 1974 [41] as a result of attempts to combine general relativity and quantum mechanics. Hawking showed that black holes radiate particles with a thermal spectrum. That is, in a quantum mechanical framework, a black hole acts as a black body with temperature given by,

$$T = \frac{\hbar\kappa}{2\pi k_B} \tag{1.1}$$

where $\hbar$ is the reduced Planck's constant, k_B is the Boltzmann constant and κ is the surface gravity at the black hole event horizon (the gradient of the gravitational potential). The surface gravity is inversely proportional to the mass of a black hole and hence the temperature has a dependence on the mass. As indicated, the surface gravity is defined at the event horizon of the black hole. The event horizon is one of the defining features of a black hole. It is a boundary of a region in space-time where the trajectory of any particle moving forward in time points inward, and hence, away from the boundary. In other words, propagation into a black hole is a one way process and once the event horizon has been crossed, and a particle is found to be within the horizon, it cannot be found outside the event horizon at a future time.

An additional characterising feature of a rotating black hole is the ergoregion. As shown in figure 1.1 this is a region surrounding the event horizon, within which a particle cannot remain stationary relative to an observer far from the black hole. It is from this region that a second notable black hole effect, first proposed by Penrose [65] in 1969, arises. Essentially, a rotating black hole will produce an effect known as frame dragging, whereby the reference frame of a nearby observer will be "dragged" along with the black hole. Consequently, any particle in the ergoregion is made to rotate with the black hole and therefore increases its rotational kinetic energy. Since

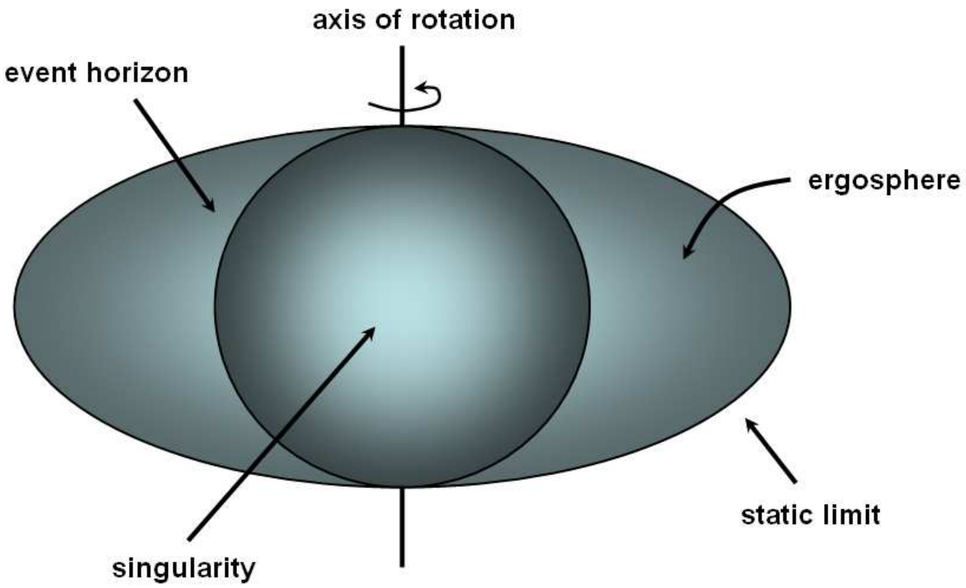

Figure 1.1: The defining features of a black hole: The Singularity, Event Horizon and the Ergoregion

the particle is outside the event horizon it is possible for it to escape the black hole, and in doing so, extract rotational energy from the black hole. This is called the Penrose process. The wave analogue of the Penrose process is otherwise known as superradiance [88, 75, 60] and is related to the Zeldovich-Starobinsky effect which has been considered in superfluid systems by Volovik [85]. More particularly, superradiance refers to the amplification of a wavepacket, of sufficiently low frequency and high angular momentum, scattered from a black hole. The reflected superradiant pulse carries energy away from the black hole and therefore the black hole loses energy. This can only take place if the incident pulse splits into a reflected pulse and a transmitted pulse that propagates into the black hole. That is, one must interpret the incident pulse as an anomalous negative energy mode [30] of the fully quantised field [52]. This will be emplained further in section 6.2.2. An upper bound on the frequency of the incoming wavepacket specifies whether extraction of rotational energy from the black hole by the wavepacket, and hence amplification, will occur. This frequency cut off is given by,

$$\omega < m\Omega \tag{1.2}$$

where ω is the frequency of the wave, m is its angular wave number and Ω is the angular speed of the black hole.

The theory predicting Hawking Radiation, the spontaneous emission of particles from the event horizon, and its stimulated counterpart, superradiance is well developed. However, experimental verification of these weak effects associated with large scale systems is implausible in a laboratory setting. Consequently, one is required to use an indirect path to study such systems. The approach taken, is that of analogue models of general relativity which aim to simulate certain aspects of black hole physics by acting as alternative physical models of gravitational systems. Such analogue gravity models not only mimic certain features of astrophysical systems, but more importantly, they permit investigation of otherwise inaccessible physics as they are amenable to experiment.

In 1981, Unruh [79] presented one such analogy, between curved space-time and superfluid flow. He showed that there exists an equivalence between the equations governing the behaviour of a sound wave propagating in a flowing fluid and a massless scalar field propagating in a (3+1)-dimensional spacetime. This analogy was later extended by Visser [81] who along with other researchers, is responsible for a comprehensive review of the field [83, 4]. Hence, the possibility of being able to mimic some of the properties of black hole physics, and of obtaining experimental evidence for analogue Hawking Radiation and sonic superradiance presents itself through these sonic analogue systems. To illustrate the analogy it is instructive to highlight that in a flowing fluid one can observe the formation of sonic horizons, where the velocity of the fluid flow goes supersonic. Sound propagating from the subsonic to the supersonic flow region cannot escape this region at a later time, as doing so would involve exceeding the speed of sound. In this sense, the boundary between the two regions is analogous to the event horizon of a black hole since only one way wave propagation is permitted. Moreover, using various fluid flow configurations one can construct a sonic black hole. Whilst the thermal spectrum of the emitted particles for a gravitational black hole depends on the surface gravity, in the case of sonic black holes one has a thermal spectrum of phonons with Hawking temperature given by the velocity gradient at the sonic horizon. Specifically,

$$T_H = \frac{\hbar}{2\pi k_B} \frac{d(|\mathbf{v} - c|)}{dx}\Big|_{horizon} \tag{1.3}$$

where x is the perpendicular distance from the sonic horizon, $\mathbf{v}$ is the velocity of the fluid flow, and c is the speed of sound. Despite these remarkable parallels, Unruh also indicated a difficulty in that the temperature of Hawking Radiation in known fluid systems, meeting the necessary criteria, would be too low to allow for experimental verification.

More recently, advances in the development of cooling techniques have resulted in the experimental realisation of Bose-Einstein Condensation. A Bose-Einstein Condensate (BEC), is a gas of indistinguishable bosons for which the single particle ground state is macroscopically occupied [66, 67]. These condensed matter systems are of relevance to the detection of analogue Hawking Radiation as they are fluid systems that possess the properties of an analogue gravity system. Furthermore, the properties of BECs suggest that it may be possible to observe evidence of analogue Hawking Radiation. Most notably, their low temperature, the absence of viscosity and low decoherence makes them ideal candidates in comparison to other fluid systems.

Research into the problem of determining whether superradiance occurs in BECs, and the conditions under which it might be possible, is so far inconclusive. One can study sonic superradiance by scattering sound waves from vortices in BECs and determining whether amplification of incoming wavepackets takes place. Vortices in BECs have been an area of active research and as a result vortex configurations and dynamics have been studied in detail [47, 76]. In 2003, Basak and Majumdar [10, 11] showed that sonic superradiance occurs for a draining vortex. However, a draining vortex configuration is difficult to realise in experiments as it requires an outcoupling mechanism. Hence, Slatyer and Savage [74] considered a non-draining vortex in a BEC which forms the analogue ergoregion and showed that sound waves scattered from this non-draining hydrodynamic vortex may also be amplified. However, they used an approximation known as the the hydrodynamic approximation which is not valid near the BEC vortex core. This provides motivation for further research in this area and for adopting a different approach to this problem.

The objective of this research is to use theoretical models of BECs to determine whether phonon superradiance occurs in BECs, and if so, to characterise it using numerical simulations. The broader aim of this work is to provide a strong theoretical foundation for experimental work with BECs as analogue gravity models, and in turn, to contribute to efforts to detect analogue Hawking Radiation in these systems. Hence, the investigation of superradiant scattering in BECs is the first goal of a larger research program. The study of sonic superradiance, as a precursor to analogue Hawking Radiation, will be undertaken because superradiance is stronger and is a stimulated effect, and consequently should be easier to observe in experiments.

Our specific approach is to conduct numerical simulations of sound waves scattered from a BEC vortex. The simulation package XMDS [25] will be used in order to perform these simulations. The choice of the XMDS package is made due to its ability to solve partial differential equations and the fact that it generates all low-level code making for an efficient programming task. A 2-D simulation of sound waves impinging on a BEC vortex will be undertaken using a mean-field approach, which involves solving the Gross-Pitaevskii (GP) equation numerically. The GP equation, which is a non-linear Schrödinger equation for the condensate wavefunction, describes the evolution of the condensate provided the number of atoms in the BEC is large and the interaction between the atoms is sufficiently weak.

In summary, this research aims to observe and characterise phonon superradiance in BECs using numerical methods, in the context of efforts to detect analogue Hawking Radiation. It has the potential to increase the understanding of black hole physics which is otherwise inaccessible to experiment. Superradiance in BECs is also an interesting problem from the view point of condensed matter physics, but in addition, the analogy relating these two fields could serve to advance both areas by providing novel approaches to existing problems.

Overview of Thesis Chapters

Following this introduction, Chapters 2-5 present a review of the literature and background theory pertinent to this thesis and in doing so establish a framework for further research, and a clear understanding of the research objectives. More particularly, Chapter 1 gives an overview of Hawking Radiation and black hole superradiance and highlights the lack of experimental or observational verification of these effects. This provides the motivation for considering the superfluid analogy in Chapter 2. In Chapter 3, a summary of Bose-Einstein Condensation (BEC) theory relevant to this thesis is given, whilst in chapter 4, BECs are presented as an analogue gravity model. Chapter 5 introduces the methodology used to investigate the problem of whether superradiant scattering from a BEC vortex occurs, by discussing the general principles of numerical modelling, the simulation package used throughout the work and the method of Imaginary Time Propagation (ITP) which is pivotal in obtaining accurate simulations. The results of numerical simulations performed in an attempt to answer this question are analysed in Chapter 6. Finally, in the concluding remarks, recommendations for future research in this area are made.

Chapter 2

Hawking Radiation and Superradiance in Black Holes

The existence of black holes was first proposed in the 1700's by Laplace, a French mathematician, when he realised that given a sufficiently massive object, the escape velocity associated with this object may exceed the speed of light. Since then, the development of general relativity and the study of black holes has led to some of the most exciting predictions of gravitational physics. Most notable is the remarkable prediction of black hole radiance, or Hawking Radiation.

This chapter will provide an overview of this cosmological phenomenon and highlight the lack of experimental evidence for Hawking Radiation as a motivation for using analogue gravity models. Superradiance, another black hole effect predicted by general relativity, will also be introduced and its significance in acting as a stepping stone to detecting analogue Hawking Radiation will be discussed.

2.1 The prediction of Hawking Radiation

Predicted by Hawking in 1974, Hawking Radiation is the spontaneous emission of thermal radiation at the event horizon of a rotating, or non-rotating, black hole. Hawking proposed that quantum gravitational effects, although negligible locally, are significant due to cumulative effects over the lifetime of the universe [41, 42]. Taking quantum physics into account, using methods developed by Parker [64], Hawking demonstrated that a black hole can radiate like a black body at a temperature T, the Hawking temperature, which is proportional to the surface gravity of the black hole (the gradient of the gravitational potential). That is, Hawking showed that particles such as neutrinos and photons could be created and emitted from black holes. Since such a black hole is radiating energy, there is a corresponding decrease in the mass of the black hole and a subsequent increase in the surface gravity. Thus, the emission rate increases and the black hole has a finite lifetime.

The original derivation predicting the existence of Hawking Radiation [41], takes the case of a massless scalar field $\hat{\phi}$, propagating in an asymptotically flat space time where a black hole is present, which satisfies the Klein-Gordon equation. In order to incorporate antiparticles, one also considers complex fields. One can express the field operator $\hat{\phi}$ as,

$$\hat{\phi} = \sum_i \left(f_i \hat{a}_i + f_i^* \hat{a}_i^\dagger \right) \tag{2.1}$$

where f_i represents a complete orthonormal set of complex valued, asymptotically ingoing, positive frequency solutions of the wave equation, and $\hat{a}_i$ and $\hat{a}_i^\dagger$ are annihilation and creation operators for incoming scalar particles. Alternatively, the operator $\hat{\phi}$ can be written as,

$$\hat{\phi} = \sum_i \left(p_i \hat{b}_i + p_i^* \hat{b}_i^\dagger + q_i \hat{c}_i + q_i^* \hat{c}_i^\dagger \right) \tag{2.2}$$

where p_i are solutions of the wave equation which are asymptotically outgoing, positive frequency waves and zero at the event horizon, and q_i are solutions of the wave equation which possess no outgoing component. Furthermore, p_i and q_i can be expressed as linear combinations of f_i and f_i^*. More particularly, the Bogoliubov transformations of equations 2.3 to 2.5, form the relationship between p_i, q_i and f_i,

$$p_i = \sum_j (\alpha_{ij} f_j + \beta_{ij} f_j^*) \tag{2.3}$$

$$q_i = \sum_j (\gamma_{ij} f_j + \eta_{ij} f_j^*) \tag{2.4}$$

$$f_j = \sum_i (\alpha_{ij}^* p_i - \beta_{ij} p_i^* + \gamma_{ij}^* q_i - \eta_{ij} q_i^*) \tag{2.5}$$

where α_{ij}, β_{ij}, γ_{ij}, and η_{ij} are the Bogoliubov coefficients. Hence, there are two expressions for the quantised field $\hat{\phi}$, equations 2.1 and 2.2. On equating these expressions, it becomes clear that one can express the outgoing annihilation operator $\hat{b}_i$ as a linear combination of the ingoing annihilation and creation operators, $\hat{a}_i$ and $\hat{a}_i^\dagger$, respectively. Explicitly, one obtains,

$$\hat{b}_i = \sum_i (\alpha_{ij}^* \hat{a}_j - \beta_{ij}^* \hat{a}_j^\dagger) \tag{2.6}$$

Thus, for the case when there are no incoming scalar particles the initial vacuum can be defined as the state anhillated by the operators $\hat{a}_i$, specifically,

$$\hat{a}_i \left| 0 \right\rangle = 0 \ \ \forall i \tag{2.7}$$

and one finds that the expectation value of the ith outgoing state is given by,

$$\left\langle 0 \left| \hat{b}_i^\dagger \hat{b}_i \right| 0. \right\rangle = \sum_j \left| \beta_{ij} \right|^2 \tag{2.8}$$

From this result, it is apparent that given no incoming particles, the number of particles created and emitted due to the formation of a black hole can be deduced from the coefficients β_{ij}. That is, particle creation will take place whenever the Bogoliubov coefficients β_{ij} are non-zero. If one then considers the formation of a black hole, produced by a spherically symmetric gravitational collapse, one can express the outgoing solutions to the wave equation, p_ω, as an integral over incoming single frequency modes $f_{\omega'}$,

$$p_\omega = \int (\alpha_{\omega\omega'} f_{\omega'} + \beta_{\omega\omega'} f^*_{\omega'}) d\omega' \tag{2.9}$$

and in turn one arrives at the result,

$$|\alpha_{\omega\omega'}|^2 = e^{2\pi\omega/\kappa} |\beta_{\omega\omega'}|^2 \tag{2.10}$$

which relates the Bogoliubov coefficients, $\alpha_{\omega\omega'}$ and $\beta_{\omega\omega'}$. When considered along with equation 2.8, it can be shown that equation 2.10 satisfies the condition for emission of a blackbody spectrum, with temperature $T = \kappa/2\pi$ where κ is the surface gravity of the black hole.

In deriving Hawking Radiation, the assumption that the gravitational field is not affected by quantum fields is made. In other words, the derivation ignores the back reaction of Hawking Radiation on the background geometry. Furthermore, it is assumed that the gravitational field is unquantised and that the wave equation for the quantum field is valid on all scales [79]. In regards to the latter, Hawking's derivation relies on high wavenumber modes and yet the dispersive nature of the wave equation for these modes is neglected, despite the fact that it is the behaviour in this high frequency regime on which the derivations hinge [20].

In 2000, a derivation of Hawking Radiation was given by Parikh and Wilczek [63] in order to incorporate back reaction on the previously fixed background in earlier derivations [38, 77, 33]. Their derivation, which enforced energy conservation, resulted in corrections to the thermal emission rate derived by Hawking. The derivation by Parikh and Wilczek is also interesting in the fact that it considers Hawking Radiation as a tunnelling process, which is the heuristic picture most often used when describing Hawking Radiation.

It should be noted that although Hawking's original derivation only considered the case of a massless scalar field and a collapse which is spherically symmetric, it is only an analytical simplification and the derivation can be carried out for electromagnetic fields, charged black holes and cases that do not possess a spherical symmetry [41, 42].

Despite the well developed theory of Hawking Radiation, no experimental evidence has as yet been produced to verify its existence. This lack of evidence is due to the fact that the Hawking temperature is low compared to the microwave background radiation and hence hard to detect. For example, for black holes of greater than or equal to one solar mass, the Hawking temperature is of the order 10^{-7} K or less [10].

Consequently, observing Hawking Radiation using current astronomy techniques, and technology, is impractical.

2.2 Motivation for Studying Analogue Gravity Models and Superradiance

In response to the lack of experimental evidence for cosmological phenomena associated with black holes, analogue gravity models have been explored as a possible avenue to verifying analogue Hawking Radiation. Analogue gravity models are physical systems that allow one to simulate certain aspects of general relativity [83]. The main significance of studying these alternative physical systems, is that they enable investigation of certain theoretical arguments of general relativity in the laboratory. Thus, they provide the opportunity to investigate quantum field theory in curved spacetime, and in turn, may permit observation of Hawking Radiation. Such models are also interesting because they link many branches of physics including gravitation, condensed matter, acoustics, electrodynamics, optics and quantum field theory. A summary of the different physical systems used as analogue gravity models is given by Barcelo et al. [3]. The sheer volume of publications relating to analogue gravity techniques in a range of seemingly dissimilar physical systems suggests the power and potential of analogue models, providing further motivation for studying analogue gravity models. In response to this, and as a precursor to experiments, a numerical study of a condensed matter analogue gravity system, Bose-Einstein Condensates, will be the approach taken in this thesis in order to build a foundation for the study of Hawking Radiation in the lab. Specifically, superradiance in BECs, an analogue black hole effect, will be of primary interest and will be considered in advance of analogue Hawking Radiation in BECs, as it may be easier to detect. Hence, in the following section an overview of black hole superradiance provides a basis for future discussion of superradiance in BECs.

At this point, it should be emphasised, that whilst BECs as an analogue gravity model are valuable in the study of otherwise inaccessible astrophysical structures, they are also worthy of investigation from a condensed matter point of view. That is, phonon scattering from a BEC and its characterisation, which forms the focus of this thesis, deserves study regardless of its connection to astrophysical phenomenon. That said, however, by studying this problem from both viewpoints, the possibility of progress and the value to the scientific community is increased. This is because this interdisciplinary research area will allow for a cross-fertilisation of ideas and this may lead to advances in both fields.

2.3 Superradiance

The investigation of superradiance in an analogue gravity system is the main objective of this research and hence an overview of the discovery and principles of superradiance, in the context of black hole physics, is valuable for obtaining a better understanding of the phenomenon in BECs.

2.3.1 Classifications of Superradiance

Superradiance is the collective term used to describe a phenomenon that is common to a variety of physical systems, from familar objects such as dielectric cylinders to the more exotic black holes. It was Dicke [24], in 1954, who coined the term superradiance. This, however, was in reference to the amplification of radiation arising from coherence in a medium emitting radiation. Outside the realm of atomic physics, there are two types of superradiance, namely inertial motion superradiance and rotational superradiance. Discovered experimentally by Vavilov and Cherenkov [80, 18] in 1934, inertial motion superradiance was the first of the two effects to be identified. Ginzburg and Frank [36, 35] characterised the effect as the emission of radiation when an inertially and superluminally moving system is excited on its transit through a medium. More particularly, when the modulus of the velocity $|\mathbf{v}|$ of the particle is greater than the phase velocity of electromagnetic waves in the medium, the frequency ω and the wave number $\mathbf{k}$ of the emitted photons satisfy the condition,

$$\omega - \mathbf{k}.\mathbf{v} < 0 \tag{2.11}$$

This bound on the frequency of the wave is known as the Ginzburg-Frank condition and the emission is referred to as spontaneous superradiance. A well known example of inertial motion superradiance is the Cherenkov effect [50], where a point charge such as an electron, moving superluminally through a dielectric medium will emit radiation at frequencies for which superluminal motion is achieved. Based on an argument presented by Einstein in 1916, it is accepted that spontaneous emission in quantum systems occurs if and only if stimulated emission, in the system having these spontaneously emitted particles initially present, is possible [86]. As a result, Ginzburg-Frank spontaneous superradiance implies the amplification of already existent radiation by an object moving superluminally in a medium, that is, superradiant amplification.

The second classification of superradiance, the amplification of radiation by a rotating absorbing object, was discovered some decades after inertial motion superradiance [88]. It is this form of superradiance with which this thesis is concerned and consequently a more detailed coverage of this phenomenon follows.

2.3.2 Development of the Theory of Rotational Superradiance

It was not until 1971, with the contribution of Zel'Dovich [88], that the notion of rotational superradiance came under consideration. He was the first to realise that a cylinder composed of an absorbing material and made to rotate about its axis with a frequency Ω can cause amplification of incoming radiation. That is, an incident scalar wave of frequency ω will be amplified on scattering provided the condition,

$$\omega < m\Omega \tag{2.12}$$

holds true, where m is the azimuthal quantum number of the incoming wave with respect to the axis of rotation. From this, and the discussion of inertial motion superradiance, it can be seen that equation 2.12 is a general form of the condition for superradiance. Moreover, there are a numerous examples of superradiant emission, some of which are reviewed in a comprehensive analysis of superradiance by Bekenstein and Schiffer [13], but they are analogous in the fact that superradiance will only occur if the generic constraint of the form of equations 2.11 and 2.12 is satisfied.

In his original derivation relating to the generation of waves by a rotating body, Zel'Dovich considered the case of an electromagnetic field incident on an ohmic cylinder rotating with angular velocity Ω [88], and he later addressed the case of a scalar field [89]. He proposed that superradiance is a generic effect common to rotating objects, regardless of the form of the incident wave. In addition, he recognised the possibility of this phenomenon occurring in black hole physics, in the Kerr (rotating) black hole, when the incoming modes satisfy equation 2.12. Besides Zel'Dovich's work, it should be noted that superradiant scattering from a rotating black hole was, independently predicted by Misner [60], in 1972. For this reason equation 2.12 is often referred to as the Zel'Dovich-Misner condition for rotational superradiance.

Black hole superradiance is essentially the wave version of the particle Penrose effect [65], proposed by Penrose in 1969. More specifically, Starobinski [75] showed that the rotational kinetic energy accumulated in a black hole can be extracted from it by low frequency, high angular momentum waves scattered from the ergosphere which satisfy the condition,

$$0 < \omega < m\Omega_H \tag{2.13}$$

where ω is the frequency of the wave, m is the azimuthal quantum number of the wave and Ω_H is the angular velocity of the black hole. Hence, if energy is extracted from the black hole, the amplitude of the scattered wave will exceed the amplitude of the incoming wave. For a wave incident on the black hole, a portion of the incoming wave will be absorbed and a portion will be reflected. The reflection coefficient can be calculated and if $|R(\omega)|^2 > 1$, where $R(\omega)$ is the complex valued reflection coefficient, then superradiant scattering has occurred. This process of superradiant scattering from a black hole, as Wald [86] points out, is analogous to stimulated emission in atomic physics when one considers the Kerr black hole as an excited state of a Schwarzschild (non-rotating) black hole.

Most derivations of superradiance are based on the consideration of the appropriate wave equations in the Kerr Background [60]. Bekenstein [12], however, provides a unique derivation of superradiance based on Hawking's black hole area theorem [39] - the surface area of a black hole is non-decreasing in time. It is illustrative to provide a derivation of superradiance in black holes and therefore an overview of Bekenstein's derivation follows. We take $G = c = 1$ and consider a chargeless Kerr black hole of mass M and angular momentum $\mathbf{J}$. The horizon area of such a black hole, A, is given by,

$$A = 4\pi\left[\left(M + \sqrt{M^2 - (\mathbf{J}/M)^2}\right)^2 + (\mathbf{J}/M)^2\right] \tag{2.14}$$

Differentiating 2.14, the expression for small changes in the horizon area is found to be,

$$dA = 2A(M^2 - (\mathbf{J}/M)^2)^{-1/2}.(dM - \mathbf{\Omega}.\mathbf{dJ}) \tag{2.15}$$

where,

$$\mathbf{\Omega} = \frac{\mathbf{J}/M}{r_H^2 + (\mathbf{J}/M)^2} \tag{2.16}$$

and r_H is the radius at the horizon. In accordance with Hawking's area theorem $dA > 0$, it follows from equation 2.15 that,

$$dM > \mathbf{\Omega}.d\mathbf{J} \tag{2.17}$$

We now take the case of a scalar wave scattered from such a Kerr black hole. The scalar wave mode can be expressed in the form,

$$\psi(r, \theta, \phi, t) = f(r, \theta)e^{im\phi}e^{-i\omega t} \tag{2.18}$$

to indicate its time t and azimuthal angle ϕ dependence, where ω is the frequency of the wave and m is the azimuthal quantum number. To make use of equation 2.17 it is necessary to find a relationship between the energy and angular momentum of the incoming waves. By considering the stress-energy tensor and equation 2.18 it can be shown [12] that the angular momentum and the energy of the waves is in the ratio m/ω, where ω is the frequency and m is the azimuthal quantum number, as before. When the incident scalar wave is scattered from the black hole it prompts changes of dM and $d\mathbf{J}$ in the original black hole M and $\mathbf{J}$. Thus, by the conservation of energy and momentum and the fact that $|d\mathbf{J}/dM| \propto m/\omega$ one obtains,

$$\mathbf{\Omega}.d\mathbf{J} = \Omega dM\frac{m}{\omega} \tag{2.19}$$

Using this result and the condition given in equation 2.17, it follows that,

$$dM(1 - m\Omega/\omega) > 0 \tag{2.20}$$

From this expression, it is clear that if the Zel'Dovich-Misner condition $\omega < m\Omega$ holds, then $dM < 0$. That is, the mass of the black hole is decreased after scattering takes place. From this one can conclude that the energy of the scattered wave exceeds the energy of the incoming wave, and therefore the scattered wave will be amplified.

One notable feature of black hole superradiance is the fact that it occurs in the case of classical scalar field waves propagating in a curved spacetime. Consequently, one is not required to use a quantum physics framework to demonstrate superradiance, despite the fact that this is possible [23], and this versatility acts as an advantage when studying the effect. However, it is interesting to note that when treated in the quantum mechanical regime, superradiance can be thought of as the stimulated emission of radiation, the stimulated counterpart of Hawking Radiation which is the spontaneous emission of radiation from a black hole.

Chapter 3

The Analogy between Curved Spacetime and Superfluid Flow

It is now well established that most dynamical systems have an associated Lorentzian-signature "effective metric" allowing one to model some properties of curved space-time [3]. That is, if one linearises a classical scalar field theory around a suitable background geometry this will give rise to an effective Lorentzian geometry, and the fluctuations, propagating in this geometry, will be governed by the effective metric.

Despite the fact that there are a range of choices for analogue gravity systems [71, 83], it is acoustic geometries that are most relevant to the case of analogue black holes, due to restrictions placed on the system resulting from the need to construct event horizons and ergoregions [10]. As a consequence of this the superfluid analogy is central to this thesis, in that it underpins the use of BECs as an analogue model of gravity, and ultimately allows us to explore phonon superradiance in BECs. Hence, this chapter will serve to illustrate the analogy between superfluid flow and curved-spacetime, so as to provide a deeper insight into the analogy.

3.1 Unruh's Analogy

In 1981, Unruh [79] presented a fascinating analogy between superfluid flow and the propagation of a massless scalar field in a Lorentzian spacetime, and the analogy was later revised by Visser [83, 81]. More precisely, under certain conditions, there exists an equivalence between the equation of motion that governs the propagation of a massless minimally coupled scalar field in a (3+1)-dimensional spacetime and the equation of motion for the velocity potential describing a sound wave in barotropic, inviscid, irrotational fluids. As will be seen in section 3.2, provided that such a fluid is described by the continuity equation, the zero-viscosity Euler equation and an equation of state, then the Klein-Gordon equation [32, 53, 59, 40],

$$\frac{1}{\sqrt{-g}}\partial_\mu(\sqrt{-g}g^{\mu\nu}\partial_\nu\psi) = 0 \tag{3.1}$$

which governs the propagation of fields in relativity will also govern the propagation of fields in the hydrodynamic case. It will also become clear that the spacetime metric $g_{\mu\nu}$ is replaced by an effective metric $\widetilde{g}_{\mu\nu}$ which governs the propagation of sound in the fluid and that this acoustic metric can be written in terms of the density, the velocity of fluid flow and the speed of sound in the fluid. In other words, the ability to mimic some aspects of black hole physics in the laboratory, using various fluid flow configurations, arises due to the possibility of generating these effective metrics.

3.2 The Klein-Gordon Equation

The derivation of the superfluid analogy is not only a beautiful piece of physics but also highlights the assumptions underlying the derivation of the acoustic metric $\widetilde{g}_{\mu\nu}$.The derivation uses the equations of fluid dynamics to identify the effective metric [81, 83].

As well known in fluid dynamics [48, 49, 58], the behaviour of a fluid is described by the continuity equation,

$$\frac{\partial \rho}{\partial t} + \nabla \cdot (\rho \mathbf{v}) = 0 \tag{3.2}$$

and the Euler equation,

$$\rho\Big(\frac{\partial \mathbf{v}}{\partial t} + (\mathbf{v}.\nabla)\mathbf{v}\Big) = \mathbf{F} \tag{3.3}$$

where $\mathbf{v}$ is the velocity of the fluid flow, ρ is the density and $\mathbf{F}$ represents all the forces acting on the fluid. We begin by assuming the fluid is inviscid (zero viscosity). Hence, the only forces acting on the fluid are those due to pressure, gravity and any external forces. It is further assumed that external forces, if present, are gradient-derived and consequently one can ignore the viscosity terms in the Navier-Stokes equation [17]. Explicitly,

$$\mathbf{F} = -\nabla p - \rho\nabla\phi - \rho\nabla\Psi \tag{3.4}$$

where p is the pressure, ϕ is the gravitational potential and Ψ is the external force potential.

It is also assumed that the field is locally irrotational, that is,

$$\nabla \times \mathbf{v} = 0 \tag{3.5}$$

which implies that the velocity can be expressed as the gradient of a scalar field, $\mathbf{v} = -\nabla\psi$. This will become useful in the fact that sound waves, which are linearised fluctuations in the velocity field, are also able to be described by a scalar field. Finally, we assume that the fluid is barotropic, meaning that the density is a function of pressure only, and this allows one to define the specific enthalpy,

$$H(\rho) = \int_0^p \frac{dp'}{\rho(p')} \tag{3.6}$$

or equivalently, in differential form,

$$\nabla H(\rho) = \frac{\nabla p}{\rho}. \tag{3.7}$$

Using standard vector identities, Euler's equation can now be recast in the more convenient form,

$$-\frac{\partial \psi}{\partial t} + H(p) + \frac{1}{2}(\nabla\psi)^2 + \phi + \Psi. \tag{3.8}$$

Now, to consider sound waves, one uses the well known method of linearising the equations of fluid dynamics around some background fluid flow, which is represented by some arbitrary but exact solution $[\rho_o(t,x), p_o(t,x), \psi_o(t,x)]$ to equations 3.2 and 3.3. That is, one writes the exact fluid variables $[\rho, p, \psi]$ as a combination of the background variables and the low amplitude acoustic disturbances $[\rho', p', \psi']$, obtaining,

$$\rho(t,x) = \rho_o(t,x) + \epsilon\rho'(t,x) + \dots \tag{3.9}$$

$$p(t,x) = p_o(t,x) + \epsilon p'(t,x) + \dots \tag{3.10}$$

$$\psi(t,x) = \psi_o(t,x) + \epsilon\psi'(t,x) + \dots \tag{3.11}$$

Applying this, and neglecting terms of $O(\epsilon^2)$ or higher, the linearised version of equations 3.2 and 3.3, can be written as,

$$\frac{\partial \rho'}{\partial t} + \nabla.(\rho'\mathbf{v}_o + \rho_o\mathbf{v}') = 0 \tag{3.12}$$

$$\rho' = \frac{\partial \rho}{\partial p}\rho_o\Big(\frac{\partial \psi'}{\partial t} + \mathbf{v}_o.\nabla\psi'\Big) \tag{3.13}$$

where in the linearised Euler equation, equation 3.13, one makes use of the linearised version of the enthalphy $H(p_o + \epsilon p') = H(p_o) + \epsilon(p'/\rho_o)$ and the fact that $\rho' = \frac{\partial\rho}{\partial p}p'$, which is a consequence of the barotropic nature of the fluid. Now, substituting the linearised continuity equation of equation 3.12 into the linearised Euler equation, yields,

$$-\partial_t\Big(\frac{\partial \rho}{\partial p}\rho_o(\partial_t\psi' + \mathbf{v}_o.\nabla\psi')\Big) + \nabla.\Big(\rho_o\nabla\psi' - \frac{\partial \rho}{\partial p}\rho_o\mathbf{v}_o(\partial_t\psi' + \mathbf{v}_o.\nabla\psi')\Big) = 0. \tag{3.14}$$

This result is in the form of a wave equation describing the propagation of the linearised scalar potential ψ', that is, sound waves propagating in the fluid. For convenience one can define the local speed of sound [49],

$$c_s = \sqrt{\frac{\partial\rho}{\partial p}} \tag{3.15}$$

and by specifying a 4 × 4 matrix,

$$\widetilde{g}^{\mu\nu} \equiv \frac{1}{\rho_o c} \begin{bmatrix} -1 & \vdots & -v_o^j \\ \cdots & \cdots & \cdots \\ -v_o^i & \vdots & (c^2\delta_{ij} - v_o^i v_o^j) \end{bmatrix} \tag{3.16}$$

and introducing the four-dimensional coordinates,

$$x^\mu = (t, x^1, x^2, x^3) \tag{3.17}$$

one obtains,

$$\frac{1}{\sqrt{-g}}\partial_\mu(\sqrt{-g}\widetilde{g}^{\mu\nu}\partial_\nu\psi') = 0 \tag{3.18}$$

which is the familiar curved space Klein-Gordon equation [81], with $g = [\det(\widetilde{g}^{\mu\nu})]^{-1}$. From this result, it can be seen that the equation of motion describing the propagation of acoustic disturbances can be written in a (3+1)-dimensional form, with the propagation the acoustic disturbances governed by the acoustic metric $\widetilde{g}_{\mu\nu}$.

3.3 The Effective Metric

The effective metric describing a Lorentzian geometry can be found by inverting the matrix given in equation 3.16 [81]. More particularly, the acoustic metric is given by,

$$\widetilde{g}_{\mu\nu} \equiv \frac{\rho_o}{c} \begin{bmatrix} -(c^2 - v_o^2) & \vdots & -v_o^j \\ \cdots & \cdots & \cdots \\ -v_o^i & \vdots & \delta_{ij} \end{bmatrix} \tag{3.19}$$

and from this it is clear that the signature of the metric (-,+,+,+) is Lorentzian. The form of the metric also highlights its dependence on the density, flow velocity and the local speed of sound. Thus, if one alters the background fluid flow this will change the acoustic metric. Another important feature of the metric is that it indicates the existence of an acoustic horizon, an analogue of a black hole event horizon, when $v_o = c$. Then, the possibility of observing analogue Hawking Radiation and sonic superradiance arises. In summary, we have observed that acoustic propagation in fluids provides an example of Lorentzian geometry, despite the dynamics of fluid flow being derived in a flat spacetime. Overall, it has been seen that the two interpretations of the Klein-Gordon equation allow one to use certain fluid flow configurations which act as effective metrics analogous to those of general relativity. In principle, by studying sound waves in fluids, this enables one to investigate the behaviour of quantum and classical fields in various metrics.

3.4 Limitations of the Analogy

The propagation of sound in a moving fluid, as an analogue model of gravity, provides a powerful avenue for probing black hole physics in the laboratory. It is important to stress, however, that this analogy is not perfect, with the acoustic metric only allowing one to mimic the kinematic aspects of general relativity, and not the dynamics [83]. Specifically, it was seen in section 3.3 that the acoustic metric depends on the engineered velocity of flow, density, and the local speed of sound, and it is this feature that sets the acoustic Lorentzian geometry and the spacetime of general relativity apart.

The acoustic metric, constrained by the choice of fluid velocity and density profiles, is governed by equations of fluid dynamics which control the background geometry, but it is Einstein's equations that describe the dynamics in the case of general relativity [70]. Furthermore, no particular choice of fluid parameter profiles will enable one to generate effective metrics yielding dynamics identical to the dynamics of general relativity. Hence, it should not be expected that all features of general relativity will be observed in the condensed matter setting, and essentially the aim becomes that of getting a similar rather than identical metric. For example, there may be no analogue for black hole entropy [82] as it is a purely dynamical effect. It is possible, however, that some aspects of the dynamics of general relativity may be contained in these analogue models when quantum effects are taken into account. This is at present an unresolved question with efforts being made by researchers, including Barceló et al. [3].

Regardless of the inability to model the dynamics of general relativity, the superfluid analogue is still worthy of investigation because it allows one to explore kinematic features of general relativity, such as Hawking Radiation and superradiance. For instance, in the case of Hawking Radiation it is a generic kinematic effect occurring in the presence of an event horizon, and consequently, it is amenable to investigation in the context of an analogue gravity model. Furthermore, since this is currently the only approach available for studying such unexplored effects, its potential benefit to the field, outways the flaws arising due to constraints on the validity of the model.

Other limitations of the model come from the fact that the wave equation given in equation 3.14 is derived under the assumption that the fluid flow is irrotational and barotropic, with the condition of a nonviscous fluid being included as an analytic simplification [81]. Failure to establish and maintain such conditions will lead to a breakdown in the analogy [83]. For example, without irrotationality being satisfied, one is unable to specify the velocity potential which acts as the analogue scalar field. In regard to the need to satisfy the equations of fluid dynamics, and specifically the zero-viscosity Euler equation, it is important to realise that some fluid systems only approximately obey it. This is the case for BECs, which are of significance in this thesis, and hence a consideration of the parameters for which the zero-viscosity Euler equation holds, is necessary. It should also be noted that inherent in the derivation, is the assumption that the fluctuations in the field are small, and this limits the validity of the model to the case of small amplitude oscillations.

Another constraint, is that it has been assumed that the density and velocity can be described as continuous classical fields. However, in doing so one necessitates that the length scales in the model are sufficiently long so microscopic effects in the fluid can be neglected. Thus, effects occurring at small length scales are not incorporated into the analogue model. Consequently, the ability to directly probe the microscopic structure of astrophysical systems, an area yet to be understood, is unfortunately not possible using the analogue model. That being said, efforts have been made into studying the dependence of large scale effects on small scale effects in acoustic analogue systems [20, 78, 45, 62] because the microscopic theory of fluids is well understood, and as a result, could provide guidance in understanding the astrophysical case.

Chapter 4

Bose-Einstein Condensation Theory

Prior to considering BECs as an analogue gravity system, it is necessary to introduce Bose-Einstein Condensation and provide an outline of the BEC theory relevant to this thesis.

As shown by Visser [83], it is possible to perform the derivation of the effective metric, given in chapter 3 for a general superfluid, for the case of a BEC system. The fluid equations obtained by such a process, contain an extra higher order derivative term, known as the quantum pressure term, which is proportional to the characteristic length in the condensate. Most work involving BEC analogue gravity models neglects this term using what has become known as the hydrodynamic approximation. The validity of such an approximation, particularly when considering superradiance in BECs, is an issue of concern. However, it should be emphasised that the effective metric derivation in the BEC case can be obtained using either equations which make use of the hydrodynamic approximation, or equations that retain the quantum pressure term where the effective metric is made up of differential operators instead of functions [83].

With the knowledge that the superfluid analogy presented in chapter 3 has been shown to hold in BECs [83], regardless of whether the hydrodynamic approximation is used, the choice of equations used to consider BECs is required. For the purposes of this thesis, it is not the form of the equations reflecting general relativity and used in the derivation by Visser [83] that are utilised. Instead, it is the equations of motion for a perturbation in the BEC that are of most relevance when considering sound waves scattering from a BEC vortex, as is central to this thesis. For the remainder of this thesis we emphasise the scattering of sound by a vortex in a BEC, rather than the general relativity analogy.

Overall, this chapter will establish the theoretical foundation for numerical work by introducing the Gross-Pitaevskii (GP) equation, the hydrodynamic approximation, elementary excitations and the occurrence of vortices in BECs. In particular, this account will provide a framework for the work presented in chapter 7, in which a numerical analysis using the GP equation, and hence retaining the quantum pressure term, is conducted in an attempt observe superradiance in BECs, without the use of the hydrodynamic approximation successfully used by Slatyer and Savage [74] to provide evidence of superradiance in BECs.

4.1 Bose-Einstein Condensation

A Bose-Einstein Condensate (BEC) is a gas comprised of a large number of indistinguishable bosons, particles of integer spin, which have been cooled below a critical transition temperature T_c, such that the macroscopic occupation of the single-particle ground state occurs. In 1995 landmark experiments involving dilute atomic gases [1, 16, 22] provided detailed quantitative verification of Bose-Einstein Condensation, predicted seventy years earlier by Bose [15] and Einstein [26]. These experimental milestones generated intense interest in BECs, as reviewed in [66], as they allowed quantum-mechanical behaviour to be observed in the laboratory on a macroscopic scale.

The experimental realisation of BEC was made challenging by the need to develop methods of confining and cooling dilute gases to the nanokelvin temperatures required for condensation to occur [56]. It is ultra-cold and dilute gases of alkali atoms such as Rubidium [1], Lithium [16] and Sodium [22] that have been successful in BEC experiments. For such atoms the atomic interactions can be approximated by an effective contact potential and this permits the mean-field description of the condensate as will be explained in the following section [66]. As an aside, Bose-Einstein Condensation was first shown to be possible in superfluid Helium [85] but in such systems the atomic interaction is too strong for the mean-field description to utilised.

4.2 The Gross-Pitaevskii Equation

From an experimental perspective, the study of BECs has been promising because of the techniques developed to accurately control BECs. In addition, an understanding of BECs has also been obtained from a theoretical basis, with the dynamics of the condensate, at the mean field level, being well described by the Gross-Pitaevskii (GP) equation [21]. The GP equation is a nonlinear Schrödinger equation which approximates the quantum many-body interaction with a classical, nonlinear interaction [66]. The following derivation of the GP equation provides a deeper insight into the GP equation which is central to this thesis.

4.2.1 Derivation of the Gross-Pitaevskii Equation

In the framework of second quantisation, the quantum state for a BEC of interacting particles, can be determined from the many-body Hamiltonian,

$$\hat{H} = \int d\mathbf{r}\hat{\psi}^{\dagger}(\mathbf{r})\hat{H}_o\hat{\psi}(\mathbf{r}) + \frac{1}{2}\int\int d\mathbf{r}'d\mathbf{r}\hat{\psi}^{\dagger}(\mathbf{r})\hat{\psi}^{\dagger}(\mathbf{r}')V(\mathbf{r}-\mathbf{r}')\hat{\psi}(\mathbf{r}',t)\hat{\psi}(\mathbf{r},t) \tag{4.1}$$

where $\hat{\psi}^{\dagger}(\mathbf{r})$ and $\hat{\psi}(\mathbf{r})$ are the field operators for atoms, which create and annihilate a particle at the point $\mathbf{r}$, respectively, and obey the usual commutation relations for bosons,

$$[\hat{\psi}(\mathbf{r}), \hat{\psi}^{\dagger}(\mathbf{r}')] = \delta(\mathbf{r}-\mathbf{r}'), \quad [\hat{\psi}(\mathbf{r}), \hat{\psi}(\mathbf{r}')] = 0. \tag{4.2}$$

The potential term $V(\mathbf{r}-\mathbf{r}')$ is the particle-particle interaction and $\hat{H}_o$ is the single-particle Hamiltonian which may contain an external trapping potential,

$$\hat{H}_o = -\frac{\hbar^2\nabla^2}{2m} + V_{trap}. \tag{4.3}$$

The dynamics of the quantum field is described by the Heisenberg equation of motion for the field operator,

$$i\hbar\partial_t\hat{\psi}(\mathbf{r},t) = [\hat{\psi}(\mathbf{r},t), \hat{H}] \tag{4.4}$$

or more particularly, using the form of $\hat{H}$ given by equation 4.1,

$$i\hbar\partial_t\hat{\psi}(\mathbf{r},t) = \Big(\hat{H}_o + \int d\mathbf{r}'\hat{\psi}^{\dagger}(\mathbf{r}')V(\mathbf{r},\mathbf{r}')\hat{\psi}(\mathbf{r}',t)\Big)\hat{\psi}(\mathbf{r},t). \tag{4.5}$$

However, when the number of atoms in the condensate is large this treatment becomes impractical. When there is a small fraction of non-condensed particles in the condensate, that is, the depletion of the condensate is small, the Bogoliubov decomposition [14] becomes useful. This occurs when the particle-particle interaction is sufficiently weak or for, sufficiently dilute gases, regardless of the strength of the interaction [67]. This mean-field approach involves writing the Bosonic field operator in two parts, namely the classical condensate wavefunction and the excitations. That is, one can write,

$$\hat{\psi} = \psi + \hat{\delta\psi} \tag{4.6}$$

where $\psi =< \hat{\psi} >$ is complex and is the expectation value of the field operator. Whilst, $\hat{\delta\psi}$ is the field operator representing the small contributions due to the non-condensed fraction of the condensate. Hence, to lowest order one can replace $\hat{\psi}$ in the many-body Heisenberg equation with the condensate wavefunction ψ, in the limit of zero temperature, yielding,

$$i\hbar\frac{\partial}{\partial t}\psi(\mathbf{r},t) = [\psi(\mathbf{r},t), \hat{H}]. \tag{4.7}$$

We also assume that the interatomic interaction $V(\mathbf{r}-\mathbf{r}')$ is short range, which is true in alkali atom BECs as these are dilute and ultra-cold ensembles of atoms where only binary collisions at low energy are significant. Thus, we can approximate the interaction as a product of a short-distance delta-function term and a coupling constant, U_o describing the binary collisions and unique to the atomic species used as it depends on the s-wave scattering length a and the atomic mass of the atoms in the condensate m. Explicitly, this effective interaction is given by,

$$V(\mathbf{r},\mathbf{r}') = U_o\delta(\mathbf{r}-\mathbf{r}') \tag{4.8}$$

where U_o is the coupling constant which characterises the strength of the repulsive interactions between the bosons, given by,

$$U_o = \frac{4\pi\hbar^2 a}{m}. \tag{4.9}$$

It follows, by substituting the effective contact potential of equation 4.8 into equation 4.7, that the time evolution of a dilute BEC at zero degrees Kelvin when the number of atoms in the condensate is large and the interaction between the atoms is sufficiently small is given by the Gross-Pitaevskii (GP) equation,

$$i\hbar\frac{\partial\psi(\mathbf{r},t)}{\partial t} = \Big(-\frac{\hbar^2\nabla^2}{2m} + V_{trap} + U_o\,|\psi(\mathbf{r},t)|^2\Big)\psi(\mathbf{r},t) \tag{4.10}$$

where $\psi(\mathbf{r},t)$ is the mean-field condensate wavefunction, ∇ is the Laplacian, V_{trap} is the potential which confines the atoms in the trap, and $\rho = |\psi(\mathbf{r},t)|^2$ is the particle density of condensate. The wavefunction is normalised to the total number of atoms $N = \int d^3\mathbf{r}\,|\psi(\mathbf{r},t)|^2$. The external potential, V_{trap}, can take various forms but is typically of harmonic form [66],

$$V_{trap} = \frac{1}{2}m(\omega_x^2x^2 + \omega_y^2y^2 + \omega_z^2z^2). \tag{4.11}$$

where $\omega_{x,y\,,z}$ are the trap frequencies and, in general, $\omega_x \neq \omega_y \neq \omega_z$.

The GP equation is in the form of a non-linear Schrödinger equation with the two-body interaction term accounting for the non-linearity in the problem. One can tune the trapping potential, the particle density and the strength of the interactions to suit ones purposes in an experimental situation. It should be noted that the GP equation is derived under the assumption that the number of atoms in the condensate is large, and neglects interaction effects due to any non-condensed atoms. For the case of a dilute Bose gas at low temperatures the depletion of the condensate is small and therefore the quantum fluctuations of the field operator are small, making the theory valid in this realm. The theory is also limited to the case of temperatures much less than the condensate temperature due to the need for thermal fluctuations to be negligible. Thus, the GP equation provides a good approximation under these conditions and, in doing so, provides a reliable model for BEC evolution with the properties of BECs being well described by the GP equation when the effects of the fluctuation field on the bulk fluid is negligible. For example, it describes the propagation of collective excitations and interference effects arising from the phase of the condensate wavefunction, that are general properties of superfluid systems [67].

4.2.2 Hydrodynamic Version of the Gross-Pitaevskii Equation

The GP equation can also be derived in the hydrodynamic context giving emphasis to the fluid characteristics of BECs. Essentially, one can obtain a set of two equations in terms of the density of the condensate, given by $|\psi|^2$, and the gradient of the phase of the condensate, which is proportional to the local velocity of the condensate [66]. Since a great deal of the research into analogue gravity in BECs makes use of such equations, as will be outlined in chapter 5, a detailed derivation of the set of hydrodynamic equations equivalent to the GP equation is provided.

Starting with the mean-field equation of motion, given by equation 4.10, and expressing the condensate wavefunction as,

$$\psi = |\psi|\, e^{i\theta} = \sqrt{\rho}e^{i\theta} \tag{4.12}$$

where the function ρ is real and positive and the function θ is real, one can rewrite the GP equation. We proceed by finding the relevant derivatives, in terms of the variables ρ and θ,

$$\nabla\psi = \nabla(\sqrt{\rho}e^{i\theta}) = \sqrt{\rho}e^{i\theta}i\nabla\theta + \frac{1}{2\sqrt{\rho}}\nabla\rho e^{i\theta} = \psi i\nabla\theta + \psi\frac{\nabla\rho}{2\rho}, \tag{4.13}$$

$$\nabla^2\psi = \nabla\psi(i\nabla\theta + \frac{\nabla\rho}{2\rho}) + \psi(i\nabla^2\theta + \frac{\nabla^2\rho}{2\rho} - \frac{|\nabla\rho|^2}{2\rho^2}), \tag{4.14}$$

$$\frac{\partial\psi}{\partial t} = i\frac{\partial\theta}{\partial t}\psi + \frac{\psi}{2\rho}\frac{\partial\rho}{\partial t}. \tag{4.15}$$

On substitution into equation 4.10 one obtains,

$$i\hbar\Big(i\frac{\partial\theta}{\partial t}+\frac{1}{2\rho}\frac{\partial\rho}{\partial t}\Big)\psi = \frac{-\hbar^2}{2m}\Big(\psi(i\nabla\theta+\frac{\nabla\rho}{2\rho})^2+(\psi(i\nabla^2\theta+\frac{\nabla^2}{2\rho}-\frac{|\nabla\rho|^2}{2\rho^2}))\Big)+V_{trap}\psi+U_o\rho\psi. \tag{4.16}$$

Cancelling ψ on both sides, and equating the real and imaginary parts of the equation gives rise to a pair of equations,

$$-\hbar\frac{\partial\theta}{\partial t} = \frac{-\hbar^2}{2m}\Big(-|\nabla\theta|^2 - \frac{|\nabla\rho|^2}{4\rho^2} + \frac{\nabla^2\rho}{2\rho}\Big) + V_{trap} + U_o\rho, \tag{4.17}$$

$$\frac{\hbar}{2\rho}\frac{\partial\rho}{\partial t} = \frac{-\hbar^2}{2m}\Big(\frac{1}{\rho}\nabla\theta\cdot\nabla\rho + \nabla^2\theta\Big). \tag{4.18}$$

We now define $\mathbf{v} = (\hbar/m)\nabla\theta$ and it follows that $\nabla\times\mathbf{v} = (\hbar/m)\nabla\times\nabla\theta = 0$ as all gradients of a function are curl free. Taking the gradient of equation 4.17, and writing both equation 4.17 and 4.18 in terms of $\mathbf{v}$ one obtains,

$$\frac{\partial \mathbf{v}}{\partial t} = \nabla\Big(-\frac{1}{2}(\mathbf{v}\cdot\mathbf{v}) + \frac{\hbar^2}{2m^2\sqrt{\rho}}\nabla^2\sqrt{\rho} - \frac{V_{trap}}{m} - \frac{U_o\rho}{m}\Big) \tag{4.19}$$

$$\frac{\partial \rho}{\partial t} + \nabla\cdot(\rho\mathbf{v}) = 0 \tag{4.20}$$

It is seen immediately that equation 4.20 is identical to the continuity equation, equation 3.2. However, the form of equation 4.19 can be written in a more intuitive manner if one exploits the well known vector identity,

$$\nabla(\mathbf{v}\cdot\mathbf{v}) = (\mathbf{v}\cdot\nabla)\mathbf{v} + (\mathbf{v}\cdot\nabla)\mathbf{v} + \mathbf{v}\times(\nabla\times\mathbf{v}) + \mathbf{v}\times(\nabla\times\mathbf{v}) \tag{4.21}$$

and realising that $\nabla\times\mathbf{v} = 0$ one obtains,

$$\nabla(\mathbf{v}.\mathbf{v}) = 2(\mathbf{v}.\nabla)\mathbf{v} \tag{4.22}$$

and substitutes this into equation 4.19, to obtain,

$$\frac{\partial \mathbf{v}}{\partial t} + (\mathbf{v}\cdot\nabla)\mathbf{v} = \frac{\hbar^2}{2m^2}\nabla\Big(\frac{1}{\sqrt{\rho}}\nabla^2\sqrt{\rho}\Big) - \nabla\Big(\frac{V_{trap}+U_o\rho}{m}\Big). \tag{4.23}$$

Referring back to equation 3.3, it is seen that this result is similar in form to the zero-viscosity Euler equation, differing only by the inclusion of a spatial derivative term dependent on ρ. This additional term is known as the quantum pressure term [66].

When the quantum pressure term is sufficiently small, it can be neglected and the condensate behaves like a zero viscosity, irrotational fluid, with $\rho = |\psi|^2$ being the density of the condensate, and $\mathbf{v}$ being the velocity of the condensate proportional to the gradient of the phase θ of the condensate and corresponding to the collective motion of many particles occupying a single quantum state. This is the essence of the hydrodynamic approximation. In summary, by using the definition of the phase and velocity in the GP equation, it has been shown that the dynamics of a BEC on the macroscopic level is governed by the equations of hydrodynamics for an irrotational nonviscous fluid.

4.2.3 The Hydrodynamic Approximation

The assumption that the quantum pressure term, in equation 4.23, is small and consequently can be neglected, forms the basis of the hydrodynamic approximation. This approximation is commonly used when dealing with BECs as analogue gravity models, as will be seen in section 5. Thus, a consideration of the parameter choices leading to validity of such an approximation is essential.

The validity of the hydrodynamic approximation can be assessed based on a comparison of the relative contribution of the quantum pressure term, $\frac{\hbar^2}{2m^2}\nabla\Big(\frac{1}{\sqrt{\rho}}\nabla^2\sqrt{\rho}\Big)$, and the other term on the right hand side of equation 4.23. More specifically, if we let ξ be the spatial scale over which the density ρ of the condensate varies, then the pressure term given by $\nabla(U_o\rho/m)$, in equation 4.23, is of order $U_o\rho/ml$, whilst the quantum pressure term is of order $\hbar^2/m^2l^3$ [66]. From this it can be concluded that the hydrodynamic approximation is valid provided that the length scale of spatial variations of the density l satisfies,

$$l \gg \frac{\hbar}{\sqrt{2mU_o\rho}}. \tag{4.24}$$

Therefore, in neglecting the quantum pressure term one limits the description of the hydrodynamic analogy to length scales l larger than this characteristic length in the condensate, denoted ξ, and known as the healing or coherence length of a BEC.

4.3 Fluctuations in the Gross-Pitaevskii Wavefunction

The research efforts, reported in chapter 7 of this thesis, rely on simulating linearised perturbations to the condensate wavefunction, that is, sound waves. Therefore, it becomes necessary to overview the theory relating to fluctuations in the various forms of the linearised GP equation.

4.3.1 Fluctuations in the Condensate using the Linearised Hydrodynamic form of the Gross-Pitaevskii Equation

Within the realm of the hydrodynamic approximation, the equation of motion for fluctuations in the mean-field ψ can be derived, as in section 3.2, using the hydrodynamic equations of motion. However, as mentioned, for this analysis to be valid the spatial length scale over which the density varies must satisfy the condition in equation 4.24, and in turn so must any perturbations to the density. Hence, the following provides a derivation using the hydrodynamic form of the GP equation, without the hydrodynamic approximation, in order to gain a deeper insight into modelling fluctuations in the condensate whilst retaining the quantum pressure term.

Let ψ_o be a background field and $\epsilon\hat{\psi}$ be a perturbation on the background field where $\epsilon \in \mathbb{R}$, $\epsilon > 0$ and $\epsilon << 1$ to ensure the perturbative nature of the field $\epsilon\hat{\psi}$. Note that here we use the notation $\epsilon\hat{\psi}$ to represent the perturbation and not an operator as in section 4.2.1. Also, the background field ψ_o and the total wavefunction $\psi = \psi_o + \epsilon\hat{\psi}$ must satisfy the GP equation, equation 4.10. In order to determine the hydrodynamic form of the GP equation, incorporating fluctuations in the condensate, one must write the wavefunctions ψ_o and $\hat{\psi}$ in terms of density ρ and phase θ of the condensate. Explicitly, $\rho = \rho_o + \epsilon\hat{\rho}$ and $\theta = \theta_o + \epsilon\hat{\theta}$, where ρ_o and θ_o are the background density and phase, whilst $\hat{\rho}$ and $\hat{\theta}$ are the perturbed density and phase. With this notation one can write the background field,

$$\psi_o = \sqrt{\rho_o} e^{i\theta_o} \tag{4.25}$$

and the total wavefunction,

$$\psi = \sqrt{\rho} e^{i\theta} = \sqrt{\rho_o + \epsilon\hat{\rho}} e^{i(\theta_o + \epsilon\hat{\theta})}. \tag{4.26}$$

Using Taylor series expansion,

$$\begin{aligned}\psi &= \rho_o^{1/2}\Big(1 + \tfrac{\epsilon\hat{\rho}}{2\rho_o}\Big)e^{i\theta_o}e^{i\epsilon\hat{\theta}} + O(\epsilon^2) \\ &= \Big(\sqrt{\rho_o} + \frac{\epsilon\hat{\rho}}{2\sqrt{\rho_o}}\Big)e^{i\theta_o}(1 + i\epsilon\hat{\theta}) + O(\epsilon^2)\end{aligned} \tag{4.27}$$

where we retain the exponential for the purposes of obtaining an expression for $\hat{\psi}$. Expanding, equation 4.27 gives,

$$\begin{aligned}\psi &= \Big(\sqrt{\rho_o}e^{i\theta_o} + \tfrac{\epsilon\hat{\rho}}{2\sqrt{\rho_o}}e^{i\theta_o}\Big)(1 + i\epsilon\hat{\theta}) + O(\epsilon^2) \\ &= \sqrt{\rho_o}e^{i\theta_o} + i\epsilon\hat{\theta}\sqrt{\rho_o}e^{i\theta_o} + \epsilon\tfrac{\hat{\rho}}{2\sqrt{\rho_o}}e^{i\theta_o} + O(\epsilon^2) \\ &= \sqrt{\rho_o}e^{i\theta_o} + \epsilon e^{i\theta_o}(i\hat{\theta}\sqrt{\rho_o} + \frac{\hat{\rho}}{2\sqrt{\rho_o}}) + O(\epsilon^2).\end{aligned} \tag{4.28}$$

Recalling that $\psi = \psi_o + \epsilon\hat{\psi}$, from this result we find that,

$$\hat{\psi} = e^{i\theta_o}\Big(i\hat{\theta}\sqrt{\rho_o} + \frac{\hat{\rho}}{2\sqrt{\rho_o}}\Big) = \psi_o\Big(i\hat{\theta} + \frac{\hat{\rho}}{2\rho_o}\Big). \tag{4.29}$$

One can now derive the equations of motion by substituting $\psi = \psi_o + \epsilon\hat{\psi}$ into the GP equation, that is,

$$i\hbar\frac{\partial(\psi_o + \epsilon\hat{\psi})}{\partial t} = \Big(-\frac{\hbar^2\nabla^2}{2m}(\psi_o + \epsilon\hat{\psi}) + V_{trap}(\psi_o + \epsilon\hat{\psi}) + U_o\left|\psi_o + \epsilon\hat{\psi}\right|^2\Big)(\psi_o + \epsilon\hat{\psi}) \tag{4.30}$$

becomes,

$$\begin{aligned}i\hbar\frac{\partial\psi_o}{\partial t} + \epsilon i\hbar\frac{\partial\hat{\psi}}{\partial t} = \Big(-\frac{\hbar^2\nabla^2}{2m} + V_{trap}\Big)\psi_o + \epsilon(-\frac{\hbar^2\nabla^2}{2m} + V_{trap})\hat{\psi} \\ +U_o\Big(\left|\psi_o\right|^2 + \epsilon(\hat{\psi}\psi_o^* + \hat{\psi}^*\psi_o) + O(\epsilon^2)\Big)(\psi_o + \epsilon\hat{\psi})\end{aligned} \tag{4.31}$$

Now, comparing terms of zero and first order in ϵ, one obtains,

$$i\hbar\frac{\partial\psi_o}{\partial t} = (-\frac{\hbar^2\nabla^2}{2m} + V_{trap})\psi_o + U_o\left|\psi_o\right|^2\psi_o \tag{4.32}$$

$$i\hbar\frac{\partial\hat{\psi}}{\partial t} = (-\frac{\hbar^2\nabla^2}{2m} + V_{trap})\hat{\psi} + U_o(\hat{\psi}\psi_o^* + \hat{\psi}^*\psi_o) + +U_o\left|\psi_o\right|^2\hat{\psi} \tag{4.33}$$

as the equations of motion, and one can write these equations in terms of density and phase, using equations 4.25 and 4.29. In doing so, and using the definition of the background fluid velocity $\mathbf{v} = (\hbar/m)\nabla\theta_o$ and the background density $\rho_o = |\psi|^2$, one arrives at a set of coupled equations for the phase and density fluctuations, given by,

$$\frac{\partial\hat{\theta}}{\partial t} = \frac{\hbar}{4m\rho_o}\nabla\cdot\Big[\rho_o\nabla\Big(\frac{\hat{\rho}}{\rho_0}\Big)\Big] - \mathbf{v}\cdot\nabla\hat{\theta} - \frac{U_o}{\hbar}\hat{\rho}, \tag{4.34}$$

$$\frac{\partial\hat{\rho}}{\partial t} + \frac{\hbar}{m}\nabla\cdot(\rho_o\nabla\hat{\theta}) + \nabla\cdot(\hat{\rho}\mathbf{v}) = 0. \tag{4.35}$$

In retaining the quantum pressure term, this system of equations is difficult to solve for either of the perturbations. Hence, neglecting the second derivative term in equation 4.34, and hence introducing the constraint given in equation 4.24, one can obtain an expression for the density fluctuations in terms of the phase fluctuations and the background field variables. This enables a single equation of motion for the phase fluctuations, and in turn the density fluctuations, to be obtained. However, it should be stressed that such equations are only valid within the context of long-length scales, as necessitated by hydrodynamic approximation. Explicitly, the resulting equations are,

$$\hat{\rho} = -\frac{\hbar}{U_o}\Big(\frac{\partial\hat{\theta}}{\partial t} + \mathbf{v}\cdot\nabla\hat{\theta}\Big), \tag{4.36}$$

$$\frac{\partial}{\partial t}\Big[\frac{1}{U_o}\Big(\frac{\partial\hat{\theta}}{\partial t} + \mathbf{v}\cdot\nabla\hat{\theta}\Big)\Big] - \frac{1}{m}\nabla\cdot(\rho_o\nabla\hat{\theta}) + \nabla\cdot\Big[\frac{1}{U_o}\Big(\frac{\partial\hat{\theta}}{\partial t} + \mathbf{v}\cdot\nabla\hat{\theta}\Big)\mathbf{v}\Big] = 0. \tag{4.37}$$

Furthermore, using the definition of the speed of sound in the condensate,

$$c_{sound} = \sqrt{\frac{\rho_o U_o}{m}} \tag{4.38}$$

as derived by Bogoliubov [14] and Lee et. al [51], one can rewrite equation 4.37, yielding,

$$\frac{\partial}{\partial t}\Big[\frac{\rho_o}{c^2}\Big(\frac{\partial\hat{\theta}}{\partial t} + \mathbf{v}\cdot\nabla\hat{\theta}\Big)\Big] - \nabla\cdot(\rho_o\nabla\hat{\theta}) + \nabla\cdot\Big[\frac{\rho_o}{c^2}\Big(\frac{\partial\hat{\theta}}{\partial t} + \mathbf{v}\cdot\nabla\hat{\theta}\Big)\mathbf{v}\Big] = 0. \tag{4.39}$$

4.3.2 Fluctuations in the Condensate using the Linearised Gross-Pitaevskii Equation

For the purposes of this thesis it is not appropriate to use the hydrodynamic form of the equations derived in section 4.3.1, as it is desired to retain the quantum pressure term in order to perform a numerical investigation of superradiant scattering from a BEC vortex. Hence, it is worthwhile to overview a more traditional approach of examining fluctuations in the condensate, representing the fluctuations by linearised perturbations to the solution of the GP equation. From this one can derive the Bogoliubov equations [66] describing the behaviour of perturbations of the condensate. That is, we take the GP equation,

$$i\hbar\frac{\partial\psi(\mathbf{r},t)}{\partial t} = \Big(-\frac{\hbar^2\nabla^2}{2m} + V_{trap} + U_o\left|\psi(\mathbf{r},t)\right|^2 \Big)\psi(\mathbf{r},t) \tag{4.40}$$

and we let $\epsilon\hat{\psi}(\mathbf{r},t)$ denote the small amplitude oscillations around the background solution describing the bulk motion of the condensate. We proceed to find the excited states of the system from the classical frequencies of the linearised GP equation [67], by writing the GP wavefunction as,

$$\psi(\mathbf{r},t) = [\psi_o(\mathbf{r}) + \epsilon\hat{\psi}(\mathbf{r},t)]e^{-i\mu t/\hbar} \tag{4.41}$$

and looking for solutions, of small oscillations of the GP wavefunction around equilibrium, in the form,

$$\epsilon\hat{\psi}(\mathbf{r},t) = \sum_i [u_i(\mathbf{r})e^{-i\omega_i t} - v_i^*(\mathbf{r})e^{i\omega_i t}] \tag{4.42}$$

where μ is the chemical potential, ω_i is the frequency of the oscillation, and $u_i(\mathbf{r})$ and $v_i(\mathbf{r})$ are the functions to be determined. Inserting 4.41 and 4.42 into the GP equation, and collecting the $e^{-i\omega_i t}$ and $e^{i\omega_i t}$ terms, the GP equation can be written as a set of two coupled equations, with the ith solution given by,

$$\hbar\omega_i u_i(\mathbf{r}) = [\hat{H}_o - \mu + 2U_o\left|\psi_o(\mathbf{r})\right|^2]u_i(\mathbf{r}) - U_o(\psi_o(\mathbf{r}))^2 v_i(\mathbf{r}), \tag{4.43}$$

$$-\hbar\omega_i v_i(\mathbf{r}) = [\hat{H}_o - \mu + 2U_o\left|\psi_o(\mathbf{r})\right|^2]v_i(\mathbf{r}) - U_o(\psi_o^*(\mathbf{r}))^2 u_i(\mathbf{r}) \tag{4.44}$$

where $\hat{H}_o$ is the single-particle Hamiltonian and U_o is the coupling constant describing the strength of the interactions.

This pair of equations, known as the Bogoliubov equations [14, 67], allow one to calculate the energies of the excitations. They also give the amplitudes u and v of the normal modes of the system. In most cases these equations must be solved numerically, however, in the case of oscillations around the ground state of a uniform gas an analytic result is possible [67]. That is, consider a uniform gas for which the confining potential $V_{trap} = 0$, $\mu = \rho U_o$ is the chemical potential for the uniform system and the density $\rho = \left|\psi_o\right|^2$ is independent of $\mathbf{r}$. It can then be shown that $u(\mathbf{r}) = u_k e^{i\mathbf{k}.\mathbf{r}}$ and $v(\mathbf{r}) = v_k e^{i\mathbf{k}.\mathbf{r}}$ are plane wave solutions to the Bogoliubov equations, which reduce to,

$$\hbar\omega u_k = \frac{\hbar^2 k^2}{2m}u_k + U_o\rho(u_k - v_k), \tag{4.45}$$

$$-\hbar\omega v_k = \frac{\hbar^2 k^2}{2m}v_k + U_o\rho(v_k - u_k). \tag{4.46}$$

It should be noted that for each solution u_i and v_i with frequency ω_i, another solution u_i^* and v_i^* with frequency $-\omega_i$ will exist, but such solutions describe identical oscillations and so can be ignored [67]. Equations 4.46 and 4.46, can be solved analytically to produce the result,

$$(\hbar\omega)^2 = \left(\frac{\hbar^2 k^2}{2m}\right)^2 + \frac{\hbar^2 k^2}{m}\rho U_o. \tag{4.47}$$

describing the dependence of the frequency, ω, on the wave vector, $\mathbf{k}$ [67]. By letting $p = \hbar k$ and $E = \hbar\omega$ it is clear that this result is equivalent to the well known Bogoliubov dispersion law for the elementary excitations of the system [14]. Therefore, if one wishes to understand the behaviour of the excitations it is useful to consider the Bogoliubov dispersion relation and the behaviour of the Bogoliubov coefficients.

The Bogoliubov Coefficients

In the spatially uniform case the Bogoliubov coefficients can be shown to be,

$$u_k^2 = \frac{1}{2}\Big(\frac{\xi_k}{\epsilon_k} + 1\Big) \tag{4.48}$$

$$v_k^2 = \frac{1}{2}\Big(\frac{\xi_k}{\epsilon_k} - 1\Big) \tag{4.49}$$

where ϵ_k^o the free-particle energy and ϵ_k the excitation energy, are given by,

$$\epsilon_k^o = \frac{(\hbar k)^2}{2m} \tag{4.50}$$

$$\epsilon_k = \hbar k c \tag{4.51}$$

and $\xi_k = \epsilon_k^o + \rho U_o$ where U_o is the coupling constant and ρ is the density of the condensate [66]. The Bogoliubov model goes beyond mean-field model theory as one can take the field operator, representing small fluctuations in the Bose field operator, into account. In other words, although here we are deriving the Bogoliubov equations in a classical setting, in the microscopic theory of BECs the excitation spectrum predicted by the Bogoliubov model agrees with that derived here using the time-dependent GP equation, but with the classical frequencies replaced by their quantum counterpart. With this in mind, the behaviour of u_k and v_k, as a function of wave number, is shown on the plot in figure 4.1. It can be seen that as k becomes large, v_k approaches zero and u_k approaches one. In the quantum description, this corresponds to adding a single particle with momentum $\hbar k$, and removal of a zero-momentum particle. Whilst for small wave numbers, or large wavelengths, $u_k \approx v_k$ and the excitations consist of linear superpositions of the states in which a particle with $\hbar k$ is added and $-\hbar k$ is removed [66]. Overall, knowing the Bogoliubov coefficients allows one to model the perturbations as plane waves and this will become useful in the work presented in chapter 7.

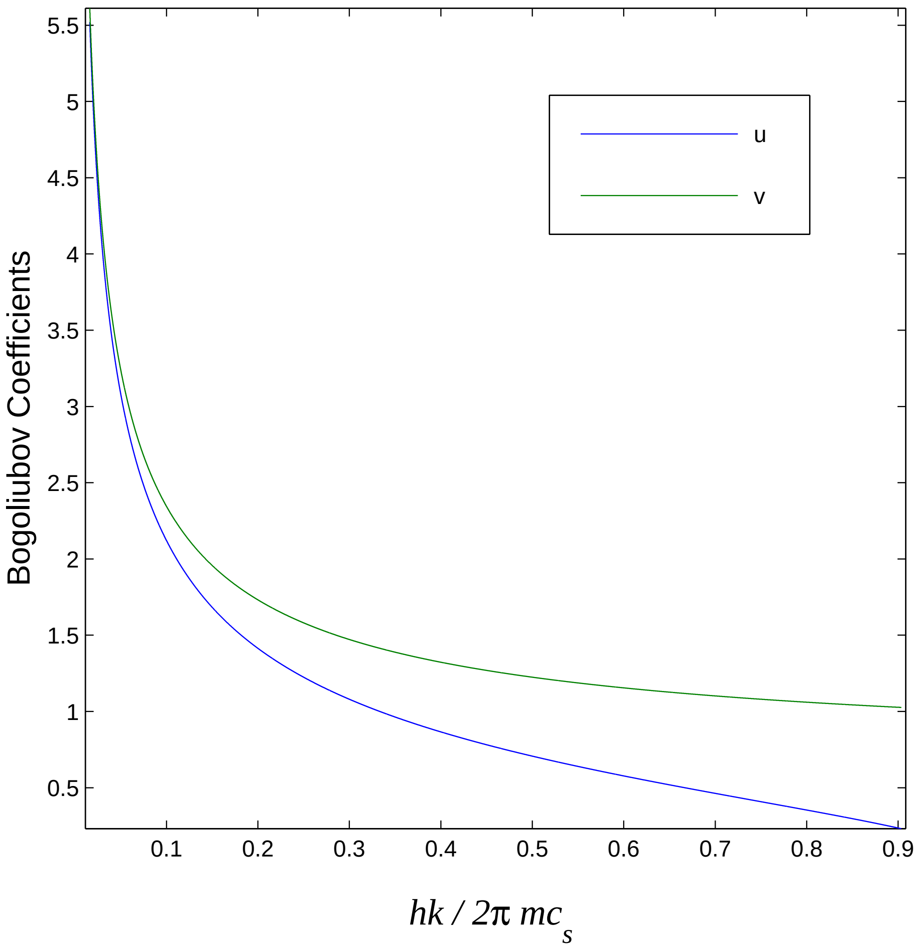

Figure 4.1: Plot of the Bogoliubov coefficients u_k and v_k, as given by equations 4.48 and 4.49, as a function of the wavenumber k given in the form of a dimensionless variable $hk/2\pi mc_s$, where h is Planck's constant, m is the atomic mass of atoms in the condensate and c_s is the Bogoliubov speed of sound in the condensate given by equation 4.38.

The Bogoliubov Dispersion Relation

The Bogoliubov dispersion relation describes the relationship between the wavenumber and energy for the solutions of the Bogoliubov equations. It was first derived from the microscopic theory of BEC by Bogoliubov [14]. In the long wavelength limit, the dispersion law takes phonon-like form, with $E(p) = pc_s$, where p is the phonon momentum. As previously defined in equation 4.38, c_s is the speed of sound in the BEC.

For small wavelengths it asymptotes to the free-particle dispersion law, with energy $p^2/2m$, where m and p are the mass and the momentum of the particles, respectively. Hence, depending on whether we are in the high or low wavenumber regime, the behaviour of excitations can make a transition from sound-like to particle-like behaviour. The transition between the two regimes occurs when the excitation wavelength is of the order of the healing length,

$$\xi = \frac{1}{\sqrt{8\pi\rho a}} = \frac{\hbar}{mc_s\sqrt{2}} \tag{4.52}$$

which as mentioned, is the typical distance over which the condensate wavefunction recovers its bulk value after being made to vanish at some point. As a result of this dispersion relation, when simulating the propagation of sound waves it is important to consider the regime under which sound waves, small perturbations on the background density, are accurately produced to ensure that all properties observed are representative of the properties of sound waves in BECs and not free particles, or some intermediate behaviour.

4.4 A Single Vortex in a Rotating Condensate

Dilute gas Bose-Einstein Condensates, and superfluids in general, in comparison to classical fluids, respond in unique ways to rotation. Of particular significance to this research is vortex motion in BECs. That is, when a BEC is made to rotate about an axis this will lead to the generation of vortices in the system. Hence, the following section will provide a brief overview of the structure of a single quantised BEC vortex in the context of mean-field theory.

The feature of BECs that leads to the formation of vortices is the fact that the velocity $\mathbf{v}$ of fluid flow in a BEC is proportional to the gradient of the phase of the condensate wavefunction, or more particularly,

$$\mathbf{v} = \frac{\hbar}{m}\nabla\theta \tag{4.53}$$

where θ is the phase and m the atomic mass of atoms in the condensate with wavefunction of the form $\psi = |\psi|\, e^{i\theta}$. Since $\mathbf{v}$ is the gradient of a scalar function, the fluid flow is irrotational, that is, $\nabla \times \mathbf{v} = 0$, and due to the single-valuedness of the condensate wavefunction, it satisfies the quantisation condition,

$$\oint_c \mathbf{v} \cdot d\mathbf{s} = \frac{\hbar}{m} \oint_c \nabla\theta \cdot d\mathbf{s} = \frac{\hbar}{m} 2\pi l = \frac{h}{m} l. \tag{4.54}$$

where $l \in \mathbb{Z}$ and is known as the vortex charge or winding number. From this it can be seen that the the circulation of $\mathbf{v}$ around a closed path C in the fluid is quantised, with $\hbar/m$ being a quantum of circulation.

As an example of a vortex structure, consider a tangential flow orientated about the z-axis with all atoms in the condensate flowing around it with quantised circulation. If the phase contribution of the wavefunction is given by $e^{il\theta}$, it follows from equation 4.54, that the tangential velocity of the flow is given by,

$$v_\theta = \frac{\hbar l}{mr} \tag{4.55}$$

where r is the distance from the axis of the trap and m is the mass of atoms in the trap. Therefore, the rotation of a BEC requires the presence of quantised vortices with cores of vanishing density, otherwise the kinetic energy will diverge as a result of the motion [66].

For the general case of a trap with axial symmetry the condensate wavefunction in cylindrical polar coordinates can be written as,

$$\psi(\mathbf{r}) = f(\rho, z)e^{il\theta} \tag{4.56}$$

where ρ is the distance from the axis of the trap, f is a real function of ρ and z, l is the vortex charge specifying the number of quanta of angular momentum in the vortex forming the background, and the energy of the system in the context of the GP formalism can be shown to be [66],

$$E = \int d\mathbf{r}\Big[\frac{\hbar^2}{2m}\Big[\Big(\frac{\partial f}{\partial \rho}\Big)^2 + (\frac{\partial f}{\partial z}\Big)^2\Big] + \frac{\hbar^2}{2m} l^2 \frac{f^2}{\rho^2} + V(\rho, z)f^2 + \frac{U_o}{2} f^4\Big]. \tag{4.57}$$

Above a critical angular velocity Ω_c, this energy functional associated with the GP equation, which includes a term due to the centrifugal contribution resulting from the rotation of the condensate, is minimised by the formation a single vortex structure [54, 66]. The amplitude f of the condensate wavefunction is found using the GP equation to be,

$$-\frac{\hbar^2}{2m}\Big[\frac{1}{\rho}\frac{d}{d\rho}\Big(\rho\frac{df}{d\rho} + \frac{d^2 f}{dz^2}\Big)\Big] + \frac{\hbar^2}{2m\rho^2} l^2 f + V(\rho, z)f + U_o f^3 = \mu f. \tag{4.58}$$

where U_o is the coupling constant, μ is the chemical potential. Making use of this expression one can find the energy of a vortex in a uniform BEC. More importantly, for the purposes of the simulations described in chapter 7, equation 4.58 reduces to an equation that can be solved numerically [66, 67]. Hence, in the case of a BEC vortex the density profile of the background can be generated by solving this equation numerically. Doing so results in a density profile that cannot be exactly matched to a function, and therefore it is convenient to make use of a function profile that is very close to the numerical solution [66]. Explicitly, as common in the literature,

$$\chi = \frac{x}{\sqrt{2 + x^2}} \tag{4.59}$$

will be the form used to approximate the profile for a singly-quantised vortex in the numerical efforts contained in this thesis. Furthermore, using a numerical technique called imaginary time propagation (ITP), explained in section 6.3, one can generate a numerically accurate profile consistent with a physical vortex.

Chapter 5

BECs as an Analogue Gravity System

After justifying the use of BECs as an analogue gravity system, this chapter will present the various BEC configurations capable of acting as analogue black holes and overview research into the study of analogue Hawking Radiation and sonic superradiance in such geometries.

As mentioned in chapter 3, Unruh showed that for particular fluid systems there exists an analogy between curved space-time and the system in question. The formation of analogue gravity models has traditionally been centred around the use of superfluid Helium [85]. However, the analogy also applies to BECs, and thus one can extend the derivation of the acoustic metric to BEC systems to show that the equations describing phonons in the condensate are equivalent to those describing a scalar field in curved spacetime [83]. Since changing the background fluid flow in a BEC system corresponds to a change of the effective metric, one can design various flow geometries to model analogue black holes. With the experimental advances in BEC research over the last decade, dilute gas Bose-Einstein condensates have come under increased interest in this context, as they possess certain properties that make them an ideal candidate for such work.

5.1 The Advantages of using BECs as Analogue Gravity Systems

BECs of atoms possess unique properties that provide a rich source of unexplored physics. These properties, including their tunable nonlinearities, also make BECs amenable to a range of experimental configurations, necessary for generating analogue acoustic black holes in the laboratory. In other words, advances in the detection and manipulation of BECs have made them promising analogues.

There are several motivating factors behind the use of BECs as analogue models of general relativity. In regards to Hawking Radiation, which is predicted by using a quantum mechanical model, BECs are a suitable candidate because they have a simple quantum mechanical description. Also, the microscopic theory of

BECs gives rise to the potential to study Hawking Radiation in systems where the hydrodynamic approximation breaks down. Furthermore, Hawking Radiation has a low temperature as do BECs, and hence it may be possible to detect the subtle presence of Hawking Radiation in such a system. Other properties making BECs a promising candidate as an analogue model, from the view of the experimentalist, include their high degree of quantum coherence and the low speed of sound in such systems.

The reason that superradiance, which is a classical effect, is suited to study in a BEC model is because of the absence of viscosity and other disturbances. To illustrate, water based models, much easier to generate in the lab than BEC systems, have been proposed by Schutzhold and Unruh [71]. However, such systems must deal with the effects of viscosity, turbulence and environmental factors which provide a source of complications. That is, a more simple fluid system could be used to model superradiance, but the accuracy of any results would be limited, whereas BECs are nonviscous and decoherence is low, so such problems are minimised.

It should be mentioned, that it is not only in regard to the analogy that superradiant scattering from BECs is studied. Understanding more about BECs and the possibility of superradiance from BEC vortices, from a condensed matter point of view, is worthy of study in its own right.

5.2 Generating Sonic Horizons and Ergoregions in BECs

A sonic horizon, in analogy with the event horizon of a black hole, occurs where the non-rotational component of the flow velocity of an inhomogeneous fluid exceeds the speed of sound. In particular, it is the boundary at which there is a transition from subsonic to supersonic fluid flow. In a rotating system, it is also possible to form an analogue ergoregion. Developing acoustic analogue models using BECs centres around the successful formation of sonic horizons and ergoregions.

Several flow configurations have been introduced in the literature, including the formation of a sonic horizon in a BEC confined to a narrow ring [34], and acceleration through a potential barrier [37], where the BEC is forced along a waveguide by an applied potential, generating supersonic speeds. Both of these configurations are considered in the realm of the hydrodynamic approximation and are not specific to the case of BEC vortex systems. Instead, to provide an insight into the general concepts of flow geometries, the simple Laval Nozzle geometry is discussed, along with BEC vortices as they are reminiscent of black holes and it is proposed that such systems realised experimentally may provide the conditions necessary to observe sonic superradiance, and in turn analogue Hawking Radiation. Hence, this section provides an overview of these acoustic geometries that have shown promise as analogue black holes and will outline research into such fluid configurations.

5.2.1 The Laval Nozzle

The Laval Nozzle is a simple geometry that allows one to observe the formation of a sonic horizon [79, 81]. The nozzle, as shown in figure 5.1, is a constriction through which a fluid, such as a condensate, is moving at a velocity u. The subsonic flow accelerates with decreasing nozzle cross-section and at the throat of the nozzle the flow becomes supersonic, that is, it exceeds the speed of sound. Furthermore, downstream from this transition region the flow will remain supersonic. The interesting feature of such a configuration is that a sound wave that has propagated through the constriction cannot be redirected to propagate to the right, because in fighting against the direction of fluid flow it is impossible to pass the supersonic region. Hence, only one way sound propagation through the nozzle is permitted and as a consequence it is possible to trap sound waves propagating in a moving fluid if a suitable configuration is used to restrict and control the fluid flow. This is where the analogy with the event horizon of a black hole arises, with the Laval Nozzle being used to generate a sonic horizon.

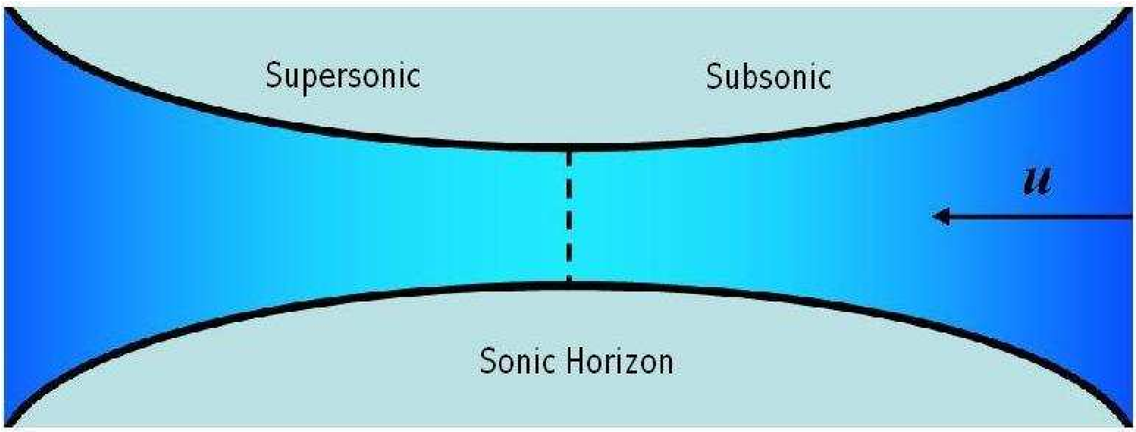

Figure 5.1: Schematic illustration of a supersonic nozzle, called the Laval Nozzle. At the constriction point, indicated by the dashed line, the flow velocity u exceeds the speed of sound. The supersonic boundary in this system gives rise to the analogy with a black hole, acting as a sonic horizon.

In the case of a BEC, the Laval Nozzle constriction can be generated by using laser beams to apply a suitable trapping potential to the atoms in the condensate. In practice, however, the Laval Nozzle is not the geometry most suited to studying analogue gravity models, such as BECs. This is because the configuration does not share many of the features of a black hole geometry and in simulating such a system it becomes necessary to introduce a second constriction into the system to force the fluid back to the subsonic regime [83], or to incorporate some form of absorbing boundary conditions [28], to remove the effects of unphysical reflection from the domain boundaries. Overall, the Laval Nozzle provides a good introduction to the concept of forming sonic horizons, but more complicated structures have been proposed as more suitable geometries for studying analogue black hole effects in BECs.

5.2.2 Vortices

As mentioned in section 4.4, a BEC vortex is a topological defect arising due to the way in which superfluid flow responds to rotation. In agreement with the fact that the energy functional, given by the expression in equation 4.57, is minimised by the formation a single vortex structure [54, 66], various experiments have shown that a vortex is formed in a BEC by simply "stirring" the condensate using laser beams [55, 54, 43]. Alternatively, one can observe spontaneous vortex formation in BECs as a result of dynamical instabilities or can generate vortices using a procedure known as phase imprinting, which involves modulating the phase of the condensate to produce a vortex structure [47].

The rotation of a condensate, and the resulting vortices, effects the propagation of sound in a BEC because the density vanishes at the core of the vortex and the sound waves are modulations in the condensate density. With this in mind, draining BEC vortices have been proposed as another fluid configuration in which it is possible to form a sonic horizon [81]. In addition to the event horizon, a vortex configuration allows one to simulate the ergosphere of a rotating black hole. The two relevant features of a draining vortex flow include that as one approaches the vortex core the magnitude of the flow velocity exceeds the local speed of sound and at a certain point the radial component of the flow velocity also exceeds the local speed of sound. The former surface acts as an analogue ergosphere. The latter acts as an analogue event horizon, because the radial component of the flow velocity is greater than the speed of sound and hence, sound in this region can no longer escape from the vortex.

The event horizon must always be contained within or coincide with an ergosphere, as it is impossible to have a surface where the perpendicular flow velocity has equal magnitude to the speed of sound if the overall magnitude of the flow velocity is not greater than or equal to the speed of sound. The two boundaries coincide for one dimensional systems and for purely radial flow in cylindrically, or spherically, symmetric systems. The latter will be discussed in section 5.4.2. On the other hand, a cylindrically symmetric draining vortex configuration has an ergosphere outside the event horizon. The horizon is located where the radial flow has greater magnitude than the speed of sound, whilst the ergosphere will be found where the total magnitude of the flow, in both radial and angular directions, is equal to the speed of sound. This vortex configuration, often called the draining bathtub configuration requires a central drain and will be considered in more detail in section 5.4.1.

5.3 Realising Analogue Gravity in the Laboratory

There are significant issues that need to be addressed before BEC flow configurations can be produced to observe analogue Hawking Radiation, or sonic superradiance, in the laboratory. For example, the experimental challenges of keeping the BEC at ultra-low temperatures, ensuring isolation from the environment and detecting single phonons radiating from a sonic horizon, whilst achievable, require substantial expertise and apparatus. Hence, this section accounts some of the requirements, and the feasibility, for bringing BEC analogue gravity models to fruition in the laboratory.

5.3.1 Analogue Hawking Radiation in BECs

Analogue Hawking Radiation, the spontaneous emission of phonons from a sonic horizon, is predicted to be a subtle effect, and hence the feasibility of detecting and measuring it in the laboratory depends on the magnitude of the Hawking temperature relative to the background temperature of the condensate [34]. This assumes that the phonons will come to thermal equilibrium raising the temperature of the condensate some distance from the sonic horizon [83].

The Hawking temperature, T_H, for the case of phonons radiated with a thermal spectrum from a sonic horizon in a BEC, is given by [52, 81],

$$T_H = \frac{\hbar}{2\pi k_B} \frac{d(|\mathbf{v} - c|)}{dx}\Big|_{horizon} \tag{5.1}$$

where $\mathbf{v}$ is the flow velocity, c is the speed of sound in the BEC, x is the perpendicular distance from the horizon and k_B is the Boltzmann constant. One can estimate the variables in this expression to approximate the magnitude of the Hawking temperature. For example, the derivative,

$$\frac{d(|\mathbf{v} - c|)}{dx} \approx \frac{6\text{mms}^{-1}}{1\mu\text{m}} \tag{5.2}$$

where the fluid is accelerated from rest to a speed of sound of about 6 mms^{-1}, typical of the speed of sound in a BEC of alkali atoms, over a distance of 1 μm which is the nozzle or vortex diameter, representing the size of the sonic black hole. Using this estimate in equation 5.1, the temperature associated with the phonon radiation is $T_H \approx 7$ nK. However, experiments have shown that these values could be made more favourable. For instance, using the Feshbach resonance [68] one can alter the scattering length for the condensate, which enables one to increase the speed of sound in the condensate, as is it is proportional to the square root of the scattering length. In turn this would lead to an increase in T_H as it is proportional to the speed of sound. Furthermore, one can also increase the density of the condensate and since it is proportional to the speed of sound, an increase in speed of sound can be achieved. However, for a given geometry there needs to be a compromise between increasing T_H by increasing the speed of sound, and making

Hawking Radiation easier to observe, as doing so makes it harder to set up the supersonic flow. At present, the most positive estimate predicted in the literature is 70 nK for a particular choice of Laval Nozzle geometry [8].

Despite the small value of T_H, an achievable condensate temperature is $T_{BEC} \approx 90$ nK [7]. Hence, T_H differs by approximately only one order of magnitude when compared to T_{BEC}. From this it can be seen that T_H is comparable to T_{BEC}, and therefore it is hoped that Hawking Radiation will fall within a range detectable in experiments.

In response to this, various flow geometries have been suggested as systems in which to observe Hawking Radiation. A single nozzle geometry was considered by Sakagami and Ohashi [69], whilst Barcelo et al. [4, 7] discussed the use of a pair of nozzles with the second constriction returning the flow to subsonic speeds so that the flows could be generated in experiments. Also, Visser [81] presents the idea of a vortex with a central sink generating a sonic horizon. Although the effective metric associated with the draining bathtub configuration is not identical to the Kerr metric, it is qualitatively similar as a result of its rotation and inflow. In experiments, a draining bathtub flow geometry could be achieved by outcoupling atoms from the BEC using a tightly focussed laser beam [34], as depicted in figure 5.2. More recently in 2006, it was shown [6, 5] that it is not necessary to create an ergoregion in the flow in order to observe Hawking Radiation.

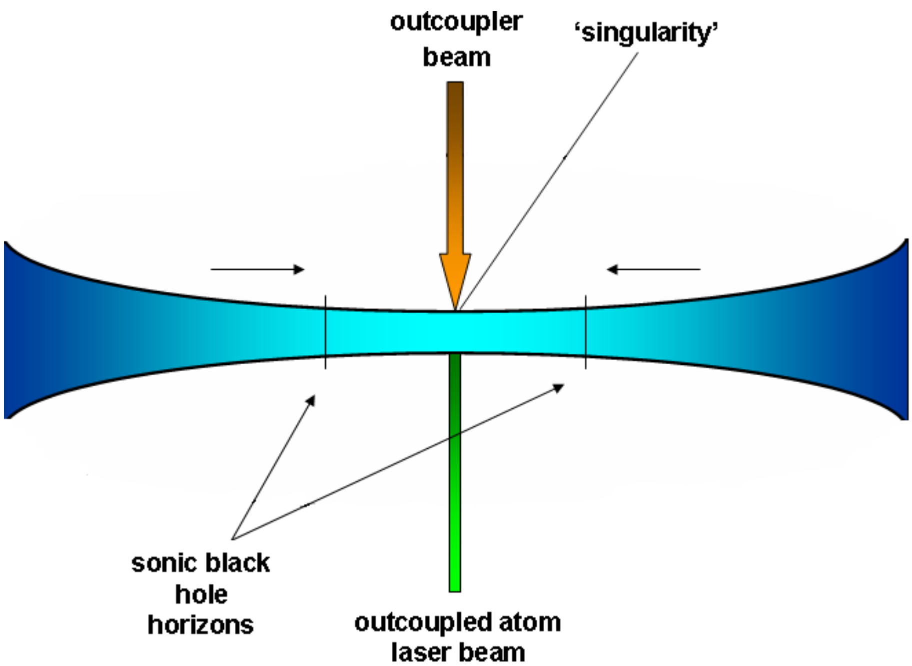

Figure 5.2: Atom outcoupling from a BEC to produce a draining vortex geometry, with a "singularity" at the outcoupling region, leading to the generation of two acoustic black hole horizons. Arrows specify the direction of the fluid flow. This experimental setup is known as the tight cigar-shaped configuration [34].

5.3.2 Sonic Superradiance in BECs

The investigation of sonic superradiance, the amplification of an incident sound wave in a fluid system, in the laboratory prior to analogue Hawking Radiation has been proposed primarily because it could be easier to detect [74, 10, 11, 9, 31]. When dealing with superradiance there is no need to quantise fields when investigating it, and this simplifies the task of determining whether an analogue system will give rise to such an effect. In addition, the stimulated nature of superradiance suggests it would easier to observe than the weaker spontaneous effect, Hawking Radiation. More particularly, in the case of superradiance the magnitude of the effect is under experimental control. Like Hawking Radiation, superradiance is also a kinematical effect and as a result is suited to investigation in an analogue gravity context. Besides interest in sonic superradiance from the point of view of understanding sound propagation in BECs, these factors warrant the study of sonic superradiance as an avenue to investigating Hawking Radiation.

In 2002, Schutzhold and Unruh [71], addressed the possibility of observing rotational superradiance in analogue black holes. They proposed an experimental setup, involving a water based model, using gravity waves in a shallow basin representing an ideal draining bathtub. Building on the ideas of this research, in 2003 Basak and Majumdar [10, 9] conducted a detailed numerical analysis of sonic superradiance in BECs within the constraints of the hydrodynamic approximation for the draining bathtub configuration presented by Visser [83]. Basak and Majumdar [11] also computed analytically the reflection coefficients in the low frequency limit, where superradiance is predicted to occur. Finally, in 2005, Slatyer and Savage [74] presented numerical evidence of sonic superradiance from a non-draining hydrodynamic vortex.

5.4 Progress using BECs as an Analogue Gravity Model

Prior to conducting analogue gravity experiments it is beneficial to undertake theoretical analysis and numerical simulations to determine how analogue gravity experiments can best be carried out. In performing such simulations, it is beneficial to choose parameters indicative of experimental scenarios. In doing so, one ensures that greater insight into the detection of sonic superradiance, and in turn Hawking Radiation. These studies have the potential to make clear exactly how sonic horizons and analogue ergoregions should be formed in the laboratory, and how sonic superradiance and analogue Hawking Radiation should be detected.

This section provides a detailed account of recent numerical efforts in considering BECs as analogue gravity systems in relation to the detection of superradiant scattering from a BEC vortex. Research so far has focussed on numerical investigations of scattering from hydrodynamic vortices. It is this work that this thesis attempts to extend.

5.4.1 Vortex with Sink: Vortex Geometry with Radial Flow

For the case of a (2+1) dimensional draining bathtub fluid configuration with a sink at the origin [10, 11], where the background density and speed of sound of the condensate are assumed to be constant, the sonic horizon and analogue ergosphere do not coincide, as shown in figure 5.3. The velocity profile in cylindrical polar coordinates [81], for such a flow geometry is given by,

$$\mathbf{v} = v_{\hat{r}}(r)\hat{r} + v_{\hat{\theta}}(r)\hat{\theta} \tag{5.3}$$

where $v_{\hat{r}}$ and $v_{\hat{\theta}}$ are the velocity components in the radial and angular directions, respectively. More particularly,

$$\mathbf{v} = \frac{A\hat{r} + B\hat{\theta}}{r} \tag{5.4}$$

where $\hat{r}$ and $\hat{\theta}$ denote unit vectors in polar coordinates, and A and B are arbitrary real positive constants associated with the radial and angular components of the background fluid velocity, respectively.

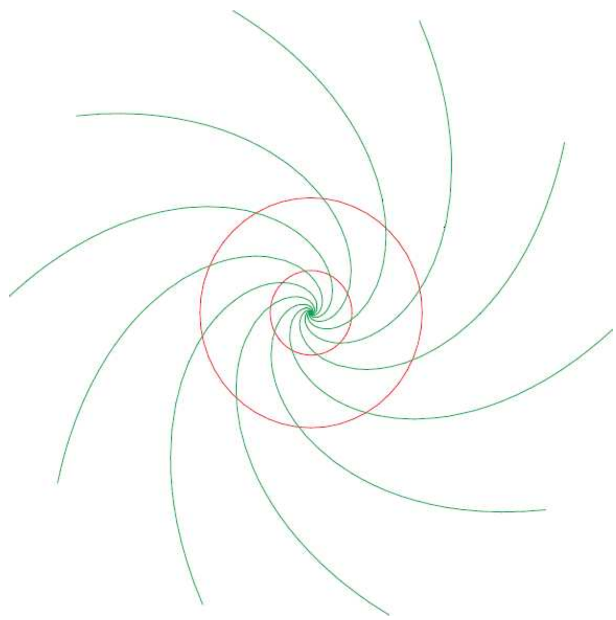

Figure 5.3: The Draining Bathtub or collapsing vortex geometry generated by the presence of a source or sink, reproduced from Visser et al. [84]. The spirals represent the contours of the fluid flow. The outer circle defines the ergoregion and the inner circle defines the event horizon, where the radial component of the flow velocity exceeds the speed of sound.

It can be shown [81] that the acoustic metric for this draining bathtub configuration is given by,

$$ds^2 = -c^2dt^2 + \Big(dr - \frac{A}{r}dt\Big)^2 + \Big(rd\theta - \frac{B}{r}dt\Big)^2 \tag{5.5}$$

or equivalently,

$$ds^2 = -\Big(c^2 - \frac{A^2+B^2}{r^2}\Big)dt^2 - \frac{2A}{r}drdt - 2Bd\theta dt + dr^2 + r^2d\theta^2 \tag{5.6}$$

The vortex fluid flow possess an ergosphere forming at the cylindrical surface where the magnitude of the flow velocity,

$$|\mathbf{v}| = \sqrt{\frac{A^2+B^2}{r^2}} \tag{5.7}$$

is equal to the speed of sound, c. The radius of the ergosphere, r_{ES}, is therefore given by,

$$r_{ES} = \sqrt{\frac{A^2+B^2}{c}} \tag{5.8}$$

where the sign of A determines whether the vortex core is a sink or source, that is, whether we have a collapsing or expanding BEC vortex, respectively. However, as seen by equation 5.8 this is not of concern in defining the ergoregion. When the radial component of the fluid velocity,

$$v_r = \frac{A}{r} \tag{5.9}$$

exceeds the speed of sound, a sonic horizon will be formed, with radius r_H defined as,

$$r_H = \frac{|A|}{c}. \tag{5.10}$$

In this instance, if $A < 0$ one has a future event horizon, which applies to the case of an analogue black hole. On the other hand, if $A > 0$ one has a past event horizon, corresponding to an analogue white hole where only one way propagation of sound waves out of the vortex is permitted [83].

As mentioned, in order to generate radial flow this configuration requires a sink at $r = 0$ which makes it hard to realise experimentally. Despite this added complexity, the draining bathtub is a good model for considering the difference between an event horizon and an ergosphere. Furthermore, using such a geometry it is possible to investigate sonic superradiance. In particular, Basak and Majumdar [10] show that with the angular velocity of the black hole given by,

$$\Omega_H = \frac{Bc}{A^2} \tag{5.11}$$

there exists a relationship between the reflection and transmission coefficients for a scalar wave incident on an acoustic black hole, explicitly,

$$1 - |\mathcal{R}|^2 = \left(\frac{\omega - m\Omega_H}{\omega}\right) |\mathcal{T}|^2 \tag{5.12}$$

where ω is the frequency of the incident wave, m is the angular wave number, and $|\mathcal{R}|$ and $|\mathcal{T}|$ are the reflection and transmission coefficients, respectively. From this result it is clear that for frequencies in the range $0 < \omega < m\Omega_H$ the reflection coefficient has a magnitude greater than one, and hence amplification of the incident wave occurs. This is exactly the condition for rotational superradiance discussed in section 2.3.

5.4.2 Non-Draining Vortex: Vortex Geometry with no Radial Flow

A non-draining vortex flow, characterised by a purely radial flow, is a special case of equation 5.4 with $A = 0$. The ergosphere occurs where the angular flow has greater speed than the speed of sound. The advantage of such a geometry is that a sonic horizon is not present and this removes the need to create a vortex sink which is useful to avoid in the initial stages of experimental work. Importantly, however, sonic superradiance can be investigated in such a system because, as with the astrophysical case, superradiance only requires the presence of an ergoregion.

For such a geometry, Slatyer and Savage [74] have shown that sound waves scattered from a BEC vortex may be amplified when working within the hydrodynamic approximation. To do so, they conducted a numerical analysis using a vortex density profile that mimics a realistic vortex in a BEC. The following presents an overview of the derivation of sonic superradiance from a BEC vortex given by Slatyer and Savage. However, as will become apparent, this approximation is of questionable validity near the scattering point.

Derivation of Superradiant Scattering from a Simple Vortex

Consider a cylindrically symmetric time-independent fluid flow with zero radial flow which generates a vortex aligned along the z axis with flow velocity,

$$\mathbf{v} = v_{\hat{\theta}}(r)\hat{\theta}. \tag{5.13}$$

where for irrotational flow, $v_\theta = \alpha/r$ for some constant α. It is assumed that the density and speed of sound depend only on the radial coordinate r, and approach asymptotic values, ρ_∞ and c_∞, as $r \to \infty$. The effective metric for this system obeys the zero-viscosity Euler equation 3.3 and the Continuity equation 3.2, under the hydrodynamic approximation.

Consider cylindrical wave solutions to the wave equation, equation 3.1, of the form $\phi(t, r, \theta, z) = \psi(t, r)e^{-im\theta}$ where m is the angular wave number. Also, assume that the square of the speed of sound is proportional to the density, as is the case for

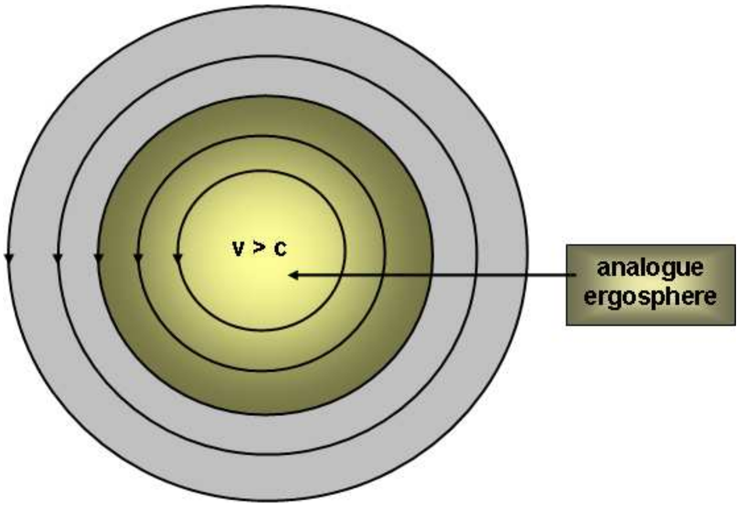

Figure 5.4: The "ergosphere" in a non-collasping vortex geometry. The circles represent the contours of the fluid flow. The inner region specifies the analogue ergosphere, where the flow velocity exceeds the speed of sound.

BECs when the interaction strength is constant [66]. This allows one to remove the density dependence in the sound wave equation, yielding,

$$\frac{\partial^2\psi}{\partial t^2} - 2i\frac{mv_\theta}{r}\frac{\partial\psi}{\partial t} - \frac{1}{r}\frac{\partial}{\partial r}\Big(rc^2\frac{\partial\psi}{\partial r}\Big) + \frac{m^2}{r^2}\Big(c^2 - v_\theta^2\Big)\psi = 0 \tag{5.14}$$

where c is the speed of sound in the unperturbed fluid and v_θ is the tangential component of the flow velocity for the unperturbed fluid. The density profile used in the derivation is,

$$\rho(r) = \rho_\infty\frac{[(r - r_o)/\sigma]^2}{2 + [(r - r_o)/\sigma]^2} \tag{5.15}$$

when $r > r_o$ and $\rho_o = 0$ when $r < r_o$, where r_o is the vortex core radius and ρ_∞ is the density of the condensate far from the vortex. This expression is similar to that for a charge l BEC vortex density profile, except that the scale length is given by the free parameter σ, instead of the healing length ξ.

It is convenient to make a further simplification to single frequency waves of the form $\psi(t, r) = r^{-1/2}G(r^*)e^{i\omega t}$, where r^* is a tortoise coordinate defined by $dr/dr^* = \tilde{c}^2$, with $r^* \to r$ for $r \to \infty$ and $\tilde{c} = c/c_\infty$. Applying these definitions equation 5.14 becomes,

$$\frac{d^2G(r^*)}{dr^{*2}} + \frac{\tilde{c}^2}{c_\infty^2}(\omega^2 - V_{eff})G(r^*) = 0 \tag{5.16}$$

where V_{eff} given by,

$$V_{eff} = \frac{2m\omega v_\theta}{r} + \frac{m^2}{r^2}(c^2 - v_\theta^2) - \frac{1}{2r}\Big(\frac{c^2}{2r} - \frac{dc^2}{dr}\Big) \tag{5.17}$$

is an effective potential defined to illustrate the similarity of equation 5.16 to the time-independent Schrödinger equation. As is typical in astrophysical based derivations, the solution to equation 5.16 can be obtained by studying the two limiting cases where the tortoise coordinate r^* approaches $\pm\infty$. For the case when r is large, one has $r^* \approx r$, and one can neglect all terms, except for those of highest order in r, as they are negligible. This gives the equation,

$$\frac{d^2G(r^*)}{dr^{*2}} + \frac{\omega^2}{c_\infty^2}G(r^*) \approx 0, \tag{5.18}$$

which has the general solution,

$$G(r^*) = Ae^{i(\omega/c_\infty)r^*} + Be^{-i(\omega/c_\infty)r^*}, \tag{5.19}$$

where A and B are the constant amplitudes of the incoming and outgoing waves, respectively. For the case when $r^* \to -\infty$ one can use the density profile described by equation 5.15 to find the other asymptotic form of equation 5.14,

$$r^{*2}\frac{d^2G(r^*)}{dr^{*2}} + \frac{2\sigma^2\Omega^2}{c_\infty^2}G(r^*) = 0, \tag{5.20}$$

$$\Omega \equiv \omega - m\alpha/r_o^2. \tag{5.21}$$

This Euler-type equation has solutions $G(r^*) = |r^*|^\delta$, where,

$$\delta = \frac{1}{2} \pm \gamma, \quad \gamma \equiv \frac{1}{2}\mathrm{sign}(\Omega)(1 - 8\sigma^2\Omega^2/c_\infty^2)^{1/2}. \tag{5.22}$$

The general solution is therefore,

$$G(r^*) = |r^*|^{1/2}\,(C\,|r^*|^\gamma + D\,|r^*|^{-\gamma}), \tag{5.23}$$

where C and D are constants. The parameter γ is either real or imaginary. In the case of γ imaginary, the solution is oscillatory and given by,

$$G(r^*) = |r^*|^{1/2}\,(Ce^{\gamma\ln|r^*|} + De^{-\gamma\ln|r^*|}) \tag{5.24}$$

where C and D represent the amplitudes of the incoming and outgoing waves, respectively. One then finds the Wronskians associated with the asymptotic solutions given in equations 5.19 and 5.24, and using Abel's Theorem which implies that the Wronskians of the solutions are constant due to the fact that no first derivative term appears in the equation for $G(r^*)$ given in equation 5.14, it can be shown [74] that,

$$\frac{2i\omega}{c_\infty}(|\mathcal{R}|^2 - 1) = -2\gamma\,|\mathcal{T}|^2\,. \tag{5.25}$$

This result indicates that provided $\Omega < 0$ and $\mathcal{T} \neq 0$ then $|\mathcal{R}| > 1$, and hence superradiance occurs. By considering the superradiance inequality for $\Omega < 0$ one obtains,

$$\omega < m\alpha/r_o^2, \tag{5.26}$$

and this can be combined with the expression for the vortex velocity constant [66] $\alpha = l\hbar/m_{atom}$, where m_{atom} is the mass of an atom in the BEC, for the case of a charge l BEC vortex, if desired.

In summary, for single frequency waves of the form $\phi(t,r) = R(r)e^{-i\omega t}$ it is seen that an incoming wave can be scattered into an outgoing reflected wave and an ingoing transmitted wave, with superradiance occuring for $\omega < m\alpha/r_o^2$. Numerical evidence of the effect was obtained for parameters satisfying this inequality, by solving the wave equation given by equation 5.14, for a dilute gas BEC system. An investigation of the magnitude of the superradiant scattering was made by taking the Fourier components of the real parts of the incident and reflected wavepackets. This revealed that the dominant Fourier power was approximately doubled [74].

Limitations of the Hydrodynamic Approach

The derivation of sonic superradiance, as presented by Slatyer and Savage [74], is limited by the use of a single equation describing the sound wave in the BEC as this makes use of the hydrodynamic approximation. As discussed in section 4.2.3, such an approximation is only valid when the quantum pressure term is small, however, the quantum pressure term is proportional to the healing length of the BEC, and in turn, inversely proportional to the density of the condensate, as indicated by equation 4.24. This presents a concern, since it is the region approaching the vortex core that is of significance when dealing with superradiance, but it is also the region in which the density drops off rapidly to zero. Hence, the quantum pressure term cannot be considered negligible and as a consequence the results of superradiant scattering obtained under the hydrodynamic approximation become suspect. Therefore, it is required to undertake analysis of the same situation retaining the quantum pressure in order to be confident that superradiance is observed when the BEC interpretation holds.

Chapter 6

Research Methodology

In this chapter, an overview of the numerical techniques used to investigate phonon supperradiance from BECs will be presented. Furthermore, a justification for the methods used will be given.

6.1 Numerical Modelling

It is often the case that a problem in physics can be written in terms of a system of differential equations. However, analytic solutions to such problems are in the majority of cases limited to the simplest cases. In response to this, the need for numerical solutions of mathematical problems occurs often in physics. With this in mind, it becomes clear that numerical techniques are a powerful tool in investigating BEC dynamics for which this is the case. Furthermore, the use of numerical simulations as a first step in characterising scattering from BEC vortices is justified on the basis that it provides an effective mechanism by which one can gain deeper understanding of phonon superradiance, and decide on the experimental requirements of detecting analogue black hole effects in the laboratory.

Numerical simulations involve specifying and solving numerically the partial or ordinary differential equations relevant to the problem under investigation. The general form of partial differential equations (PDEs), which will be relevant to this thesis, is given by the second - order linear equation,

$$\begin{aligned} A(x,y)U_{xx} + 2B(x,y)U_{xy} + C(x,y)U_{yy} + D(x,y)U_x \\ +E(x,y)U_y + F(x,y)U + G(x,y) = 0 \end{aligned} \tag{6.1}$$

where U is the dependent variable, x and y are the independent variables, $A(x,y)$ to $G(x,y)$ are constants or functions of x and y, and the subscripts represent differentiation with respect to the relevant variable. The equations represented by equation 6.1 can be classified as either hyperbolic, elliptic or parabolic depending on whether, for regions in the $x-y$ plane, the discriminant $B^2 - 4AC$ is greater than, less than or equal to zero [57], as summarised in table 6.1.

When working with PDEs one must limit the computational domain, in order for efficiency to be maintained. Hence, there is a need to introduce boundary conditions

PDE classification	Discriminant $B^2 - 4AC$
hyperbolic	$\Delta > 0$
elliptic	$\Delta < 0$
parabolic	$\Delta = 0$

Table 6.1: Classification of Partial Differential Equations

specifying the behaviour at the domain boundaries. The most common boundary conditions, besides the initial state, are Dirichlet boundary conditions, Neumann boundary conditions and periodic boundary conditions [46, 44]. The Dirichlet boundary condition involves specifying the function U along the boundary. Whilst for the Neumann boundary condition, the derivative of the function is specified along the boundary. Finally, periodic boundary conditions are where the value of the function is the same at beginning and end points of a given dimension.

A variety of methods can be used for solving differential equations of the form discussed above. They can be divided into two categories, namely explicit picture and interaction picture methods, with the distinction being how one choses to perform the evolution due to the transverse derivatives [25]. For both methods the choice of the semi-implicit and Runge-Kutta algorithms can then be made [44].

6.2 Programming Considerations

6.2.1 The XMDS Package

XMDS, the e**X**tensible **M**ulti-**D**imensional **S**imulator, is a numerical simulation package used in this investigation for the purposes of simulating the scattering of waves from a BEC vortex. Hence, a brief overview of XMDS and its main attributes is warranted, in order to fully grasp the concepts underpinning the simulations performed. For a more comprehensive coverage of this topic the reader is referred to the XMDS manual [25].

XMDS is a computer program which takes the high level description of a given problem, written by the user in XML (the extensible markup language), and generates the low level C++ code which can then be compiled to produce an executable file that solves the problem. As a result, the user is left with a simpler and more efficient programming task.

The XMDS package solves ordinary or partial differential equations and therefore is ideal for use in simulating phonon superradiance, which involves solving partial differential equations. It also allows one to solve stochastic differential equations, which are differential equations with noise terms introduced. XMDS has several advantages over traditional programming approaches. Firstly, it allows one to write code in a standard form so that simulation results can be easily verified by different research groups. It also enables the user to take full advantage of the similarities of physical problems by applying the same general format in simulating an array of unique physical systems. Furthermore, it ensures an error free process following debugging of the XML script. These features are what motivates and justifies the use of XMDS, over other programming approaches, in this research.

Another important feature of XMDS, is that it allows the user to make use of various algorithms. In the one-dimensional simulations outlined in chapter 7, the Fourth-order Runge-Kutta algorithm in the Interaction Picture (RK4IP) is used. The algorithm of particular significance in simulating scattering from a BEC vortex, in the two-dimensional case presented in chapter 7, is the adaptive step size Runge-Kutta-Fehlberg algorithm in the interaction picture (ARK45IP). This adaptive time step algorithm is useful in our simulations as for much of the propagation time there are small changes in the background density, whilst in the vortex region rapid changes take place. This algorithm is more computationally expensive than the equivalent Runge-Kutta algorithm in the constant time step case. However, this increased computational burden is still worthwhile in simulations where the rate of change of the solution is substantial, or simply when an appropriate step size is not known.

The algorithm circumvents the problem of determining a suitable time step for the problem, by selecting the optimal time step for each iteration. This is achieved by computing the results of the simulation for a particular time step, halving this time step, and computing the results for this new time step. A comparison of the two sets of results is then made and the difference between them is used as an estimate of the discretisation error. Essentially, the algorithm continues this process until it reaches an optimum time step for which the discretisation error is minimised, but the time step is sufficiently long to maintain computational efficiency.

6.2.2 Justification of the GP Approach

Primarily, the choice of the GP equation to model the condensate is made because the GP equation provides a good description of BEC evolution. In regards to modelling sound waves impinging on a BEC vortex, the GP equation retains the quantum pressure term and therefore allows one to probe the behaviour of the transmitted wave, that propagates into the vortex, generated due to the scattering of the incomimg wavepacket from the vortex. This is not possible under the hydrodynamic approximation since the model breaks down as one approaches the vortex core. Due to the equivalence of the linearised GP approach and the full quantum theory of excitations, discussed in section 4.3.2, the phonon modes can be considered as negative energy uncondensed modes [30], called anomalous modes, of the fully quantised field [52] and this is necessary if we are to observe superradiance. In particular, the background field is in the ground state of the GP equation, and consequently the vortex has the lowest possible energy, meaning that no rotational energy can be extracted from the vortex to produce superradiance. However, when dealing with perturbations one is not restricted by the mean-field approximation implicit in the GP equation and instead can consider perturbations as uncondensed modes, that is, the non-condensed fraction of the BEC. Such modes are not governed by the GP equation and due to their fully quantum nature are permitted to have negative energy. Thus, these modes could give rise to a transmitted wave propagating into the vortex. In turn, this allows the reflected wave to have an increased energy, relative to the incident wave, by an amount equal to the magnitude of the negative energy transmitted mode. From this it can be seen that using this interpretation superradiance could be observed in the framework of the GP equation.

In selecting the GP approach, discussed in section 4.2, one also needs to consider how the code generated by XMDS performs the propagation. Due to the appearance of spatial derivatives in the equations of motion, XMDS takes the Fourier transform of each field throughout the problem space. This is a computationally expensive process as such calculations must be performed at each time step. As a result, the run time for simulations increases with the number of dimensions and the number of spatial lattice points used.

From this it is clear that the choice of equations becomes important if one is to limit computational burden. For example, one could choose the hydrodynamic form of the equations of motion (equations 4.34 and 4.35), without the hydrodynamic approximation, but this involves solving two coupled equations with two perturbation fields. This is a computationally expensive endeavour as the two fields need to be Fourier transformed at each time step. Although possible to convert these coupled equations into a single equation using the hydrodynamic approximation, for the purposes of this research we wish to avoid this. Using the GP approach, XMDS only needs to transform one complex field. Hence, this equation of motion can be easily and efficiently implemented in XMDS.

6.3 Imaginary Time Propagation

Imaginary time propagation (ITP), also known as the method of steepest descent, is a numerical technique generally used for obtaining the ground state of a given system [27, 29].

The process works by propagating the wavefunction in imaginary time, using a trial form of the wavefunction as the initial state. Consider a wavefunction $\psi(\mathbf{r}, t)$ given by,

$$\psi(\mathbf{r}, t) = \sum_{n=0}^{\infty} c_n(t)\phi_n(\mathbf{r}) \tag{6.2}$$

as a superposition of eigenstates $\phi_n(\mathbf{r})$ with time-dependent amplitudes $c_n(t)$ and eigenenergies $E_n(t)$. After a time Δt the wavefunction, found by integration of the Schrödinger equation, is given by,

$$\psi(\mathbf{r}, t + \Delta t) = e^{-i\Delta t H}\psi(\mathbf{r}, t) \tag{6.3}$$

where H is the Hamiltonian of the system, here assumed time-independent. We set $\Delta t \mapsto -i\Delta t$ in the unitary evolution operator in equation 6.3, and substituting the form of the wavefunction given in equation 6.2 into equation 6.3, yields,

$$\psi(\mathbf{r}, t + \Delta t) = \sum_{n=0}^{\infty} c_n(t)\phi_n(\mathbf{r})e^{-E_n\Delta t}. \tag{6.4}$$

From equations 6.3 and 6.4, it is seen that for positive eigenenergies the eigenstates decay exponentially with time. The important point here is that the decay rate is dependent on E_n, and it follows that the eigenstate ϕ_n with the lowest energy, generally the the ground state of the system, decays the slowest. As a consequence, if one selects a trial wavefunction and evolves the system for a sufficient amount of imaginary time, the lowest energy state for the system under consideration will dominate. The trial wavefunction, merely a guess of the lowest energy state, will contain some contribution from excited states in the decomposition of equation 6.4. However, these contributions will decay away at a greater rate compared to the ground state contribution to the decomposition. Specifically, for our vortex background, the imaginary time propagation output can be used as an initial condition in the real time evolution and in turn this allows vortex stability to be achieved for the real time propagation.

In this thesis ITP is used to ensure that vortex stability is maintained over time by finding the lowest energy state for an $l = 1$ vortex. That is, strictly speaking it is the ground state with $l = 1$ topology that one obtains, and not the actual ground state of the system. The reason that ITP is successful in obtaining the ground state within a topological constraint is that the method only permits local changes to achieve the lowest energy state, whilst vortices of different l are globally different structures.

There is one additional issue that needs to be addressed in order to obtain the ground state with $l = 1$ topology, namely, periodic renormalisation of the wavefunction [27]. As the evolution of the wavefunction takes place, this maintains the background density $|\psi|^2$ and prevents errors that would be inevitable due to the decaying norm of the solution [87]. This can be achieved by the inclusion of the chemical potential into the GP equation [29]. Alternatively, this can be done by preserving the norm, that is the number of atoms in the condensate, using a renormalisation procedure. It is the latter method that is employed in the numeric work pertaining to this thesis, because of the difficultly in accurately determining the chemical potential in the presence of the vortex.

Chapter 7

Simulation Results

This chapter is devoted to describing the Gross-Pitaevskii (GP) simulation of the propagation of sound waves in a BEC and the interaction of such waves with a BEC vortex. The results of both the one and two-dimensional simulations exhibit the propagation of sound waves in BECs and the reflection of sound waves from regions of varying density in the 1-D case, and a vortex structure in the 2-D case. An analysis of vortex stability resulting from the use of the method of Imaginary Time Propagation is also provided. Finally, a consideration of the frequency regime, in which superradiance has been shown to occur within the hydrodynamic approximation [74], is used as a basis for determining simulation parameters for which superradiant scattering from a BEC vortex should be observed in the GP case.

7.1 One-Dimensional Simulation of Sound Wave Propagation in a BEC

7.1.1 Constant Density Background

Prior to performing two-dimensional simulations of scattering from a BEC vortex, the intermediate goal of observing sound waves propagating in a BEC in one dimension was instructive. That is, by first considering sound wave propagation in the one-dimensional case a clear understanding of the behaviour of such waves is obtained in advance of the complications introduced by an extra spatial dimension. As a result of this, one-dimensional simulations were conducted as a precursor to the higher dimensional case.

A sound wave is a small amplitude oscillatory motion in a compressible fluid, such as BECs, which causes compression and rarefaction as it propagates through the fluid [49]. More particularly, sound waves are linearised fluctuations around a given background field corresponding to modulations in the condensate density. One can use a wavepacket, that is, a weighted superposition of plane waves or modes, to model sound waves. In analytic work, sound waves are expressed as single frequency waves, however, in experiments and simulations it is more practical to make use of wavepackets. This is because one can obtain the additional information arising from the frequency spectrum and use it for diagnostic purposes. For instance, by taking the Fourier transform of a given wavepacket one can measure the amplitude of the

Fourier components of the wavepacket. Hence, in an investigation of superradiant scattering using a wavepacket to model sound waves, it is possible to determine amplification as a function of frequency.

In the one-dimensional simulation performed, the spatial dimension x had the domain $(-6.0 \times 10^{-5}$ m, -2.5×10^{-5} m) and a Gaussian modulated pulse was initialised at $x_o = -5.0 \times 10^{-5}$ m. Using XMDS and the RK4IP algorithm [25], the GP equation with $V_{trap} = 0$, was then integrated for $t = 0.8$ ms and the density, $\rho = |\psi|^2$, as a function of position was obtained.

In performing such simulations the time step was determined by the point at which numerical stability and accuracy is achieved. Accuracy is ensured by considering the sampling limit,

$$\pi \gg \frac{kL}{N_{grid}} \tag{7.1}$$

where k is the wavenumber and N_{grid} is the number of lattice points sampled in the domain of length L. This constraint is determined from the fact that the spatial lattice step Δx must be substantially less than $\lambda/2$, where λ is the wavelength of the propagating wave. This is known as the Nyquist sampling limit [19] and it acts as an upper limit to the cell size as it must be satisfied in order to adequately sample the spatial information. So one must reduce cell size to limit numerical error and this in turn determines the computational time. In other words, a large cell size decreases computational burden, but a compromise must be reached between this and minimising numerical error.

A plot of the perturbation on a constant density background, generated using MATLAB™, is shown in figure 7.1. This output was used to ensure consistency of the simulation results with expectations formed from a theoretical basis. The wavelength, corresponding to wavenumber $k = 1 \times 10^7$ m, is easily verified from this plot to be $\lambda = 6.3 \times 10^{-7}$ m, as expected. The Bogoliubov speed of sound [14, 51], given by,

$$c = \sqrt{\frac{\rho_o U_o}{m}} \tag{7.2}$$

was also verified for the scattering length $a = 5.29 \times 10^{-9}$ m, $m = 1.41 \times 10^{-25}$ kg and $\rho_o = 1 \times 10^{22}$ m^{-3} to be $c = 0.02$ ms^{-1}. These parameters are consistent with realistic BEC parameters for Rubidium-85 atoms. Furthermore, the amplitude of the initial perturbation was made small, to ensure that the perturbation was behaving as a sound wave, with the amplitude being approximately 0.1% of the background density.

The form of the initial Gaussian modulated pulse is given by,

$$\psi = \sqrt{\rho_o} + Ae^{-(x-x_o)^2/2\sigma^2}(u_k e^{+ikx} - v_k e^{-ikx}) \tag{7.3}$$

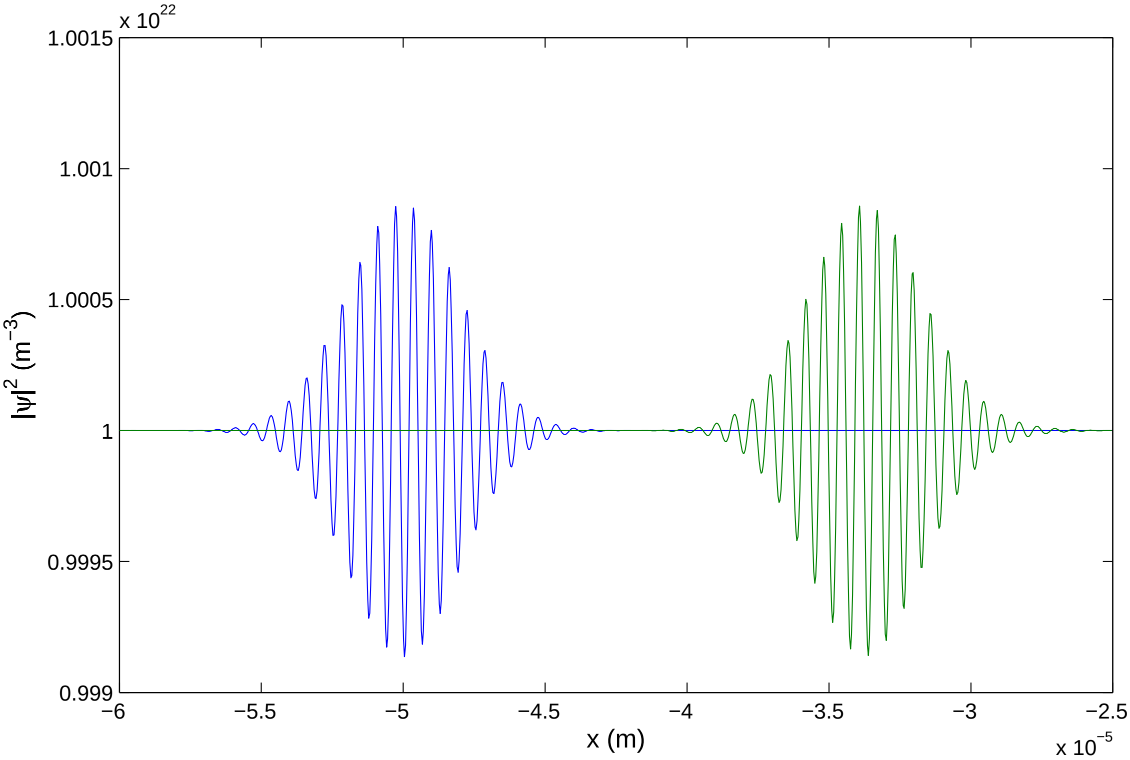

Figure 7.1: Propagation of sound wave travelling to the right at $c = 0.02$ ms^{-1} in a constant density background. The initial wavepacket, shown in blue, is centred at $x_o = -5.0 \times 10^{-5}$ m in the domain $(-6.0 \times 10^{-5}$ m, -2.5×10^{-5} m). The wavepacket shown in green, is for a time $t = 0.8$ ms later. The time step used in the simulation was $\Delta t = 1.6 \times 10^{-7}$ s, the cell size was $\Delta x = 4.3 \times 10^{-8}$ m where the number of spatial lattice points used was $N_{grid} = 2000$.

where u_k and v_k are the Bogoliubov coefficients [66] given in section 4.3.2, A is the wave amplitude, ρ_o is the background density, and x_o is the centre of the wavepacket. The Bogoliubov coefficients, calculated to be $u_k = 1.3641$ and $v_k = 0.9277$, are dependent on the wavenumber, and hence the wavelength of the sound wave. The Bogoliubov form of equation 7.3 was chosen to prevent the wavepacket splitting into two equal amplitude wavepackets propagating in opposite directions [2], after a given evolution time. That is, for the purposes of investigating scattering from the vortex-like geometry, this additional wavepacket was not required and for convenience the form of the initial perturbation was engineered to obtain one-way wave propagation in the constant density background.

A problem inherent in the model, is the sensitivity of the Bogoliubov coefficients. Although not obvious in the plots shown, the wave packet does split into two wave packets on propagation in the medium, with one being of substantially smaller amplitude. Hence, despite designing the model to permit only one way wave propagation, we do see a small degree of splitting when the wave propagates through the constant density medium. This effect, however, is not of huge concern as it is small and if the need arises could be eliminated by the use of absorbing boundary conditions.

7.1.2 Position Dependent Density Profile

Since the problem of superradiance in BECs involves scattering from BEC vortices it is valuable to consider a simplification of this scenario in the 1-D case to ensure that the underlying physics of sound waves travelling through an inhomogeneous medium is well understood. Therefore, although the concept of a vortex in 1-D is unrealistic, in the sense that a vortex is by definition a structure which rotates about an axis, studying this problem is still worthwhile.

The vortex-like density profile has the approximate form [66, 67],

$$\frac{|x/\xi|}{\sqrt{2+(x/\xi)^2}} \tag{7.4}$$

where ξ is the healing length of the condensate far from the vortex, as discussed in section 4.4. From this it follows that the vortex density ρ_{vortex} is given by,

$$\rho_{vortex} = \rho_o\Big(\frac{|x/\xi|}{\sqrt{2+(x/\xi)^2}}\Big) \tag{7.5}$$

where ρ_o is the background density, that is, the density far from the vortex. The background density profile corresponding to equation 7.5 is shown in figure 7.2.

In order to incorporate a vortex-like structure into the model, it was necessary to reformulate the GP equation in terms of the vortex density. More specifically, to implement a density profile which varies as a function of position, one cannot simply insert a static density profile in the expression for the initial perturbation. This is due to the fact that the profile will not be preserved as in the 1-D case it becomes unstable as time proceeds.

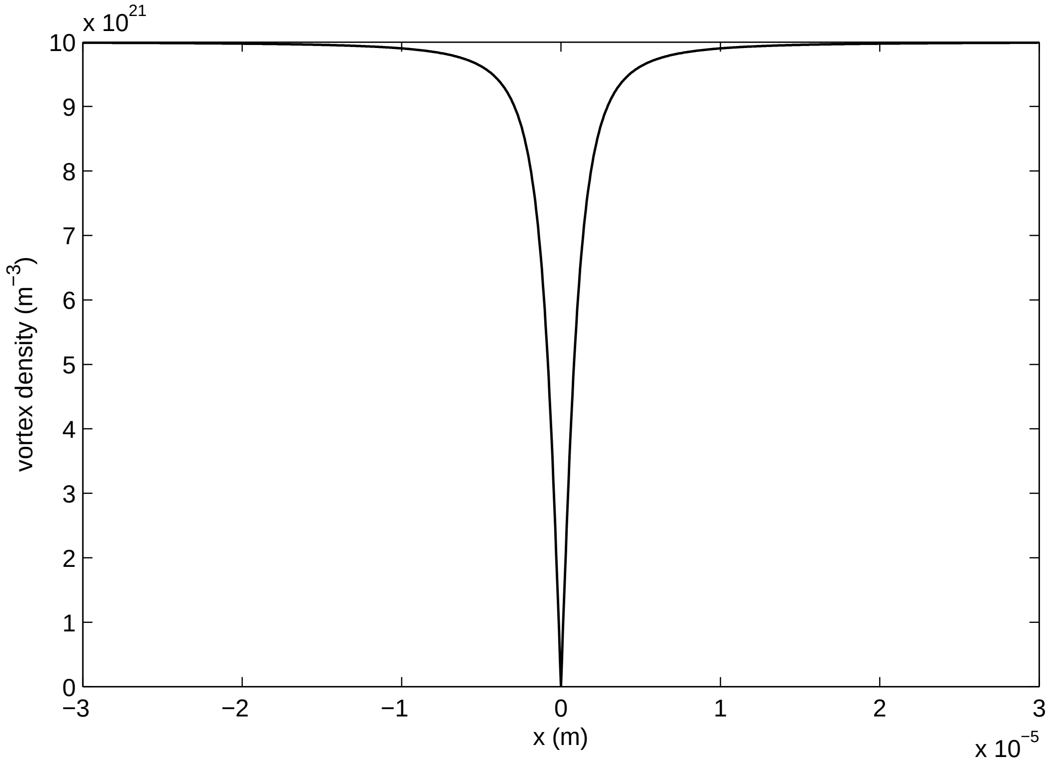

Figure 7.2: Plot of the background density of the vortex-like structure.

To write the GP equation in terms of ρ_{vortex}, the total condensate wavefunction can be expressed as $\psi = B + \epsilon\tilde{\psi}$ where B is the background field, $\epsilon\tilde{\psi}$ is some perturbation to the field and $\epsilon \in \mathbb{R}^+$ and $\epsilon << 1$. Hence, the GP equation can be written as,

$$i\hbar\frac{\partial(B+\epsilon\tilde{\psi})}{\partial t} = \Big(-\frac{\hbar^2\nabla^2}{2m} + V_{trap} + U_o\left|B+\epsilon\tilde{\psi}\right|^2\Big)(B+\epsilon\tilde{\psi}) \tag{7.6}$$

In our model, no trapping potential has been incorporated for simplicity and hence, $V_{trap} = 0$. Considering B as a time-dependent background field with no spatial dependence, of the form,

$$B = |B|e^{-i\mu t/\hbar} \tag{7.7}$$

where $\mu = |B|^2 U_o$ is the chemical potential, the GP equation becomes,

$$i\hbar\frac{\partial\epsilon\tilde{\psi}}{\partial t} = -\mu B - \frac{\hbar^2}{2m}\nabla^2\epsilon\tilde{\psi} + U_o(|B|^2B + \epsilon(B^2\tilde{\psi}^* + 2|B|^2\tilde{\psi})) \tag{7.8}$$

where the interaction term is calculated as follows,

$$\begin{aligned} |\psi|^2 \psi &= \left|B + \epsilon\tilde{\psi}\right|^2 (B + \epsilon\tilde{\psi}) \\ &= (B + \epsilon\tilde{\psi})(B^* + \epsilon\tilde{\psi}^*)(B + \epsilon\tilde{\psi}) \\ &\approx |B|^2 B + \epsilon(B^2\tilde{\psi}^* + |B|^2\tilde{\psi} + |B|^2\tilde{\psi}). \end{aligned} \tag{7.9}$$

and $\nabla^2 B$ is assumed small compared to the interaction term, and hence neglected. Since $-\mu B = U_o|B|^2 B$, equation 7.8 becomes,

$$i\hbar\frac{\partial\tilde{\psi}}{\partial t} = -\frac{\hbar^2}{2m}\nabla^2\tilde{\psi} + U_o(B^2\tilde{\psi}^* + 2|B|^2\tilde{\psi})) \tag{7.10}$$

or equivalently,

$$i\hbar\frac{\partial\tilde{\psi}}{\partial t} = -\frac{\hbar^2}{2m}\nabla^2\tilde{\psi} + U_o|B|^2(e^{-2i\mu t/\hbar}\tilde{\psi}^* + 2\tilde{\psi}) \tag{7.11}$$

where $\rho_{vortex} = |B|^2$. This result was then implemented in a discretised form using XMDS, and hence it was possible to generate plots of the density $\rho = |\psi|^2$ as a function of position for a sound wave propagating in the non-uniform density background.

7.1.3 Interaction with the Vortex-like Structure: Reflection due to Non-uniform Density

The next stage in the simulation process was to incorporate the spatially varying profile specified in equation 7.5 and to characterise the interaction between the wavepacket and the vortex-like geometry. For completeness, an example of the XMDS code used for this purpose, is given in appendix A.1.

The parameters used in the simulations were the same as in the constant density case, with the exception of the spatial domain of $(-2.5 \times 10^{-5}$ m, 0.5×10^{-5} m) and the position of the initial wavepacket $x_o = -1 \times 10^{-5}$ m. A plot of the initial perturbation is given in figure 7.3 with the vortex-like core located at $x = 0$ m. In addition, the total propagation time was increased to 1.0 ms in order to observe the entirety of the interaction, and this necessitated increasing the number of lattice points to maintain numerical stability.

The plots in figure 7.4 provide an overview of the results of the simulation of the wavepacket impinging on the vortex-like profile. The plots are generated at different times during the propagation and the wavepacket is moving in the positive x-direction. The numerical stability of the results is verified by confirming that the behaviour of the wave remains invariant with respect to changes in the number of spatial and temporal lattice points. A video file of this simulation, named vortex1D.avi, accompanies this thesis and provides a more intuitive presentation of the data as the evolution of the wavepacket in time can be observed directly. From the plots in figures 7.4, it is seen that the wavepacket interacts with and reflects from the region of varying density. This is in agreement with the well known behaviour of the response of a sound wave to a change in the density of the transmission medium [49].

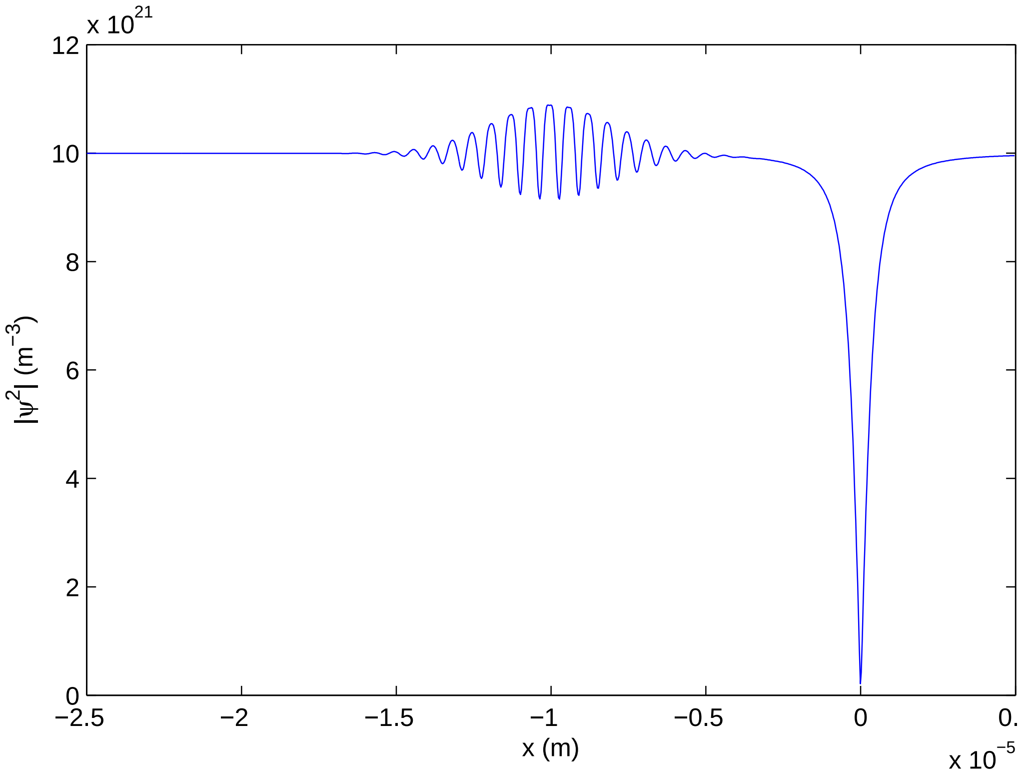

Figure 7.3: Plot of the initial perturbation centred at $x_o = -10$ μm and the vortex-like profile centred at the origin. The numerical parameters are $\Delta t = 1 \times 10^{-7}$ s, $\Delta x = 1.5 \times 10^{-8}$ m and $N_{grid} = 2000$. The amplitude of the perturbation has been magnified by a factor of 100 for visualisation purposes, as described in section 7.1.3.

It should be mentioned, that the plotted quantity in the simulations performed is the density. However, because the amplitude of the perturbation is small, compared to the background density used in the computation, the amplitude of the perturbation needed to be scaled in order to observe the behaviour of the wavepacket impinging on the region of varying density. Moreover, the wavefunction can be written in the form $\psi = B + \alpha\epsilon\tilde{\psi}$, where B is the background field, $\epsilon\tilde{\psi}$ is some perturbation to the field, $\epsilon \in \mathbb{R}^+$ and $\epsilon << 1$, and α is a scale factor which increases the size of the sound wave for visualisation purposes. Hence, one can output the density as,

$$\begin{aligned}\rho &= (B + \alpha\epsilon\tilde{\psi})(B^* + \alpha\epsilon\tilde{\psi}^*) \\ &= |B|^2 + \alpha\epsilon(B\psi^* + B^*\psi) + \alpha^2\epsilon^2|\psi|^2 \qquad (7.12)\end{aligned}$$

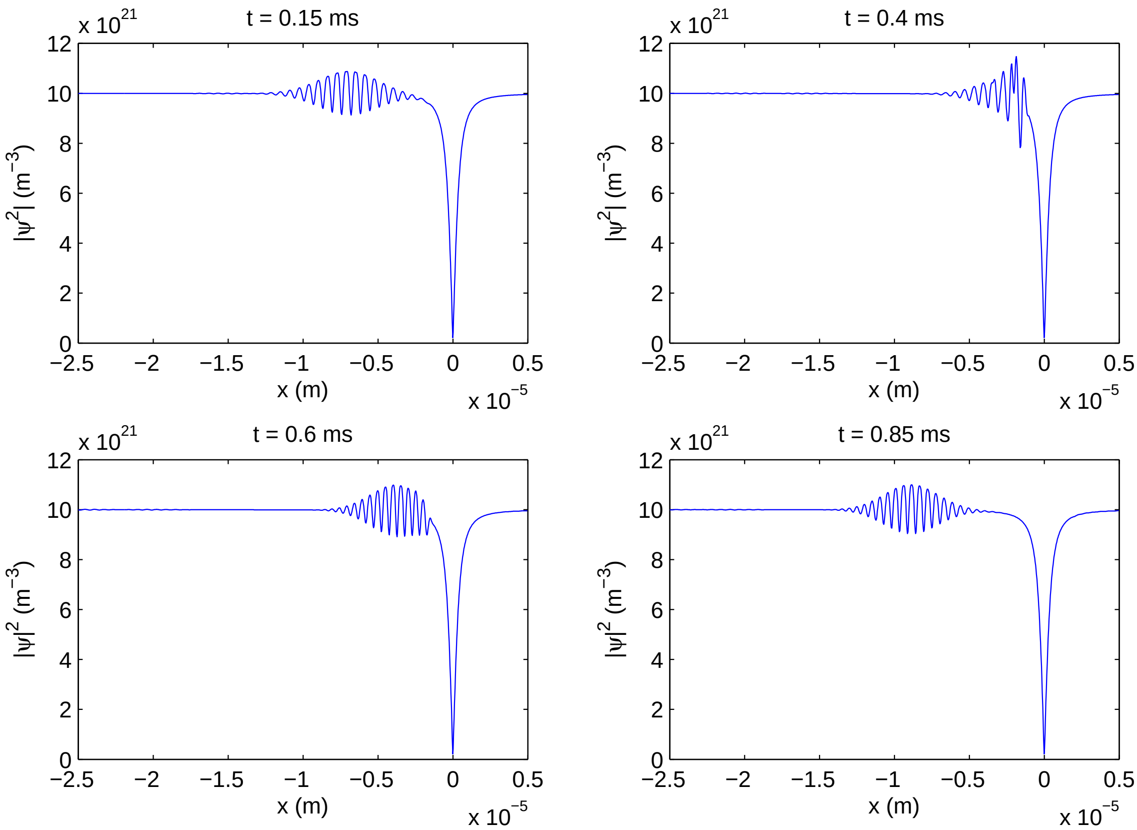

Figure 7.4: Plot of the wave packet, initialised as in figure 7.3, propagating in the non-uniform density background. The wave is seen impinging on the vortex-like structure at t=0.15 ms and t=0.4 ms. At t=0.6 ms, the wave packet has been reflected from the vortex-like structure. The reflected wave packet is shown at t=0.85 ms. The numerical parameters correspond to those used to generate the plot of the initial perturbation in figure 7.3.

The term $O(\epsilon^2)$ can be neglected, as usual, provided that the scale factor is not too large. In the results obtained a scale factor of $\alpha = 10^2$ was used, increasing the amplitude of the perturbation by a factor of 100 and this was sufficient to clearly observe the evolution of the wavepacket.

7.2 Two-Dimensional Simulation of Sound Wave Propagation in a BEC

This section provides an account of the results obtained from simulations investigating the propagation of sound waves in a BEC in the two-dimensional case. In turn these efforts put in place the foundations for studying scattering from a BEC vortex. The main components of such simulations include incorporating a vortex structure in the constant density background, ensuring the vortex is stable during the evolution, implementing the initial state of the perturbation and observing propagation of the wavepacket.

7.2.1 The Vortex Background

In order to construct a BEC vortex the density profile discussed in section 4.4, and of a similar form to the profile used in the one-dimensional case, was implemented in a two-dimensional grid with domain $(-15 \times 10^{-6}$ m, 15×10^{-6} m$)$. In particular, the vortex is initialised as the background field,

$$\psi_B = \sqrt{\rho_o}\frac{r/l\xi}{\sqrt{2 + (r/l\xi)^2}}e^{il\theta} \tag{7.13}$$

with density profile,

$$\rho = \rho_o\frac{(r/l\xi)^2}{2 + (r/l\xi)^2} \tag{7.14}$$

and where the phase factor $e^{il\theta}$ ensures angular momentum is incorporated into the model and l is the winding number, or charge, of the vortex [66]. For the purposes of this thesis, only vortices with vortex charge $l = 1$ are considered. This is justified by the fact that higher l vortices are unstable and split into l, $l = 1$ vortices [61], which although possible to stabilise using vortex pinning are not very practical from an experimental perspective. It should be stressed that the profile represented by Equation 7.14 provides only an approximate form of the numerically generated vortex profile discussed in section 4.4 and 6.3.

A vortex structure, representative of those used in this work, is provided by the plot of the vortex background given in Figure 7.5. In the two-dimensional simulations performed, the adaptive time step algorithm ARK45IP [25], discussed in section 6.2.1 as a method for controlling the error per step, is used to circumvent the need to manually determine the optimal time step. Throughout the investigation outlined in this chapter, invariance of the results for different tolerance values was used to verify accuracy of the simulation results. Furthermore, spatial sampling was considered with simulation results verified as accurate by checking for invariance under change in the number of spatial lattice points.

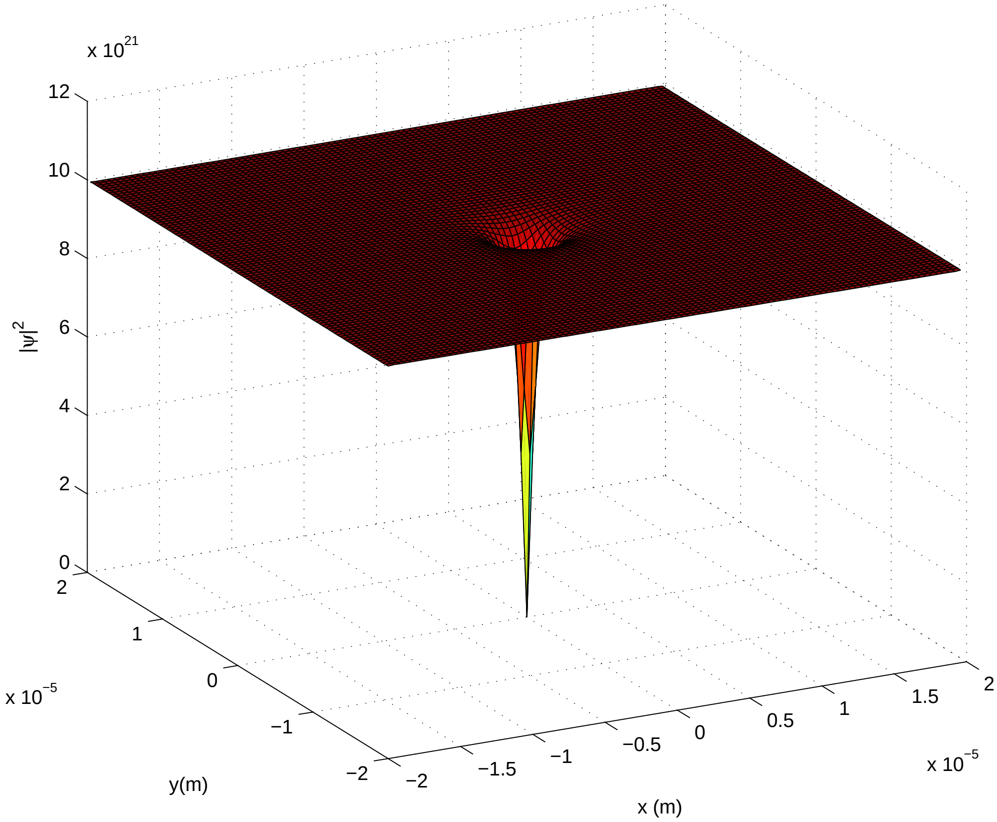

Figure 7.5: Two-dimensional image of the initial background density for the vortex geometry. The domain is $(-20 \times 10^{-6}$ m, 20×10^{-6} m) and the density far from the vortex is $\rho_o = 10^{22}$ m^{-3}.

An investigation of vortex stability during time evolution was undertaken for the vortex background shown in figure 7.5. The vortex was observed to become unstable as time progresses. As a consequence, it is necessary to develop a method for achieving a vortex background that preserves its initial form over time.

Another issue apparent in this analysis was unphysical effects on the boundary of the domain. This can be attributed to the phase discontinuity arising due to the presence of the vortex and the fact that periodic boundary conditions are defined at the domain boundary. That is, the numerical method tries to force the edges opposite each other to have the same value but this not possible because of the phase variation of the vortex. During the evolution, these boundary effects grow and hence need to be eliminated if one is to perform accurate simulations. The solution to both of these problems is discussed in sections 7.2.2 and 7.2.3.

7.2.2 Vortex Stability using Imaginary Time Propagation

The method of Imaginary Time Propagation is used in the simulations for the purposes of obtaining a vortex structure in the otherwise uniform density medium. To observe the interaction of sound waves with the BEC vortex one requires sufficient real time propagation. When using the ITP method, the amount of imaginary time evolution must be large enough to ensure convergence to the ground state for a given real time propagation. Hence, one must determine the optimal value for the imaginary time so that convergence is achieved but computational burden is minimised.

To verify that the amount of imaginary time propagation is sufficient for ensuring the ground state of the system has been obtained, it is necessary to confirm the convergence of the solution. In this investigation, a 128×128 grid was used to keep computation time at a minimum. The GP equation describing the real time evolution and given by equation 4.10, was expressed using $t \mapsto -it$, as,

$$\frac{\partial \psi(\mathbf{r},t)}{\partial t} = \Big(\frac{\hbar \nabla^2}{2m} - \frac{V_{trap}}{\hbar} - \frac{U_o\,|\psi(\mathbf{r},t)|^2}{\hbar}\Big)\psi(\mathbf{r},t) \tag{7.15}$$

and this was then solved numerically using a renormalisation procedure to preserve the norm of the wavefunction throughout the imaginary time evolution. For a total imaginary propagation time of $t_i = 8 \times 10^{-5}$ s, the total number of atoms,

$$N = \int |\psi|^2 dxdy \tag{7.16}$$

was found to converge to $N = 8.9490 \times 10^{10}$, after renormalisation, as revealed by the plot in figure 7.6. The number of atoms was calculated in XMDS by summing the amplitudes at each spatial lattice point throughout the imaginary time evolution. The initial drop from the starting norm of $N = 8.9501 \times 10^{10}$ occurs after the first iteration of the imaginary time evolution and then the solution proceeds to relax to the ground state, as indicated by the constant renormalised N.

An image of the initial state used in the imaginary time evolution is provided in Figure 7.7. The density far from the vortex $\rho_o = 10^{20}$ m^{-3} is chosen so that the radius of the vortex is large enough so that computational problems do not arise when waves impinge on the vortex. More specifically, since $\xi \propto 1/\sqrt{\rho}$, a decrease in the density increases the healing length and hence the size of the vortex. Figure 7.8 shows the vortex background after convergence to the ground state. That is, it represents the initial state used as input in the real time propagation. A potential defined over the domain forces the density to zero at the boundaries and hence the boundary effects are eliminated. This is explained in section 7.2.3.

The output of the imaginary time evolution was then used as an initial state for the real time evolution, with a real time propagation of $t_r = 1 \times 10^{-4}$ s. Appendix B.1 and Appendix B.2 provide examples illustrative of the XMDS code used

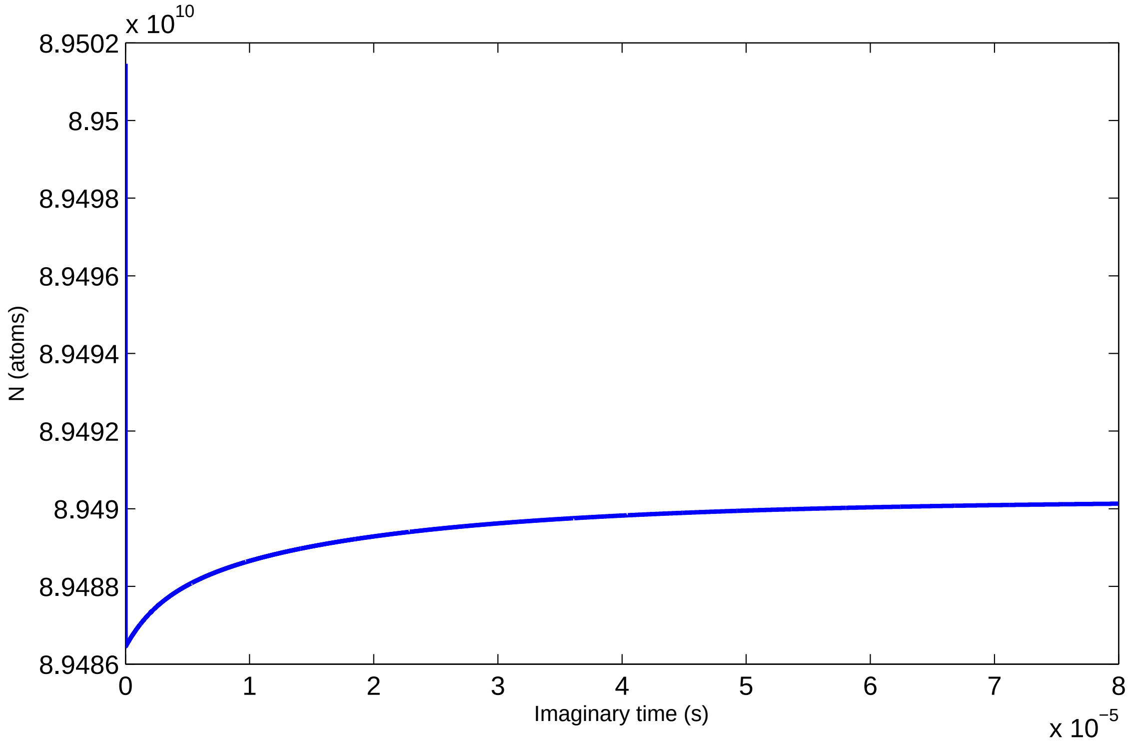

Figure 7.6: Convergence to the ground state of the system using the Imaginary Time Propagation method. As t_i increases, $N \rightarrow 8.9490 \times 10^{10}$ and hence the solution has converged to the ground state. In the simulation an integration time of 1×10^{-8} s is used and 8000 cycles of the imaginary time sequence are performed, yielding $t_i = 8 \times 10^{-5}$ s. Also, $N_{grid} = 128$ and the ARK45IP algorithm [25] is used with a tolerance of 1×10^{-6}.

for the imaginary time and real time evolution, respectively. From the previously established convergence behaviour, and the fact that the output after t_r real time propagation is seen to preserve the vortex background depicted in figure 7.8, it can be concluded that the method was successful in generating an initial state capable of producing a stable vortex background for the amount of time required to observe propagation of a wavepacket into the vortex.

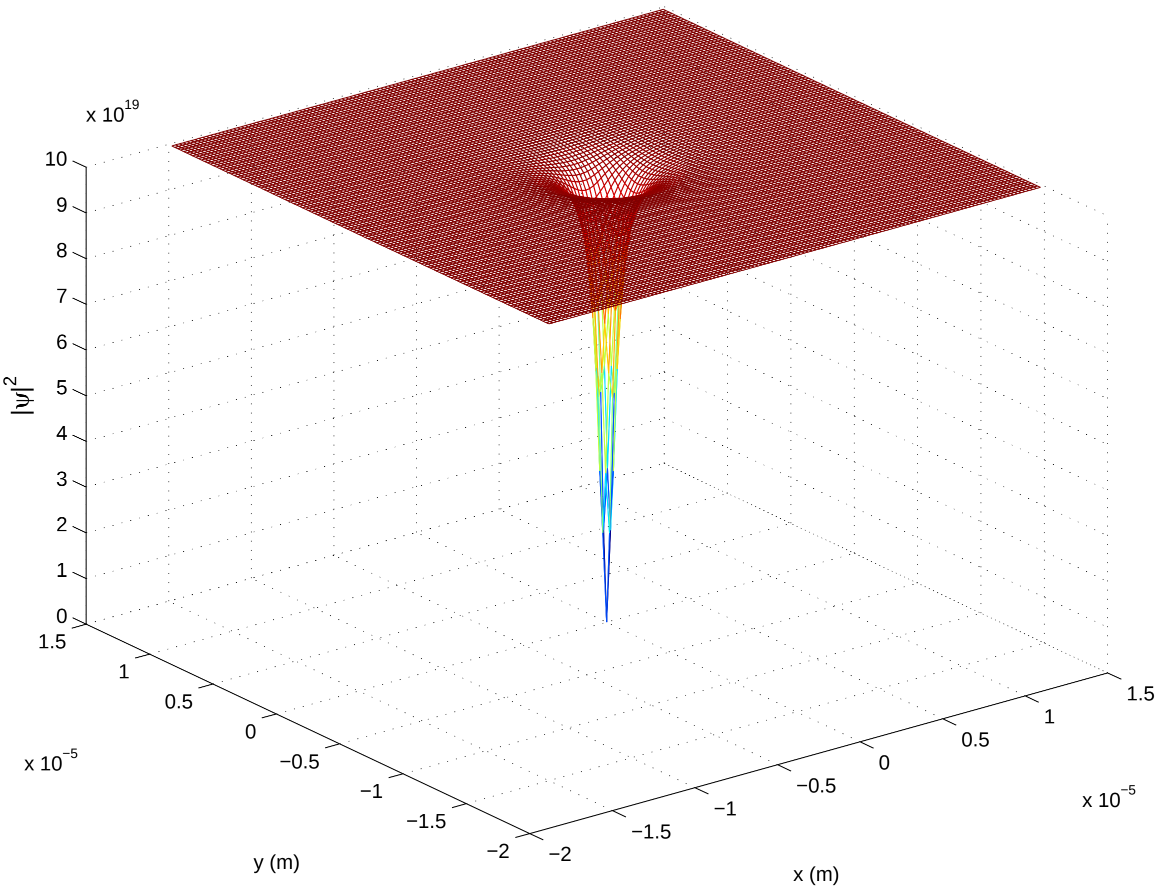

Figure 7.7: Background field describing the vortex geometry used as the initial state for the imaginary time evolution. A 128^2 grid is used along with a density of $\rho_o = 10^{20}$ m^{-3} to ensure a large vortex radius was obtained after convergence to the ground state.

7.2.3 Elimination of Domain Boundary Effects

As mentioned in section 7.2.2, the need to eliminate the unphysical edge effects, observed at the boundary of the computational domain during real time evolution, is an issue of great importance to ensuring the accuracy of the simulation results. In particular, these effects grow as the solution evolves and cause problems in the interior of the grid, in addition to the edges.

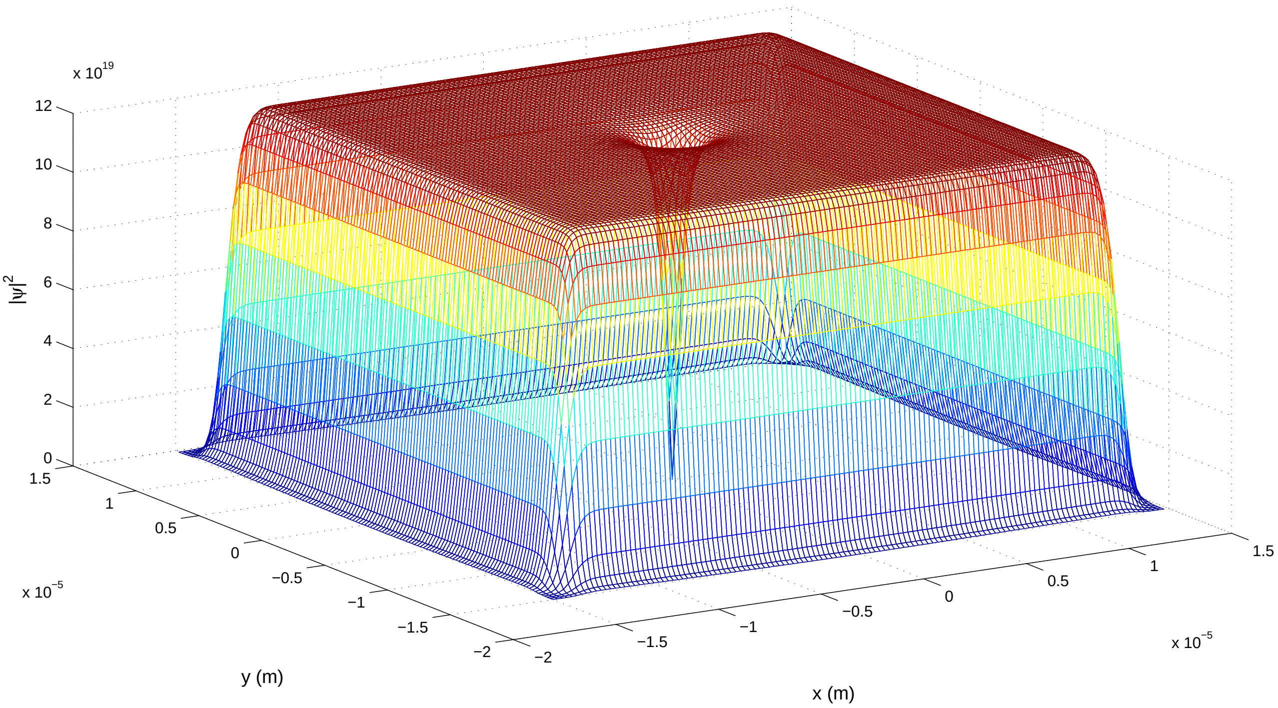

Figure 7.8: Image of the vortex background after convergence to the ground state, corresponding to the parameters in the plot of figure 7.6 with $N_{grid} = 128$. This output from the imaginary time XMDS script, with $t_i = 8 \times 10^{-5}$ s, is used as input in the real time evolution XMDS script, with $t_r = 1 \times 10^{-4}$ s. The vortex remains stable for the duration of the real time evolution as desired. The parameters in the potential are $V_o = 2 \times 10^{-30}$ m^{2}kgs^{-2}, $s = 1 \times 10^{-6}$ m and $L = 15 \times 10^{-6}$ m.

In figure 7.8, the effects at the boundary have been suppressed with the intention of allowing one to obtain accurate simulations of sound waves interacting with the BEC vortex. The form of the potential used for this purpose is given by,

$$V = V_o(e^{-(L-|x|)^2/s^2} + e^{-(L-|y|)^2/s^2}) \tag{7.17}$$

where $L = 15 \times 10^{-6}$ m and the grid goes from $(L, -L)$ in each dimension, $V_o = 2 \times 10^{-30}$ m^{2}kgs^{-2} is the amplitude of the potential and $s = 1 \times 10^{-6}$ m is the length scale over which the potential decays. This works as a potential barrier making the density fall off rapidly to zero over a small distance in from the grid boundary on all edges. Thus, the effectiveness of the potential in eliminating the effects that arise due to the violation of the periodic boundary conditions is apparent. Hence, this leaves the majority of the domain unaffected except for a 20% increase in density over the entire domain due to the boundary potential. This does not present a problem, however it is necessary to be aware of the actual density of $\rho_o = 1.2236 \times 10^{20}$ m^{-3} when incorporating sound waves into the simulations.

7.2.4 Initial Perturbation

The first consideration when implementing sound waves in the computational domain is to ensure that the perturbations are representative of phonon behaviour. In particular, it is necessary to choose a sufficiently low wavenumber so that the waves are described by the phonon-like region of the Bogoliubov dispersion curve. The transition between phonon and free particle behaviour occurs when the wavenumber is equal to the inverse of the healing length. For example, figure 7.9 shows the dispersion curve for a density of $\rho_o = 3.03 \times 10^{20}$ m^{-3} where the phonon region exhibits a linear relationship between energy and momentum below $p \approx \hbar/\xi$. The healing length can be calculated from the density, using equation 4.52, and hence one is able to ensure phonon-like behaviour by selecting a wavenumber below the relevant cutoff.

With this in mind, to incorporate sound waves into the model the wave function is written as the sum of the contribution of the background field ψ_B and the perturbative field ψ_S, that is,

$$\psi = \psi_B + \psi_S. \tag{7.18}$$

Two forms of initial perturbations were used in order to observe scattering of sound waves from a BEC vortex. In the simulations performed both Gaussian plane waves and a Gaussian ring source were implemented by using appropriate forms of ψ_S to investigate fluctuations in a BEC vortex system.

Gaussian Plane Wave

A Gaussian plane wave was initialised in the grid using,

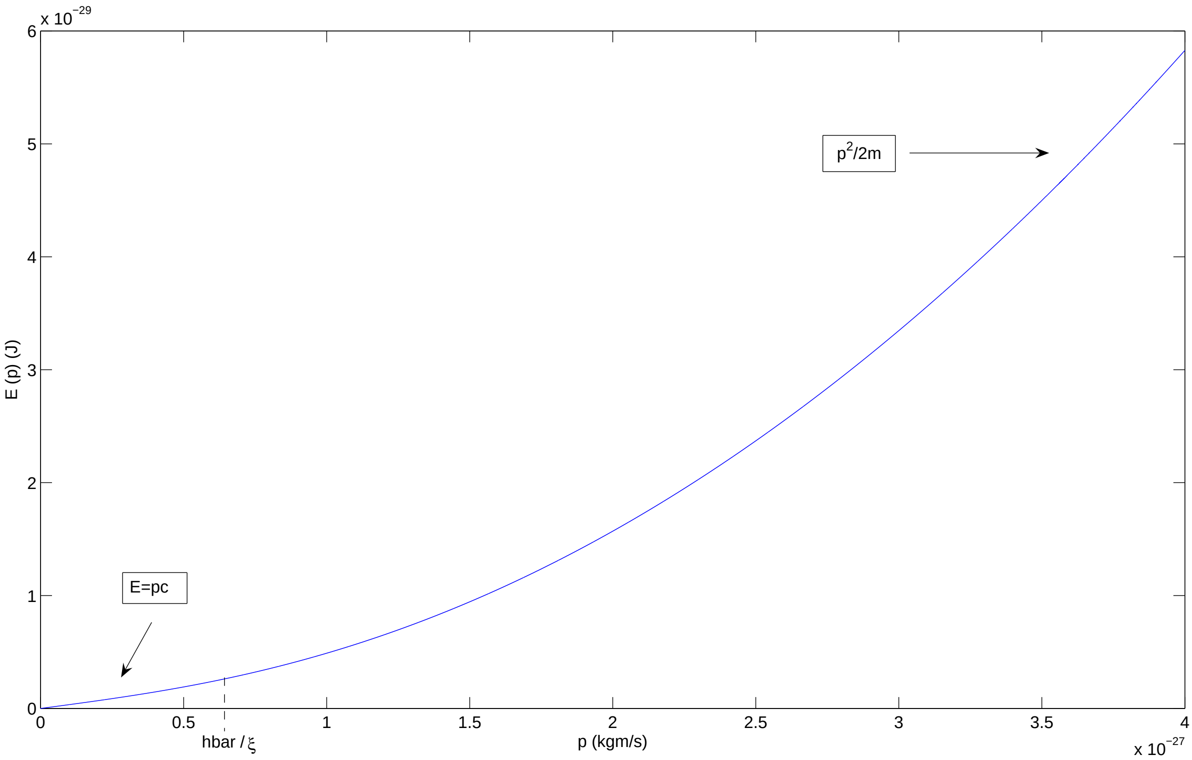

Figure 7.9: The Bogoliubov dispersion curve of elementary excitations, plotting energy E as a function of momentum p as described by equation 4.47, for $\rho_o = 3.03 \times 10^{20} m^{-3}$ and $a = 5.29 \times 10^{-9}$ m. The transition between phonon and free particle behaviour occurs at $p \approx \hbar/\xi$ that is, $p \approx 6.34 \times 10^{-28}$ kgms^{-1}.

$$\psi = \psi_B + Ae^{-(r-r_o)^2/2\sigma^2}(u_k e^{ikr} - v_k^* e^{-ikr}) \tag{7.19}$$

where the Bogoliubov coefficients u_k and v_k are obtained as in the one-dimensional case, A is the amplitude of the perturbation, σ is the spread of the wavepacket, k is the wavenumber and r_o defines the centre of the wavepacket.

Gaussian Cylindrical Wave

A cylindrical Gaussian wave can also be implemented in the computational domain using the form,

$$\psi = \psi_B + Ae^{-(r-r_o)^2/2\sigma^2}(u_k e^{ikr} - v_k^* e^{-ikr})e^{im\theta} \tag{7.20}$$

where $e^{im\theta}$ provides angular variation and m is the angular wavenumber. Thus, this ring shaped wavefunction is Gaussian in the radial direction and has only a phase variation in the angular direction. In all the simulations performed a value of $m = 1$ is used.

7.3 Sound Wave Impinging on a BEC Vortex

This section provides an overview of efforts to observe reflection from a BEC vortex and to determine whether superradiance occurs in the relevant frequency regime.

7.3.1 Verifying the Accuracy of Simulation Results

Throughout the simulation process various methods are used to provide an indication of simulation accuracy. Firstly, the discretisation of time and space domains can introduce errors and therefore requires attention. The optimal time step is determined using the adaptive step size algorithm. In order to verify that the time step is small enough to produce accurate simulation results the tolerance, or error threshold, was altered. By confirming invariance of the results for such changes it was possible to ensure that the time step is a not source of error.

It was also necessary to consider whether the lattice point separation is small enough to accurately model the variation of the field throughout the domain. This is of particular importance in the vortex region, where spatial discretisation error could occur as the wavelength of sound waves decreases with density. Hence, the decreasing density as one approaches the vortex core means that a greater number of lattice points over this region are required to correctly model the propagation of sound waves. However, as usual a compromise between this and computational expense needs to be made. For the purposes of this work, a 1024×1024 grid is found to provide sufficient sampling throughout the domain for the wave frequencies we wish to model. This was determined by checking that the solution remained the same despite changing the number of spatial lattice points.

Another method used to assess the accuracy of the simulation results involves verifying that the results agree with the known characteristics of sound wave propagation. This includes verifying that the speed of sound is consistent with that derived from theoretical results. Further quantitative checks can be made by monitoring certain parameters during the evolution. For example, throughout the real time evolution the norm of the wavefunction, discussed in section 7.2.2, should be constant in time. The features of a vortex include that the density drops off to zero at the core of the vortex whilst the phase of the condensate varies from 0 to 2π as $e^{-i\mu t}$. Whilst, the zero density core is obvious from surface plots such as figure 7.8, the latter is verified during the real time evolution by plotting the phase throughout the computational domain, with the phase seen to vary from π to $-\pi$ as shown in figure 7.10. The effectiveness of the imaginary time propagation method can be further verified by evolving the solution in real time and checking for evidence of non-convergence, that is, collective motion emanating from the vortex.

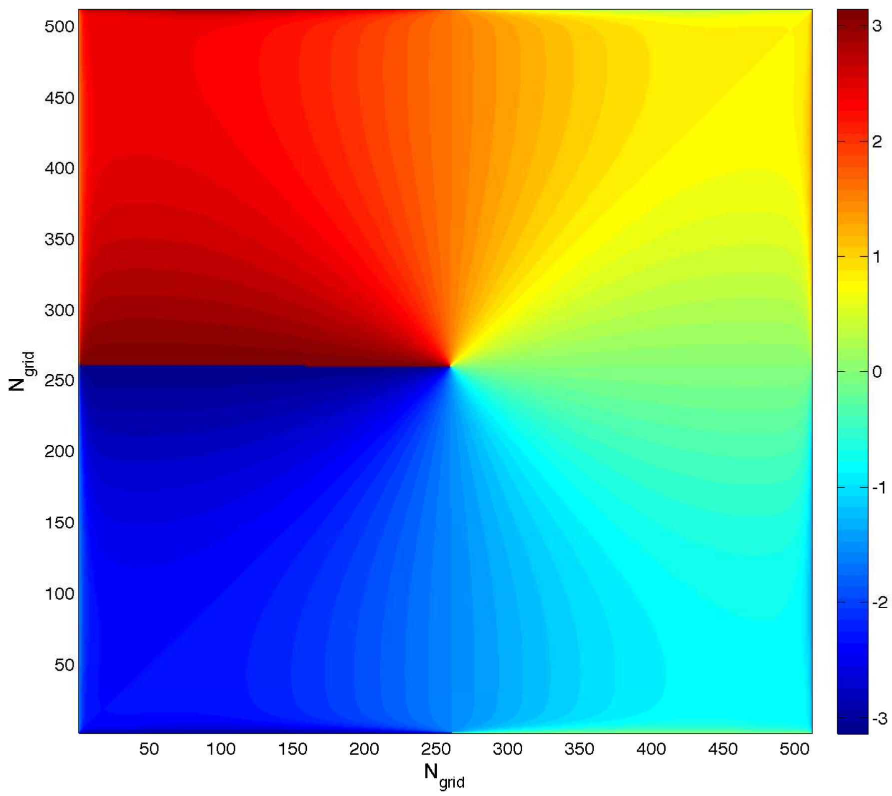

Figure 7.10: Plot of the phase variation around the vortex core after the imaginary time evolution. In this case, the computational grid is generated using $N_{grid} = 512$ lattice points.

7.3.2 Reflection from a BEC Vortex

As in the one-dimensional case, preliminary investigations of reflection from a BEC vortex indicated that the point of reflection from the vortex structure varies with vortex parameters. In particular, an increase in the condensate density far from the vortex corresponds to a decrease in healing length and this yields a smaller vortex core. In turn, this leads to reflection as the density change is more pronounced. Hence, simulations revealed the need to compromise between generating reflection and the computational expense in obtaining a narrow vortex using the method of Imaginary Time Propagation. The computation time increases as the vortex diameter decreases because the number of time steps and the number of lattice points must be increased if one is to effectively simulate these small scale features.

For the vortex parameters described in section 7.2 with $\rho_o = 1.2236 \times 10^{20}$ m^{-3} an analysis of reflection and its dependence on the size of the vortex core was made by comparing to higher density cases. Reflection was observed for this case, however, it occurred further into the vortex and consequently within the real time of $t_r = 1 \times 10^{-4}$ s for which the vortex background was stable the reflected wave only just started to emerge from the vortex. As a result of this investigation, a density of $\rho_o = 3.027 \times 10^{20}$ m^{-3} was used instead of $\rho_o = 1.2236 \times 10^{20}$ m^{-3} which meant that the topological ground state had to be found for the new parameters. To summarise, the reason for choosing this higher density was because of the advantages arising from the resulting increase in the speed of sound in the condensate, which enables one to simulate the entirety of the interaction with the vortex within the real time evolution. Furthermore, the phonon frequency threshold for such densities is increased making the sound waves easier to model in the domain of $(-15\times10^{-6}$ m, 15×10^{-6} m$)$ used in the simulations.

A more thorough analysis of the imaginary time parameters required to achieve convergence to the topological ground state was conducted for the $\rho_o = 3.027 \times 10^{20}$ m^{-3} case, with parameters $V_o = 2 \times 10^{-30}$ $\mathrm{m^2kgs^{-2}}$ and $s = 2 \times 10^{-6}$ m used in specifying the potential. Initially, great difficultly was met in finding the converged solution with ripples in the vortex background after the real time evolution indicating collective motion, a signature of non-convergence. As a result, the convergence behaviour for a range of values for the number of cycles through the imaginary time evolution and the imaginary time per cycle, t_i, was investigated. It was found that the total imaginary time must be comparable to the desired duration of the real time evolution t_r. Furthermore, t_i is sensitive to the variation in density and in particular the density variation during each cycle cannot be too large relative to t_i. Failure to meet such criteria results in lack of convergence. With these findings it was possible to generate a converged $l = 1$ BEC vortex, using 35000 cycles and $t_i = 1 \times 10^{-7}$ s, which in turn preserved the form of the vortex background for a real time evolution of duration $t_r = 2$ ms. A 1-D slice of the converged vortex background is shown in figure 7.11.

Prior to implementing a Gaussian-enveloped cylindrical wave in the computational domain various calculations were performed to find the wavenumber for which phonon behaviour will be observed. In particular, for the density $\rho_o = 3.027 \times 10^{20}$ m^{-3} sound waves are generated for $k_{sound} < \xi^{-1} = 6.34 \times 10^{6}$ m^{-1}. Despite

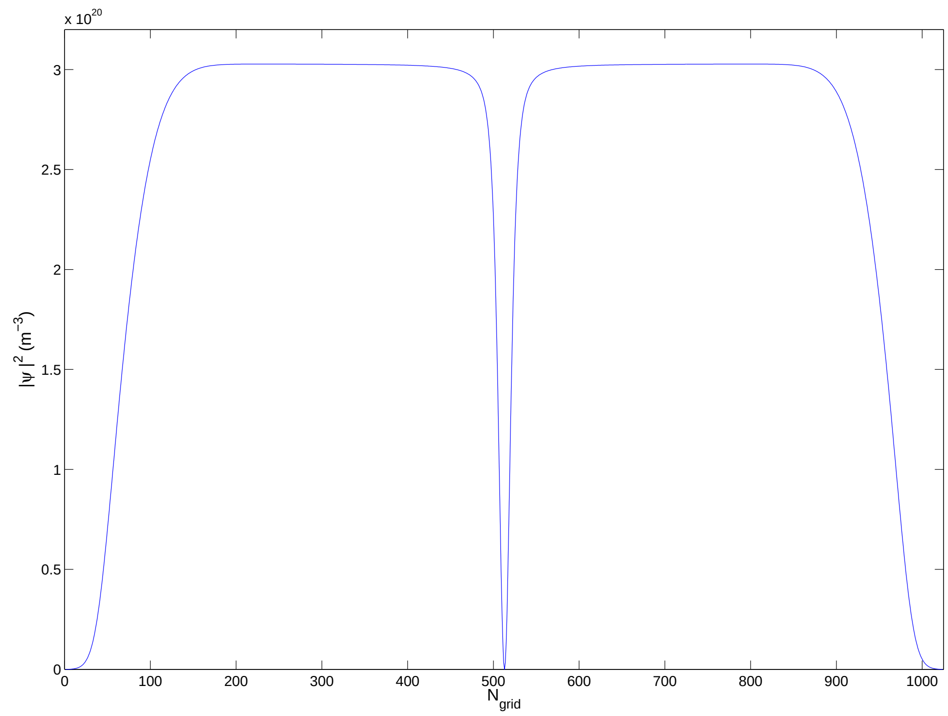

Figure 7.11: Stable vortex background obtained using imaginary time propagation with 35000 cycles through the imaginary time evolution with $t_i = 1 \times 10^{-7}$ s. The vortex background preserves this profile for a real time evolution of $t_r = 2$ ms. The density far from the vortex is $\rho_o = 3.027 \times 10^{20}$ m^{-3}. The potential is implemented with parameters $V_o = 2 \times 10^{-30}$ m^{2}kgs^{-2} and $s = 2 \times 10^{-6}$ m. The domain is $(-15 \times 10^{-6}$ m, 15×10^{-6} m) and $N_{grid} = 1024$.

this, initial simulations used a wavenumber of $k = 1 \times 10^7$ m^{-1} as such waves were investigated in the 1-D case. Hence, the following simulation results are not representative of pure sound waves but are described by the transition between the phonon regime and the free-particle regime of the Bogoliubov excitation spectrum, shown for the density under consideration in figure 7.9. The Bogoliubov coefficients for this particular wavenumber were found in the usual manner to be $u_k = 1.1321$ and $v_k = 0.5307$. Unfortunately, due to the density gradient as one approaches the vortex core, suppression of the outgoing wavepacket resulting from the splitting of the initial wavepacket was not achieved. That is, attempts to model a purely ingoing wavepacket using the Bogoliubov coefficients were unsuccessful on the non-constant density background. However, this was not an major issue in the simulations as the wave was slowed at the boundary due to the fact that the density drops off rapidly to zero. It should be noted, that this steep drop to zero density has the disadvantage that reflection from the boundary occurs toward the end of the real time evolution. However, reflection from the vortex is observed prior to any complications introduced by these boundary reflections.

Using the parameters described above, reflection from a charge $l = 1$ BEC vortex was observed for the case of density $\rho_o = 3.027 \times 10^{20}$ m^{-3} and an incoming cylindrical wave with $k = 1 \times 10^7$ m^{-1}. Although outside the low frequency regime describing phonon propagation these results are included to demonstrate general reflection from a BEC vortex. They also indicate the potential of the model for analysing reflection in the phonon regime, and moreover the superradiant regime, discussed in section 7.3.4.

The simulation was performed using a 1024^2 grid to ensure adequate spatial sampling. A total real time evolution of $t_r = 2$ ms was used. The two-dimensional surface plot in figure 7.12 shows the incoming Gaussian-modulated wave, initially centred at $r_o = 6 \times 10^{-6}$ m with spread $\sigma = 1 \times 10^{-6}$ m, after $t = 0.33$ s. Figure 7.13 shows samples of the density throughout the domain at four different times during the real time evolution in order to provide greater details of the reflection. The first image shows the wavepacket at $t = 0.11$ ms prior to splitting into an outgoing and ingoing wave. At $t = 0.33$ ms the wavepackets have split and the ingoing wave is beginning to interact with the vortex. At $t = 0.55$ ms and $t = 0.88$ ms the wave continues to make its way further into the vortex, decreasing its wavelength as it approaches the vortex core. Figure 7.14 provides four more images at later times in the simulation. At $t = 0.99$ ms the wave starts to reflect from the vortex and continues to propagate away from the vortex for later samples. By comparing the incoming and reflected wave form imaged in figures 7.13 and 7.14 one can see that the form of the wave is preserved and this provides a good indication of simulation accuracy. As explained in section 7.3.1, the accuracy of the results is also ensured using a range of diagnostics, including invariance for different N_{grid} and tolerance values. It should be emphasised that the results are not equivalent to the 1-D simulation results due to the different density profiles used. Specifically, in the 2-D case the wave propagates further into the vortex before reflecting as the density gradient is not as sharp as in the 1-D case. Overall, the results demonstrate the reflection of waves from a BEC vortex and indicate the possibility of using the model to simulate reflection from a BEC vortex in the phonon frequency regime and superradiant frequency regime.

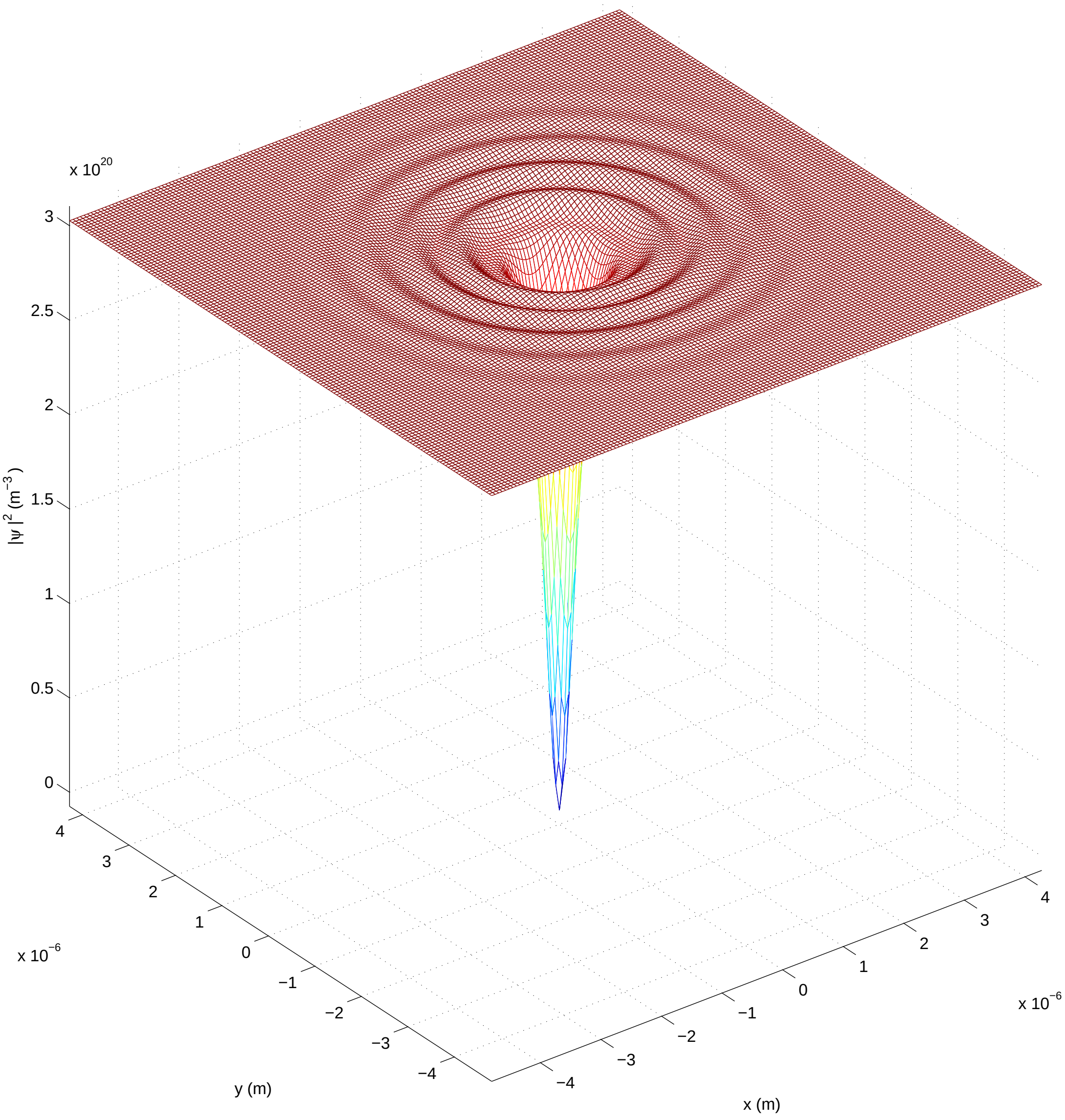

Figure 7.12: Two-dimensional surface plot of the incoming Gaussian-enveloped cylindrical wave with $k = 1 \times 10^7$ m^{-1} at $t = 0.33$ s for the converged vortex with density $\rho_o = 3.027 \times 10^{20}$ m^{-3}. A 1024^2 grid was used, however, only a subsection of the entire grid is shown.

7.3.3 The Superradiance Condition

In the case of superradiant scattering from a hydrodynamic vortex [74], discussed in section 5.4.2, the condition for superradiant scattering from a BEC vortex was

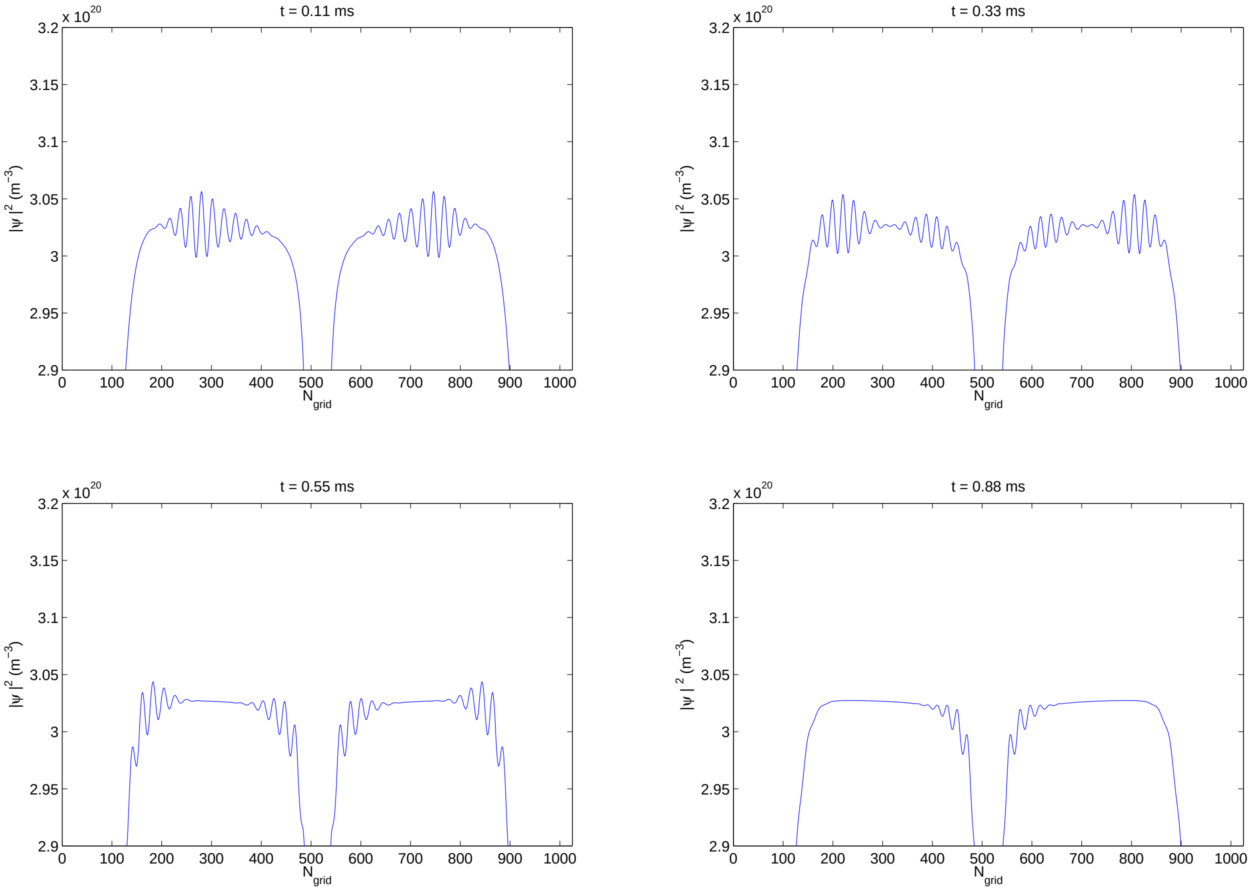

Figure 7.13: Incoming Gaussian-enveloped cylindrical wave, of figure 7.12, showing 1-D samples of the density throughout the domain at four different times during the real time evolution. The first image shows the wavepacket at $t = 0.11$ ms. At $t = 0.33$ ms the wavepackets have split and the ingoing wave is beginning to interact with the vortex. At $t = 0.55$ ms and $t = 0.88$ ms the wave continues to make its way further into the vortex. The outgoing wave at the boundary is a result of inaccuracy in the Bogoliubov coefficients leading to splitting of the wave. This was not an problem in the simulations as the wave was supressed at the boundary, due to the fact that the density drops off rapidly to zero, for the majority of the real time evolution.

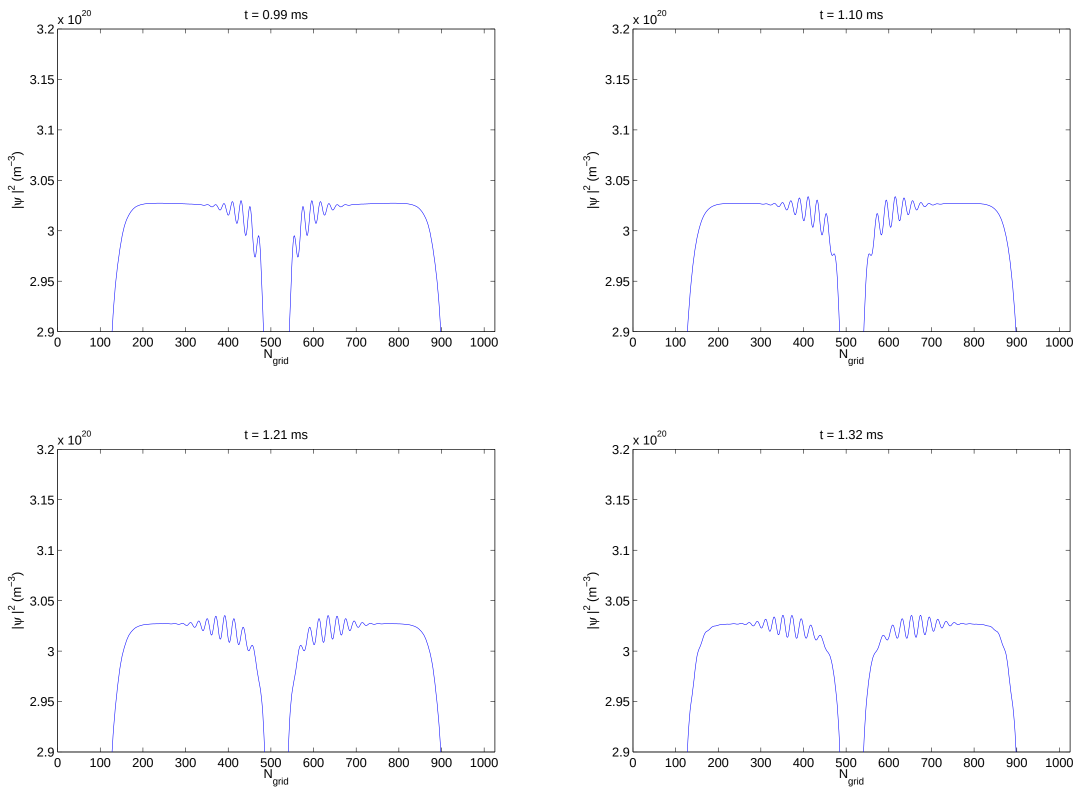

Figure 7.14: Images of four 1-D samples of the reflected wave after $t = 0.99$ ms, corresponding to the incoming wave in figure 7.13.

found to be,

$$\omega < \frac{m\alpha}{r_o^2} \tag{7.21}$$

where ω is the frequency of the wave, m is the angular wave number of the incoming wave, r_o is the radius of the zero density core used in the density profile in [74], and α is the vortex velocity constant appearing in the speed of rotation $v_\theta = \alpha/r$ given by,

$$\alpha = \frac{l\hbar}{m_{atom}} \tag{7.22}$$

for a charge l vortex [66]. Hence, the superradiance condition for a charge l BEC vortex within the hydrodynamic approximation becomes,

$$\omega < \frac{ml\hbar}{r_o^2 m_{atom}}. \tag{7.23}$$

The approach taken in determining whether superradiant scattering occurs in the GP simulations is to analyse the incident and reflected wavepackets in the frequency regime satisfied by equation 7.23. That is, in the hydrodynamic case superradiance was observed within this frequency regime and it follows that one would also expect to see superradiance in the same regime for the GP case. From equation 7.23 the constraint on the wavenumber of the incoming wave is,

$$k < \frac{ml\hbar}{r_o^2 m_{atom} c_s}. \tag{7.24}$$

In the GP simulations, the vortex charge $l = 1$, the angular wavenumber $m = 1$, and $m_{atom} = 1.41 \times 10^{-25}$ kg. We assume that the radius of zero density will be of an order of the healing length of the condensate, that is, $r_o = \epsilon\xi$ where $\epsilon \in \mathbb{R}$ and $\epsilon \ll 1$. This simplifies the superradiance condition and it can be easily seen that for a density of $\rho_o = 3.03 \times 10^{20}$ m^{-3}, as used in the simulations discussed in section 7.3.2, superradiance should occur when $k < 8.98 \times 10^6$ m^{-1}.

7.3.4 Investigation of Phonon Superradiance from a BEC Vortex

The main aim of this work is to determine whether a wavepacket reflected from a BEC vortex is amplified, in order to see if the analogy with astrophysical superradiance can be realised in BECs. Whilst, the simulation results reported in section 7.3.2 are an example of reflection of waves from a BEC vortex they do not lie within the phonon frequency regime or the frequency regime necessary to observe superradiance. In particular, phonon behaviour is only ensured if $k < \xi^{-1}$ and superradiance should only occur below the threshold wavenumber given by equation 7.24. These conditions confine the occurrence of superradiance to the low frequency regime.

Analysis of reflection of sound waves from a BEC vortex in the superradiant regime is made difficult by these constraints on the frequency of the incoming wave. The low frequencies required, and corresponding long wavelengths, raises the need to compromise between the superradiant frequency cutoff and the need to have a high frequency wave so that the wavelength of the wave can be observed over a distance smaller than the domain size.

Analysis of Reflection from a BEC Vortex in the Superradiant Regime

As mentioned, initial simulations were performed for a wavenumber of $k = 1 \times 10^7$ m^{-1} which is not in the phonon regime for the density $\rho_o = 3.03 \times 10^{20}$ m^{-3}. From the calculation in section 7.3.3 it is also clear that superradiance is not excepted for this wavenumber and density combination. Hence, simulations were conducted in the phonon regime with $k = 6 \times 10^6$ m^{-1} which is both phononic and falls under the frequency cutoff specified by the superradiance condition. Simulation parameters are identical to those used in the previous reflection simulations except that the spread of the wave was decreased to $\sigma = 0.8 \times 10^{-6}$ m and the wavepacket is centred at $r_o = 5 \times 10^{-6}$ m, in order to optimise interaction with the vortex. Furthermore, due to the new choice of wavenumber the Bogoliubov coefficients were calculated to be $u_k = 1.0992$ and $v_k = 0.4563$.

Figure 7.15 shows 1-D slices through the 2-D grid for four different time samples during the real time evolution. At $t = 0.11$ ms the wave has yet to split into outgoing and ingoing parts. Splitting occurs at $t = 0.33$ ms and the ingoing wave continues to propagate into the vortex at $t = 0.55$ ms. The reflected wave at $t = 1.43$ ms is also shown. As in the higher wavenumber case, the waveform is preserved after reflection from the vortex, and this is further evidence of numerical stability of the simulation and accuracy of the model. Although in a frequency regime theorised to generate superradiant scattering no increase of the reflected wave amplitude relative to the incident wave was observed. However, tests for a range of frequency values were not conducted due to time constraints. Hence, further analysis is required before one can determine whether or not superradiant scattering from a BEC vortex occurs.

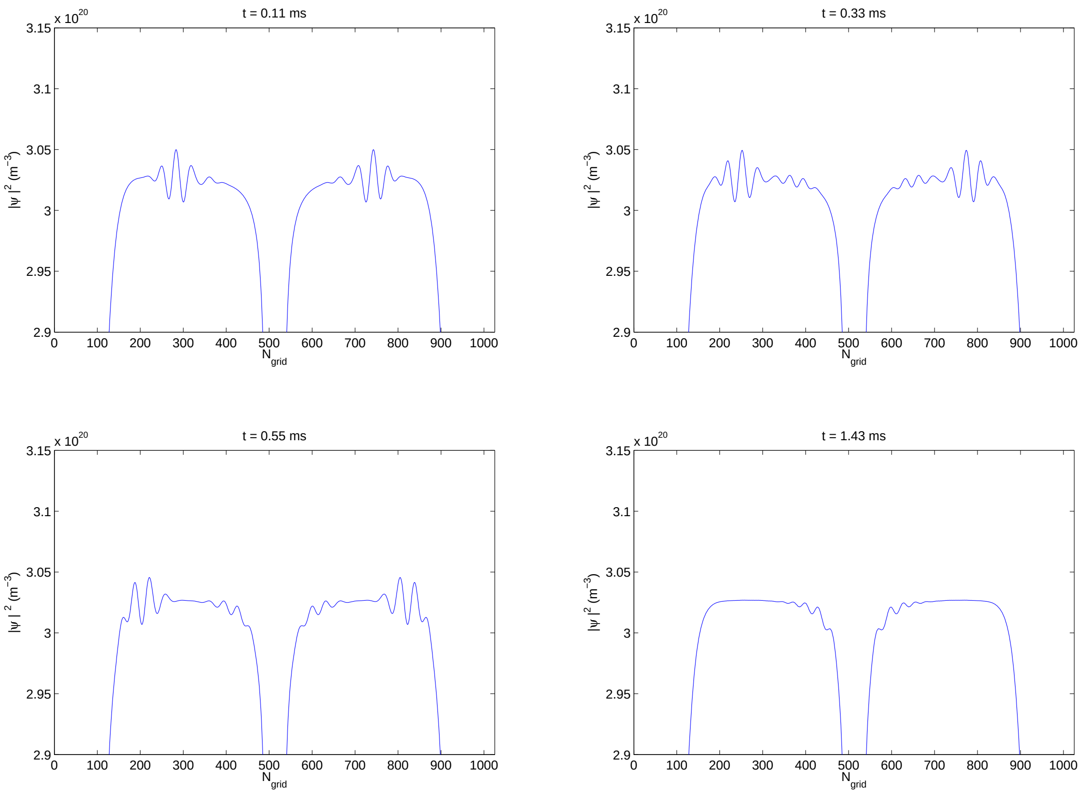

Figure 7.15: Incoming Gaussian-enveloped cylindrical wave, shown at $t = 0.11$ ms for a wavenumber of $k = 6 \times 10^6$ m^{-1}. Interaction with the vortex is imaged for $t = 0.33$ ms and $t = 0.55$ ms.The reflected wave after $t = 1.43$ ms is also shown.

Chapter 8

Conclusions and Future Directions

There exists a well established analogy between the propagation of a massless scalar field in a curved spacetime and the propagation of sound waves in an inviscid, barotropic and irrotational fluid such as a dilute gas Bose-Einstein Condensate. The unique properties of BECs make them a superior candidate as an analogue gravity model providing potential for the investigation of sonic superradiance and analogue Hawking Radiation in the laboratory. In advance of experiments it is beneficial to determine, from a theoretical and numerical basis, whether sonic superradiance is possible and under what conditions. It would also be useful, to ensuring a successful experimental program, to investigate the optimal fluid configuration and experimental setup for detecting these analogue black hole effects in the lab. Basak and Majumdar [10] have made steps towards this goal by considering the draining bathtub configuration. Whilst Slatyer and Savage [74] showed that superradiance is possible for the case of a non-draining BEC vortex, omitting the need for a central drain which somewhat simplifies experimental requirements. However, such work relies on the hydrodynamic approximation which is not valid as one approaches BEC vortex core and it is this region that is expected to give rise to superradiance.

In response to this issue, we have used a GP numerical analysis retaining the quantum pressure term to simulate sound waves interacting with a BEC vortex. We conducted 1-D simulations of sound waves propagating in a uniform BEC. Introducing a vortex-like density profile into the medium it was possible to observe reflection of sound waves from this region of varying density. Within the mean-field formalism the model was extended to observe the 2-D evolution of the condensate wavefunction with the time-dependent GP equation. In order to obtain a 2-D vortex structure the method of imaginary time propagation was employed. For a suitable choice of parameters reflection from a charge $l = 1$ vortex was observed for an incoming Gaussian-modulated cylindrical wave. Simulations were performed within the frequency regime where superradiance is expected to occur, however, results were inconclusive as efforts to perform a detailed analysis in such regimes were limited by time constraints. Despite the unresolved question of whether superradiant scattering from a BEC vortex is possible, this research provides a good foundation for future numerical work concerning phonon superradiance in dilute gas Bose-Einstein Condensates.

Future Research

As a first step in extending the work presented in this thesis, it will be necessary to carry out further analysis of the Imaginary Time Propagation method and in doing so obtain converged vortices for different vortex parameters. This will allow greater flexibilility when analysing reflection in various frequency regimes. In particular, if one obtains a converged vortex for a higher background density than that used in the numerical work in this thesis, the phonon regime will have a higher frequency cutoff. Furthermore, the increased speed of sound resulting from a higher background density will allow sound wave interaction with the vortex to be observed for a shorter real time evolution, and hence computation time for the imaginary time evolution can be lessened.

The thorough investigation of reflection in frequency regimes expected to give rise to superradiance is also achievable without much alteration to the present simulations. One problem that may be encountered, however, is the need to increase the domain size to adequately image the long wavelength waves expected to produce amplification on reflection from the vortex. Furthermore, if part of the incoming wave forms a transmitted wave propagating into the vortex, as suggested by the negative energy mode interpretation, this transmitted wave would need to be monitored. This would be to ensure that the transmitted wave is not giving rise to unphysical reflections due to inadequate sampling, since as one approaches the vortex core the wavelength of the sound waves decreases. Once these issues are resolved, a 3-D GP simulation could be undertaken in order to gain greater insight into the problem.

Another issue that may arise, in attempts to build on the results presented in this thesis, is the need to simulate the vortex in a rotating frame. In certain cases a rotating frame would be required to stabilise a vortex against drift to lower density regions. In a uniform BEC medium there is no density gradient and so drift will not occur. Hence, for such circumstances there is no need to consider the problem in a rotating frame as stability is not an issue. However, in the simulations contained in this thesis the presence of a trapping potential forcing the density to zero at the domain boundaries could lead to vortex drift. Implementing the vortex in a rotating frame in XMDS involves incorporating the energy contribution $\mathbf{\Omega} \cdot \mathbf{L}$ due the rotation of the trap, where $\mathbf{\Omega}$ is the angular velocity vector and $\mathbf{L}$ is the angular momentum vector, into the GP equation.

Depending on the outcome of the GP approach, it may be necessary to extend to a full quantum approach in order to observe superradiance. This would involve using a truncated Wigner method [72, 73], a classical field approximation in the Wigner representation, which unlike the GP approach incorporates the interaction between the condensate and the non-condensed atoms. More specifically, it enables one to account for quantum mechanical vacuum fluctuations by introducing noise terms into the GP equation, yielding a stochastic differential equation which can be solved numerically.

Bibliography

[1] M. H. Anderson, J. R. Ensher, M. R. Matthews, C. E. Wieman, and E. A. Cornell. Observation of bose-einstein condensation in a dilute atomic vapor. *Science*, 269:5221, 1995.

[2] M.R. Andrews, D.M. Kurn, H.-J. Miesner, D.S. Durfee, C.G. Townsend, S. Inouye, and W. Ketterle. Propagation of sound in a Bose-Einstein condensate. *Physical Review Letters*, 79:4, 1997.

[3] C. Barceló, S. Liberati, and M. Visser. Analogue gravity from field theory normal modes? *Quantum Grav.*, 18, 2001.

[4] C. Barceló, S. Liberati, and M. Visser. Analogue Gravity. *Living Rev. Relativity*, 8, URL (cited on 18/7/06): http://www.livingreviews.org/lrr-2005-12, 2005.

[5] C. Barcelo, S. Liberati, S. Sonego, and M. Visser. Hawking-like radiation does not require a trapped region. *Phys. Rev. Lett.*, 2006.

[6] C. Barcelo, S. Liberati, S. Sonego, and M. Visser. Quasi-particle creation by analogue black holes. *Class. Quant. Grav.*, 23, 2006.

[7] C. Barcelo, S. Liberati, and M. Visser. gr-qc/0110036. *Towards the observation of* H*awking radiation in* B*ose-*E*instein* C*ondensates*, 2001.

[8] C. Barcelo, S. Liberati, and M. Visser. Towards the observation of Hawking radiation in Bose-Einstein Condensates. *Int. J. of Mod. Phys.*, A18, 2003.

[9] S. Basak. gr-qc/0501097. *Analog of Superradiance effect in B*EC, 2005.

[10] S. Basak and P. Majumdar. 'Superresonance' from a rotating acoustic black hole. *Class. Quantum Grav.*, 20:3097, 2003.

[11] S. Basak and P. Majumdar. Reflection coefficient for superresonant scattering. *Class. Quantum Grav.*, 20:2929, 2003.

[12] J. D. Bekenstein. Extraction of energy and charge from a black hole. *Phys. Rev. D*, 7:4, 1973.

[13] J.D. Bekenstein and M. Schiffer. The many faces of superradiance. *Physical Review* D, 58, 1998.

[14] N. Bogoliubov. On the theory of superfluidity. *J. Phys.(USSR)*, 11:23, 1947.

[15] S. N. Bose. *Z Phys*, 26:178, 1924.

[16] C. C. Bradley, C. A. Sackett, J. J. Tollett, and R. G. Hulet. Evidence of bose-einstein condensation in an atomic gas with attractive interactions. *Phys. Rev. Lett.*, 75:1687, 1995.

[17] V. Cardoso. physics/0503042. *Acoustic black holes*, 2005.

[18] P. A. Cherenkov. Visible radiation produced by electrons moving in a medium with velocities exceeding that of light. *Phys. Rev.*, 52, 1937.

[19] R. L. Cook. Stochastic sampling in computer graphics. *ACM Transactions on graphics*, 5:1, 1986.

[20] S. Corley. Computing the spectrum of black hole radiation in the presence of high frequency dispersion: An analytical approach. *Phys. Rev. D*, 57:10, 1998.

[21] F. Dalfovo, S. Giorgini, L. P. Pitaevskii, and S. Stringari. Theory of bose-einstein condensation in trapped gases. *Rev. Mod. Phys.*, 71, 1999.

[22] K. B. Davis, M. O. Mewes, M. R. Andrews, and N. J. van Druten. Bose-einstein condensation in a gas of sodium atoms. *Phys. Rev. Lett.*, 75:3969, 1995.

[23] B. DeWitt. Quantum field theory in curved space time. *Phys. Rep.*, 19:295, 1975.

[24] R. H. Dicke. Coherence in spontaneous radiation processes. *Phys. Rev.*, 93:99, 1954.

[25] XMDS documentation available at http://www.xmds.org.au.

[26] A. Einstein. *Sitzungber. K. Preuss. Akad. Wiss.*, 3, 1925.

[27] B. D. Esry, C. H. Greene, J. P. Burke, and J. L. Bohn. Hartree-fock theory for double condensates. *Phys. Rev. Lett.*, 78:19, 1997.

[28] C. Farrell and U. Leonhardt. The perfectly matched layer in numerical simulations of nonlinear and matter waves. *J.* O*pt.* B*:* Q*uantum* S*emiclass.* O*pt*, 7, 2005.

[29] D. L. Feder, C. W. Clark, and B. I. Schneider. Vortex stability of interacting bose-einstein condensates confined in anisotropic harmonic traps. *Phys. Rev. Lett.*, 82:25, 1999.

[30] D. L. Feder, A. A. Svidzinsky, A. L. Fetter, and C. W. Clark. Anomalous modes drive vortex dynamics in confined bose-einstein condensates. *Phys. Rev. Lett.*, 86:564, 2001.

[31] F. Federici, C. Cherubini, S. Succi, and M.P. Tosi. Superradiance from hydrodynamic vortices: A numerical study. *Physical Review* A, 73, 2006.

[32] V. Fock. *The Theory of Space, Time and Gravitation, 2nd Ed.* Pergamon, New York, 1964.

[33] K. Fredenhagen and R. Haag. On the derivation of Hawking radiation associated with the formation of a black hole. *Commun. Math Phys.*, 127:273, 1990.

[34] L.J. Garay, J.R. Anglin, J.I. Cirac, and P. Zoller. Sonic black holes in dilute bose-einstein condensates. *Physical Review* A, 63, 2001.

[35] V. L. Ginzburg. *Progress in Optics* XXXII. Elsevier Science, Amsterdam, 1993.

[36] V. L. Ginzburg and I. M. Frank. On a doppler efffect at the superlight velocity. *Dokl. Akadem. Nauk SSSR*, 56:583, 1947.

[37] S. Giovanazzi, C. Farrell, T. Kiss, and U. Leonhardt. Conditions for one-dimensional supersonic flow of quantum gases. *Physical Review* A, 70, 2004.

[38] J. B. Hartle and S. W. Hawking. Path-integral derivation of black-hole radiance. *Phys. Rev.* D, 13:2188, 1976.

[39] S. W. Hawking. Gravitational radiation from colliding black holes. *Phys. Rev. Lett.*, 26:1344, 1971.

[40] S. W. Hawking and G. F. R. Ellis. *The Large Scale Structure of Spacetime.* Cambridge University Press, Cambridge, 1973.

[41] S.W. Hawking. Black hole explosions? *Nature*, 248:30, 1974.

[42] S.W. Hawking. Particle creation by black holes. *Commun. Math. Phys.*, 43:199, 1975.

[43] S. Inouye, S. Gupta, T. Rosenband, A. P. Chikkatur, A. Gorlitz, T. L. Gustavson, A. E. Leanhardt, D. E. Pritchard, and W. Ketterle. Observation of vortex phase singularities in Bose-Einstein Condensates. *Phys. Rev. Lett.*, 87, 2001.

[44] A. Iserles. *A First Course in the Numerical Analysis of Differential Equations.* Cambridge university Press, United Kingdom, 1996.

[45] T. Jacobson. Black-hole evaporation and ultrashort distances. *Phys. Rev.* D, 44:6, 1991.

[46] M. K. Jain. *Numerical Solution of Differential Equations.* John Wiley and Sons, New York, 1979.

[47] P.G. Kevrekidis, R. Carretero-Gonzalez, D.J. Frantzeskakis, and I.G. Kevrekidis. Vortices in bose-einstein condensates: Some Recent Developments. *Moden Physics Letters B*, 18:30, 2004.

[48] H. Lamb. *Hydrodynamics.* Dover, New York, 1932.

[49] L. D. Landau and E. M. Lifshitz. *Fluid Mechanics.* Pergamon, London, 1959.

[50] L. D. Landau, E. M. Lifshitz, and L. P. Pitaevskii. *Electrodynamics of Continuous Media, 2nd Ed.* Pergamon, Oxford, 1984.

[51] T. D. Lee, K. Huang, and C. N. Yang. Eigenvalues and eigenfunctions of a bose system of hard spheres and its low-temperature properties. *Phys. Rev.*, 106:1135, 1957.

[52] U. Leonhardt, T. Kiss, and P. Öhberg. Bogoliubov theory of the Hawking effect in Bose-Einstein condensates. *J. Opt. B: Quantum Semiclass. Opt*, 5, 2003.

[53] C. Møller. *The Theory of Relativity, 2nd Ed.* Claredon, Oxford, 1972.

[54] K. W. Madison, F. Chevy, W. Wohlleben, and J. Dalibard. Vortex formation in a stirred Bose-Einstein Condensate. *Phys. Rev. Lett.*, 84, 1999.

[55] M. R. Matthews, B. P. Anderson, P. C. Haljan, D. S. Hall, C. E. Wieman, and E. A. Cornell. Vortices in a Bose-Einstein Condensate. *Phys. Rev. Lett.*, 83, 1999.

[56] H. J. Metcalf and P. Van der Straten. *Laser Cooling and Trapping.* Springer-Verlag, New York, 1999.

[57] W.E. Milne. *Numerical solution of differential equations.* John Wiley and Sons, New York, 1953.

[58] L. M. Milne-Thomson. *Theoretical Hydrodynamics 5th Ed.* MacMillian, London, 1968.

[59] C. W. Misner, K. Thorne, and J. A. Wheeler. *Gravitation.* Freeman, San Franciso, 1973.

[60] V.W. Misner. Quantum field theory in curved spacetime. *Phys. Rev. Lett.*, 25, 1972.

[61] M. Mottonen, T. Mizushima, T. Isoshima, M. M. Salomaa, and K. Machida. Splitting of a doubly quantised vortex through intertwinning in bose-einstein condensates. *Physical Review A*, 68, 2003.

[62] R. Parentani. Beyond the semiclassical description of black hole evaporation. *Int. J. Mod. Phys.*, A17:2721, 2002.

[63] M. K. Parikh and F. Wilczek. Hawking radiation as tunneling. *Phys. Rev. Lett.*, 85:24, 2000.

[64] L. Parker. Quantised fields and particle creation in an expanding universe. *Phys. Rev.*, 183, 169.

[65] R. Penrose. Gravitational collapse: The role of general relativity. *General Relativity and Gravitation*, 34:7, 2002.

[66] C.J. Pethick and H. Smith. *Bose-Einstein Condensation in Dilute Gases.* Cambridge University Press, United Kingdom, 2002.

[67] L. Pitaevskii and S. Stringari. *Bose-Einstein Condensation.* Oxford University Press, United Kingdom, 2003.

[68] J. L. Roberts, N. R. Claussen, S. L. Cornish, and C. E. Wieman. Magnetic field dependence of ultracold inelastic collisions near a Feshbach resonance. *Phys. Rev. Lett.*, 85:728, 2000.

[69] M. Sakagami and A. Ohashi. Hawking radiation in laboratories. *Prog. Theor. Phys.*, 107, 2002.

[70] B.F. Schutz. *A first course in general relativity.* Cambridge University Press, United Kingdom, 1985.

[71] R. Schutzhold and W.G. Unruh. Gravity wave analogues of black holes. *Physical Review* D, 66, 2002.

[72] A. Sinatra, C. Lobo, and Y. Castin. Classical-field method for time dependent Bose-Einstein condensed gases. *Phys. Rev. Lett.*, 87(21), 2001.

[73] A. Sinatra, C. Lobo, and Y. Castin. The truncated Wigner method for Bose-condensed gases: limits of validity and applications. *Journal of Physics* B*:* A*tomic,* M*olecular and* O*ptical* P*hysics*, 35, 2002.

[74] T. Slatyer and C.M. Savage. Superradiant scattering from a hydrodynamic vortex. *Class. Quantum Grav.*, 22, 2005.

[75] A. A. Starobinski. Amplification of waves during reflection from a rotating 'black hole'. *Sov. Phys. - Journal of Experimental and Theoretical Physics*, 37:28, 1973.

[76] M. Tsubota. Quantised vortices in superfluid helium and Bose-Einstein Condensates. *Journal of Physics: Conference Series*, 31, 2006.

[77] W. G. Unruh. Notes on black-hole evaporation. *Phys. Rev.* D, 14:870, 1976.

[78] W. G. Unruh. Sonic analogue of black holes and the effects of high frequencies on black hole evaporation. *Phys. Rev.* D, 51:6, 1995.

[79] W.G. Unruh. Experimental black hole evaporation? *Phys. Rev. Lett.*, 46, 1981.

[80] S.I. Vavilov. On the possible reasons for the blue g luminescence of fluids. *Dokl. Akad. Nauk SSSR 2*, 457, 1934.

[81] M. Visser. Acoustic black holes: horizons, ergospheres and Hawking radiation. *Class. Quantum Gravity*, 15:6, 1998.

[82] M. Visser. Hawking radiation without black hole entropy. *Physical Review Letters*, 80:16, 1998.

[83] M. Visser. *Artifical* B*lack* H*oles.* edited by M. Novello, M. Visser and G. Volovik, World Scientific, Singapore, 2002.

[84] M. Visser and S. Weinfurtner. Vortex analogue for the equatorial geometry of the Kerr black hole. *Class. Quant. Grav.*, 22:2493, 2005.

[85] G.E. Volovik. Superfluid analogies of cosmological phenomena. *Phys. Rep.*, 351:4, 2001.

[86] R.W. Wald. Stimulated-emission effects in particle creation near black holes. *Physical Review* D, 13:12, 1976.

[87] J. E. Williams. *The Preparation of Topological Modes in a Strongly-Coupled Two-Component Bose-Einstein Condensate.* PhD thesis, University of Colorado, 1999. Appendix C.

[88] Y.B. Zel'Dovich. The generation of waves by a rotating body. *Journal of Experimental and Theoretical Physics Letters*, 14:180, 1971.

[89] Y.B. Zel'Dovich. Amplification of cylindrical electromagnetic waves reflected from a rotating body. *Journal of Experimental and Theoretical Physics*, 35:1085, 1972.

Appendix A

1-D Simulation of Sound Wave Propagation in a BEC

A.1 1-D Simulation Code

```
<?xml version="1.0"?>
<!- -Example simulation: GP equation- ->

<simulation>

<!- - Global system parameters and functionality - ->
<name>vortex1D</name>
<author>Sarah Midgley</author>
<description>
Example GP equation simulation with realistic BEC parameters and non-uniform density
</description>

<prop_dim>t</prop_dim>
<error_check>no</error_check>
<use_wisdom>yes</use_wisdom>
<benchmark>yes</benchmark>

<!- - Global variables for the simulation - ->
<globals>
<![CDATA[

const double m = 1.41e-25;//mass of rubidium 85 atom
const double hbar = 1.054e-34;
const double wave_amplitude = 1e8;
const double a = 5.29e-9;//scattering length
const double x0 =-50e-6;//centre of initial wavepacket
const double sigma =2e-6;//spread of the wave
const double k = 1e7;//wavenumber
const double V = 0.0;//trapping potential
const double U = 4.0*M_PI*hbar*hbar*a/m;//coupling constant
```

```
const double background_density = 1e22;

const double Bexp = 2.0*background_density*U/hbar;

]]>
</globals>

<!- - Field to be integrated over - ->
<field>
<name>main</name>
<dimensions> x </dimensions>
<lattice> 2000 </lattice>
<domains> (-60e-6,30e-6) </domains>
<samples>1</samples>

<vector>
<name>main</name>
<type>complex</type>
<components>phi vortex_density</components>
<fourier_space>no</fourier_space>
<![CDATA[

const double uco = 1.3641; const double vco = 0.92777;

vortex_density = background_density*(fabs(5e5*x)/sqrt(2+(5e5*x*5e5*x));

phi = wave_amplitude*exp(-(x-x0)*(x-x0)/(2.0*sigma*sigma))*
((uco*rcomplex(cos(k*x),sin(k*x)))-(vco*rcomplex(cos(k*x),-sin(k*x))));

]]>
</vector>
</field>

<!- - The sequence of integrations to perform - ->
<sequence>
<integrate>

<algorithm>RK4IP</algorithm>
<interval>2e-3</interval>
<lattice> 5000</lattice>
<samples>1</samples>
< k_operators>
<constant>yes</constant>
<operator_names>L</operator_names>
<![CDATA[
```

```
L = rcomplex(0.0,-kx*kx*hbar/(2 *m));
]]>
</k_operators>
<vectors>main</vectors>
<![CDATA[

dphi_dt = L[phi] - i*V*phi/hbar - U*i *vortex_density*(2*phi + ~phi *c_exp(-i*Bexp*t)
)/hbar;
]]>
</integrate>
</sequence>

<!- - The output to generate - ->
<output format="binary" precision="single">
<filename>vortex1D.xsil</filename>
<group>
<sampling>
<fourier_space> no </fourier_space>
<lattice> 1000</lattice>
<moments>density</moments>
<![CDATA[
density =~phi*phi;
]]>
</sampling>
</group>
</output>
</simulation>
```

Appendix B

2-D Simulation of Sound Wave Propagation in a BEC

B.1 Imaginary Time Propagation Code

```
<?xml version="1.0"?>
<!- -Example simulation: GP equation- ->

<simulation>

<!- - Global system parameters and functionality - ->
<name>imagtime</name>
<author>Sarah Midgley</author>
<description>
2 dimensional simulation: generation of imagtime.xsil data file for input into real-
time.xmds as initial state
</description>

<prop_dim>t</prop_dim>
<use_prefs>yes</use_prefs>
<use_mpi>yes</use_mpi>
<error_check>no</error_check>
<use_wisdom>yes</use_wisdom>
<benchmark> no </benchmark>

<!- - Global variables for the simulation - ->
<globals>
<![CDATA[

const double m = 1.41146e-25 ;
const double hbar = 1.05457266e-34 ;
const double wave_amplitude =1e8;
const double a = 5.29e-9;
const double x0 =-5e-6;
const double sigma =1e-6;
```

```
const double k = 1e7 ;
const double s = 1e-6; //scale factor in the potential
const double U = 4.0*M_PI*hbar*hbar*a/m ;
const double background_density = 1e20 ;
const double winding_num= 1.0;//winding number
const double b=15e-6; //half domain length
const double V0= 2e-30;//amplitude of the potential
const double norm_start = 8.9501e10; //starting norm

]]>
</globals>

<!- - Field to be integrated over - ->
<field>
<name>main</name>
<dimensions> x y</dimensions>
<lattice> 512 512</lattice>
<domains> (-15e-6,15e-6)(-15e-6,15e-6) </domains>
<samples> 1 </samples>

<vector>
<name>main</name>
<type>complex</type>
<components>phi</components>
<fourier_space>no no</fourier_space>
<![CDATA[

double r = sqrt(x*x+y*y);

phi = sqrt(background_density)*(rcomplex(x,y))*3e6/(sqrt(2.0+(3e6*r*3e6*r)));

]]>
</vector>

<vector>
<name>vc1</name>
<type>double</type>
<components>V</components>
<fourier_space>no no</fourier_space>

<![CDATA[
V=V0*(exp(-(b-fabs(x))*(b-fabs(x))/(s*s))+exp(-(b-fabs(y))*(b-fabs(y))/(s*s)));
]]>

</vector>
```

```
</field>

<!- - The sequence of integrations to perform - ->
<sequence>
<sequence>
<cycles>25000</cycles>
<integrate>

<algorithm>ARK45IP</algorithm>
<tolerance>1e-6</tolerance>
<interval>1e-6</interval>
<lattice>10000</lattice>
<samples> 0 </samples>
<k_operators>
<constant>yes</constant>
<operator_names>L</operator_names>
<![CDATA[
L = rcomplex( -(kx*kx*hbar/(2*m))- (ky*ky*hbar/(2*m)),0.0);
]]>
</k_operators>
<vectors>main vc1</vectors>
<![CDATA[

dphi_dt = L[phi] -V*phi/hbar - (U*phi*~phi)*phi/hbar;

]]>
</integrate>

<filter>
<moment_group>
<moments> n_norm</moments>
<integrate_dimension> yes yes </integrate_dimension>

<![CDATA[

n_norm+=phi*~phi;

]]>

</moment_group>

<vectors>main</vectors>
<fourier_space>no no</fourier_space>
```

```
<![CDATA[

phi *= sqrt( norm_start / n_norm.re );

]]>

</filter>

</sequence>

<breakpoint>
<filename>imagtime.xsil</filename>
<fourier_space>no no</fourier_space>
<vectors>main</vectors>
</breakpoint>

</sequence>

<!- - The output to generate - ->
<output format="binary">
<filename>imagtime2.xsil</filename>

<group>
<sampling>
<fourier_space>no no</fourier_space>
<lattice>0 0</lattice>
<moments>totnum</moments>
<![CDATA[

totnum=phi *~phi;

]]>
</sampling>
</group>

</output>
</simulation>
```

B.2 Real Time Propagation Code

```
<?xml version="1.0"?>
<!- -Example simulation: GP equation- ->
```

```
<simulation>

<!- - Global system parameters and functionality - ->
<name>realtime</name>
<author>Sarah Midgley</author>
<description>
2 dimensional simulation: real time evolution using imagtime.xsil as input
</description>

<prop_dim>t</prop_dim>
<use_prefs>yes</use_prefs>
<use_mpi>yes </use_mpi>
<error_check>no</error_check>
<use_wisdom>yes</use_wisdom>
<benchmark> no </benchmark>

<!- - Global variables for the simulation - ->
<globals>
<![CDATA[

const double m = 1.41146e-25 ;
const double hbar = 1.05457266e-34 ;
const double wave_amplitude =1e8;// 1e8 ;
const double a = 5.29e-9;
const double x0 =-5e-6;
const double r0 = 5e-6;
const double sigma =1e-6;
const double k = 1e7 ;
const double s = 1e-6;
const double U = 4.0 *M_PI*hbar*hbar*a/m ;
const double background_density = 1e20 ;
const double winding_num= 1.0;
const double m_ang=1;//angular wave number
const double b=15e-6;
const double V0= 2e-30;

]]>
</globals>

<!- - Field to be integrated over - ->
<field>
<name>main</name>
<dimensions> x y</dimensions>
<lattice> 512 512 </lattice>
<domains>(-15e-6,15e-6)(-15e-6,15e-6) </domains>
```

```
<samples> 1 1</samples>

<vector>
<name>main</name>
<type>complex</type>
<components>phi V </components>
<fourier_space>no no</fourier_space>
<filename format="xsil">imagtime.xsil</filename>
<![CDATA[

]]>
</vector>
</field>

<!- - The sequence of integrations to perform - ->
<sequence>

<filter>

<vectors>main</vectors>
<![CDATA[

const double uco =1.23254617;
const double vco =0.7205345566;

double r = sqrt(x*x+y*y);

if ((r>0.05e-6))

{phi = phi+wave_amplitude*exp(-(r-r0)*(r-r0)/(2.0*sigma*sigma))*
((uco*rcomplex(cos(k*r),sin(k*r)))-(vco*rcomplex(cos(k*r),-
sin(k*r))))*(rcomplex(x,y)/r);}

V=V0*(exp(-(b-fabs(x))*(b-fabs(x))/(s*s))+exp(-(b-fabs(y))*(b-fabs(y))/(s*s)));

]]>

</filter>

<integrate>

<algorithm>ARK45IP</algorithm>
<tolerance>1e-6</tolerance>
<interval>1e-3</interval>
<lattice>10000</lattice>
```

```
<samples> 10 10</samples>
<k_operators>
<constant>yes</constant>
<operator_names>L</operator_names>
<![CDATA[
L = rcomplex(0.0,(-kx*kx*hbar/(2*m))-(ky*ky*hbar/(2*m)));
]]>
</k_operators>
<vectors>main</vectors>
<![CDATA[

dphi_dt = L[phi] - i*V*phi/hbar - U*i*phi*phi*~phi/hbar;

]]>
</integrate>

</sequence>

<!- - The output to generate - ->
<output format="binary" precision="double">
<filename>realtime.xsil</filename>
<group>
<sampling>
<fourier_space> no no</fourier_space>
<lattice> 128 128</lattice>
<moments>den2D</moments>
<![CDATA[
den2D=phi*~phi;
]]>
</sampling>
</group>

<group>
<sampling>
<fourier_space> no no</fourier_space>
<lattice>128 32</lattice>
<moments> den2Dslice </moments>
<![CDATA[
den2Dslice = phi* ~ phi;
]]>
</sampling>
</group>

</output>
</simulation>
```